

Feasibility Study of Heavy Gas Dispersion Experiments in Complex Environments in Physical Modelling

Dissertation

zur Erlangung des Doktorgrades
an der Fakultät für Mathematik, Informatik und Naturwissenschaften
Fachbereich Erdsystemwissenschaften der Universität Hamburg

vorgelegt von

Simon Josef Michel

aus Hamburg

Hamburg, 2023

Fachbereich Erdsystemwissenschaften

Datum der Disputation:

07.06.2023

Gutachter/innen der Disertation:

Prof. Dr. Bernd Leitl

Dr. Frank Harms

Zusammensetzung der Prüfungskommission:

Prof. Dr. Bernd Leitl

Dr. Frank Harms

Prof. Dr. Felix Ament

Prof. Dr. Lars Kutzbach

Prof. Dr. Ulrich Seifert

Vorsitzender des Fach-Promotionsausschusses

Erdsystemwissenschaften:

Prof. Dr. Hermann Held

Dekan der Fakultät MIN:

Prof. Dr. Ing. Norbert Ritter

Abstract

Despite more than 50 years of research of accidental heavy gas releases, high qualitative and extensive reference data sets for heavy gas dispersions in complex environments are rare and knowledge gaps still persist. Accidental releases of heavy gases, mostly toxic or flammable, still pose severe health and environmental risks.

This thesis presents a feasibility study of physical modelling of heavy gas dispersion experiments in complex environments and findings of heavy gas dispersion experiments. Measurements have been performed in the WOTAN boundary layer wind tunnel of the Environmental Wind Tunnel Laboratory of the Meteorological Institute of the University of Hamburg. Three models of increasing complexity are used to showcase the necessary planning and setup of a heavy gas dispersion scenario and how measurements are performed to successfully model a heavy gas dispersion. The model with the highest complexity is a part of an industrial chemical park in the city of Ludwigshafen of the company of BASF, which includes a multitude of different types of obstacles and buildings. Constraints and potential problems which can arise during a wind tunnel heavy gas dispersion measurement campaign are discussed and solutions to the potential issues are presented. The heavy gas dispersions are realised with a release of a CO₂-butane mixture. Concentration measurements are performed with a flame ionisation detector.

During the thesis more than 2000 flow measurements, 1200 neutral density and 1000 heavy gas dispersion measurements were performed in the three different model geometries. Measurements have been performed with variations in the wind tunnel boundary layer, wind direction, source volume flow and wind speed. In this thesis the influence of these factors, which effect heavy gas dispersions, are investigated and discussed.

All flow, neutral density and heavy gas dispersion measurements, including the wind tunnel boundary layer measurements and model geometries are compiled in a reference data set which has been published.

Kurzfassung

Trotz mehr als 50 Jahren Forschung zu störfallartigen Schwergasausbreitungen sind qualitativ hochwertige und umfassende Referenzdatensätze für Schwergasausbreitungen in komplexen Umgebungen selten und es bestehen weiterhin Wissenslücken. Störfallartige Freisetzungen von meist giftigen oder brennbaren Schwergasen stellen nach wie vor schwere Gesundheits- und Umweltrisiken dar.

In dieser Arbeit wird eine Machbarkeitsstudie zur physikalischen Modellierung von Schwergasausbreitungsexperimenten in komplexen Umgebungen vorgestellt und die Ergebnisse von Schwergasausbreitungsexperimente werden vorgestellt. Die Messungen wurden im WOTAN Grenzschichtwindkanal des 'Environmental Wind Tunnel Laboratory' des Meteorologischen Instituts der Universität Hamburg durchgeführt. Mit drei Modellen mit zunehmender Komplexität wird die Planung von Schwergasausbreitungsszenarios und die Durchführung von Messungen zur erfolgreichen Modellierung von Schwergasausbreitungen exemplarisch präsentiert. Das Modell mit der höchsten Komplexität ist ein Teil eines Chemieparks der Firma BASF in Ludwigshafen, das eine Vielzahl von verschiedenen Hindernissen umfasst. Einschränkungen und mögliche Probleme, die bei einer Windkanalmesskampagne für Schwergasausbreitungen auftreten können, werden erörtert und es werden Lösungen für die potentiell auftretenden Probleme vorgestellt. Die Schwergasausbreitungsexperimente werden durch eine Freisetzung eines CO₂-Butan-Gemisches realisiert. Die Konzentrationsmessungen werden mit einem Flammenionisationsdetektor durchgeführt.

Im Rahmen dieser Arbeit wurden mehr als 2000 Strömungsmessungen, 1200 dichteneutrale und 1000 Schwergasausbreitungsmessungen in den drei verschiedenen Modellgeometrien durchgeführt. Bei den Messungen wurden die Anströmwindgrenzschicht, die Windrichtung, der Quellvolumenstrom und die Windgeschwindigkeit variiert. In dieser Arbeit wird der Einfluss dieser Faktoren auf die Schwergasausbreitung untersucht und diskutiert.

Alle Strömungsmessungen, Ausbreitungsmessungen von dichteneutralen und Schwergasen, sowie der Windgrenzschichtmessungen und der Modellgeometrien sind in einem Referenzdatensatz zusammengefasst und veröffentlicht.

Acknowledgements

When I meet God, I am going to ask him two questions:
Why relativity? And why turbulence?
I really believe he will have an answer for the first.

attributed to **Werner Heisenberg** (1976)

I want to thank everyone who has supported and motivated me over the course of the last three and a half years.

Special thanks go to my supervisors Prof. Dr. Bernd Leitl and Dr. Frank Harms for their helpful comments, indepth discussions about heavy gas dispersion and suggestions. They always had time to talk and help with various technical and other issues which arose during my PhD. I also want to thank them for their confidence and encouragement in me, which allowed me to work and plan several measurement campaigns independently.

I also want to thank Benedikt Seitzer for many interesting discussions, all his support over the course of the past years and the coffee and tea breaks and brief respites from the work during lunch. Furthermore I want to thank Theresa Lang and Marc Prange for proofreading and comments. Thanks go to Theresa Lang, Marc Prange, Jule Radtke, Lukas Kluft, Daniel Krieger, Henning Franke, Henning Dorff, Lara Hellmich, Finn Burgemeister and others for the lunch breaks and interesting discussions.

I want to acknowledge the help provided by the workshop of the University of Hamburg creating the model buildings, the sources and general help in the wind tunnel laboratory. Thanks also go the wind tunnel working group for the nice and welcoming working environment.

Further thanks is directed to my project partners from the University of Rostock, the Bundesanstalt für Materialforschung und -prüfung and the supporting members of the AiF-project who contributed helpful comments over the course of the project.

I thank the members of my doctoral committee for taking the time to review this work of three and a half years.

Special thank also goes to my parents and my family who always supported and encouraged me.

Publications related to this Dissertation

As a PhD student I contributed to five publications.

Leitl, B., Harms, F., Michel, S., Turnow, J., Plischka, H., Schalau, B., and Schalau, S. (2021). Simulation kurzzeitiger Gefahrstofffreisetzungen aus Industrieanlagen/simulation of short-term hazmat releases from industrial facilities – challenges and possible solutions. *Gefahrstoffe*, 81(07-08):257–270

Schalau, S., Habib, A., and Michel, S. (2021). Atmospheric wind field modelling with OpenFOAM for near-ground gas dispersion. *Atmosphere*, 12(8):933

Plischka, H., Michel, S., Turnow, J., Leitl, B., and Kornev, N. (2022). Comparison of turbulent inflow conditions for neutral stratified atmospheric boundary layer flow. *Journal of Wind Engineering and Industrial Aerodynamics*, 230:105145

Schalau, S., Habib, A., and Michel, S. (2023). A modified k-epsilon turbulence model for heavy gas dispersion in built-up environment. *Atmosphere*, 14(1):161

Michel, S., Leitl, B., Harms, F., Schalau, S., Schalau, B., Plischka, H., Turnow, J., and Kornev, N. (2023). Störfallartige Ausbreitung von dichte-neutralen und schweren Gasen in komplexen Umgebungen. 10.25592/UHHFDM.11779

Contents

| | | |
|----------|--|-----------|
| 1 | Introduction | 1 |
| 1.1 | Motivation | 1 |
| 1.2 | Contribution of this Thesis | 3 |
| 1.2.1 | Structure of the Thesis | 4 |
| 2 | Heavy Gas Dispersion Experiments in the Past | 5 |
| 3 | Theoretical Background | 13 |
| 3.1 | Turbulence Theory | 13 |
| 3.1.1 | Reynolds Number Independence | 14 |
| 3.2 | Atmospheric Boundary Layer | 15 |
| 3.2.1 | Physical Modelling of the Atmospheric Boundary Layer | 16 |
| 3.3 | Physical Modelling of Neutral Density and Heavy Gas Dispersion | 17 |
| 3.3.1 | Idealized Heavy Gas Dispersion | 18 |
| 3.3.2 | Dimensional Analysis of Continuous Release Scenarios | 20 |
| 4 | Experimental Setup | 23 |
| 4.1 | Boundary Layer Wind Tunnel WOTAN | 23 |
| 4.2 | Measurement Techniques | 24 |
| 4.3 | Model configurations | 26 |
| 4.3.1 | Area Source in a Horizontally Homogenous Rough Boundary Layer | 27 |
| 4.3.2 | Idealized Industrial Park | 27 |
| 4.3.3 | Industrial Chemical Park | 29 |
| 4.3.4 | Source Design | 31 |
| 4.4 | Modelled Wind Tunnel Boundary Layer Flows | 32 |
| 4.4.1 | Boundary Layer Development | 33 |
| 4.4.2 | Moderate Rough Boundary Layer | 35 |
| 4.4.3 | Rough Boundary Layer | 43 |
| 5 | Technical and Modelling Aspects | 49 |
| 5.1 | Froude Number | 49 |
| 5.2 | Selection of the Boundary Layer Flow | 52 |
| 5.3 | Development of the Dispersion Scenarios | 53 |
| 5.4 | Measurement Locations | 54 |
| 5.5 | Achieving a Heavy Gas Effect | 54 |

| | | |
|----------|---|------------|
| 6 | Research Questions | 59 |
| 6.1 | Influence of the Boundary Layer Inflow on the Gas Dispersion | 59 |
| 6.1.1 | Influence of a Boundary Layer Change on the Flow | 59 |
| 6.1.2 | Influence of a Boundary Layer Change on the Neutral Density Gas Dispersion . . . | 63 |
| 6.1.3 | Influence of a Boundary Layer Change on the Heavy Gas Dispersion | 66 |
| 6.2 | Statistical Characterization of Measured Concentration | 68 |
| 6.2.1 | Issues with the Arithmetic Mean | 68 |
| 6.2.2 | Suitable Statistical Measures for the Analysis of Gas Dispersion | 70 |
| 6.3 | Local Concentration Statistics | 72 |
| 6.4 | Influence of Individual Roughness Elements on the Flow and the Gas Dispersion | 82 |
| 6.4.1 | Influence of Individual Roughness Elements on the Flow | 82 |
| 6.4.2 | Influence of Individual Roughness Elements on the Gas Dispersion | 87 |
| 7 | Conclusion | 89 |
| 7.1 | Outlook | 92 |
| | Appendices | 93 |
| | Appendix A Quality Assurance | 95 |
| A.1 | Quality Assurance of the Boundary Layers | 95 |
| | Appendix B Boundary Layer Setup | 99 |
| | Appendix C Additional Measurement Results | 103 |
| C.1 | Measurement results: Model 1 | 103 |
| C.2 | Measurement results: Model 2 | 106 |
| C.3 | Measurement results: Model 3 | 108 |
| | Appendix D Measurement results: Area Source without Obstacles Model | 111 |
| | Appendix E Measurement results: Industrial Chemical Park Model | 113 |
| | References | 116 |

Acronyms

| | |
|-----------------------|--|
| ABL | Atmospheric Boundary Layer |
| BAM | Bundesanstalt für Materialforschung und -prüfung |
| CFD | computational fluid dynamics |
| CO₂ | carbon dioxide |
| FID | Flame Ionization Detector |
| LDA | Laser Doppler Anemometry |
| LES | large eddy simulation |
| LFL | lower flammability limit |
| LH₂ | Liquid Hydrogen |
| LNG | liquefied natural gas |
| LPG | Liquefied Petroleum Gas |
| MIC | Methyl Isocyanate |
| MODITIC | 'Modelling the Dispersion of Toxic Industrial Chemicals in Urban Environments' |
| MOST | Monin–Obukhov similarity theory |
| MRBL | moderate rough boundary layer |
| PDF | probability density function |
| PERF | Petroleum Environmental Research Forum |
| RANS | Reynolds-averaged Navier–Stokes |
| RBL | rough boundary layer |
| RPT | Rapid Phase Transitions |
| SF₆ | sulphur hexafluoride |
| TCDD | Tetrachlorodibenzodioxin |
| TICs | toxic industrial chemicals |
| UBL | Urban Boundary Layer |
| UCL | Urban Canopy Layer |
| USA | Ultra Sonic Anemometer |
| VDI | Verein Deutscher Ingenieure |
| WSWD | wind speed and wind direction |

Chapter 1

Introduction

Many toxic or flammable gases are heavier than air due to their high molar mass and/or their low temperature resulting from an accidental release from a pressurized state. During transport or storage gases are often pressure liquefied and kept at very low temperatures. Due to the higher weight of heavy gases, compared to air, their dispersion is effected by buoyancy. When a heavy gas is released into the atmosphere it experiences gravity-induced slumping and initially moves towards or along the ground. The buoyancy forces acting on the heavy gas reduce the influence of advection and turbulent mixing with the surrounding air is reduced due to the density jump at the interface between the gas cloud and the surrounding air (Meroney, 1982 and Britter and McQuiad, 1988).

With growing distance from the source more and more surrounding air is entrained into the heavy gas cloud and the density difference is reduced until the released gas is completely mixed into the air. This entrainment process depends on a multitude of parameters, where the dominating factors are the amount of the released material, the density excess of the released gas, the mean wind speed, the dimension of the source and the surrounding obstacles (Britter and McQuiad, 1988).

1.1 Motivation

Accidental releases of hazardous materials in factories or during transport to the atmosphere pose a serious danger to the general population and the environment. Especially in cases of releases of flammable or toxic industrial chemicals (TICs) major safety and health risks can emerge. In most cases these types of gases have a higher density than air, which further increases the danger of these releases.

In the 1970s an interest grew in the dispersion of heavy gases in the atmosphere. The growing interest was motivated by the rise of the liquefied natural gas (LNG) industry, its associated risks (Hardee et al., 1978, Philipson, 1978 and Fay, 1980) and major accidents in Staten Island, USA (1973), Flixborough, England (1974) and Seveso, Italy (1976) (Havens, 1992).

Probably the worst accidental release of a heavy gas occurred in Bhopal, India in 1984. Here, more than 40 tons of Methyl Isocyanate (MIC) was released from a pesticide plant (Broughton, 2005). The MIC cloud likely contained chloroform, dichloromethane, hydrogen chloride, carbon dioxide and other methyl compounds (D'Silva, 2006). Furthermore the cloud most likely contained liquid or solid aerosols, which further increased the density of the MIC cloud. Havens et al. (2012) estimated the initial density of the MIC cloud aerosol mixture to be greater than 4.3 kg/m^3 . The high density of the cloud and the low ambient wind speed led to a dispersion of the gas cloud close to the ground. This led to high concentrations of MIC in the surrounding area of the pesticide plant.

MIC is extremely toxic, NRC (2007) lists health exposure limits for an exposure of one hour at 0.067 ppm which result in irreversible damage. Life-threatening health effects or death can be experienced at an exposure of just 0.025 ppm for eight hours. This toxic MIC cloud moved through the dense inhabited area at night, without any warning for the mostly sleeping population. Due to the lack of warning people fled from the relative safety of their homes and inhaled the toxic gases. Children and small people were exposed to higher concentrations due to the higher concentration of the heavy and toxic gas near the ground. Havens et al. (2012) estimated MIC concentrations above 1000 ppm downwind of the pesticide plant.

The effects on the people living in the vicinity of the plant were devastating. Broughton (2005) lists 3,800 immediate deaths, with 15,000 to 20,000 premature deaths in the following two decades. More than half a million people were exposed to the toxic gas and injured.

Another hazard risk is the handling of LNG. LNG is mostly transported by large gas carrier vessels and unloaded at specified LNG-terminals. Due to the Russian invasion of Ukraine in 2022 and the resulting economic embargoes against Russia, Germany started investing into several LNG-terminals in cities on its North and Baltic sea coast (NDR, 2022).

During the approach to the harbour and the terminal and the transfer of the LNG the highest risks are present (Fay, 1980). The largest carrier ships have a capacity of more than 250,000 m³ (Ulvestad and Overland, 2012). In the worst case a total spillage of the LNG must be assumed. Due to the high heat capacity of the water the LNG would evaporate in a very short time and increase its volume 600-fold (Hardee et al., 1978 and Fay, 1980).

Due to the low boiling temperature of LNG and the resulting high density of the gas the dispersion of the gas cloud will be near the ground until it has been sufficiently warmed by the water and air and is entrained into the surrounding air. Early mathematical models from the 1970s for instantaneous LNG spills of 25,000 m³ on water showed lower flammability distances of several kilometres (Havens, 1977).

Similar risks apply to the usage of Liquid Hydrogen (LH₂). LH₂ is a potential zero-emission fuel that can play an essential role in reaching global emission goals set by the Paris agreement. A spill of LH₂ is very similar to a spill of LNG and poses a significant fire and explosion hazard for the surrounding area. Due to the very low boiling temperature the freshly evaporated H₂ will also initially disperse as a heavy gas (Odsæter et al., 2021).

Another severe accident occurred in Seveso, which resulted in a release of various toxic materials including 2,3,7,8-Tetrachlorodibenzodioxin (TCDD), Trichlorophenol and Tetrachlorobenzene, over an area of approximately 1700 ha. Thousands of people were potentially exposed to dioxin, 193 cases of chloracne and an increased cardiovascular mortality resulted from the accidental release (Bertazzi, 1991).

Since the 1970s and 1980s major advances in the safe handling of hazardous materials have been achieved. An example is the Seveso-III Directive (EU, 2012) of the European Union which aims to control major chemical accident hazards.

These examples of accidental releases of TICs and potential risks of pressurized gases show the importance of an in-depth understanding of the processes involved in the dispersion of heavy gases. Due to the higher density of heavy gases the dispersion process is initially close to the ground, which increases the danger to humans. Most historic major field and wind tunnel heavy gas dispersion measurement campaigns were performed without obstacles or only investigate dispersions in simple obstacle configurations. Data for heavy gas releases in complex environments is still rare and presents

a knowledge gap. With the continuing advances in the development of large eddy simulation (LES) models and the further increasing availability of computational power, LES models are starting to enter the domain of the computational modelling of heavy gas dispersion. Today in practise mostly box models, Gaussian plume models, shallow layer models (SLAB) or empirical models are used for heavy gas dispersion modelling. However, most of these models are not able to account for complex geometries or topography and major knowledge gaps still persist (Hanna et al., 2021). This modelling gap could be bridged by using more sophisticated computational fluid dynamics (CFD) models, like for example Reynolds-averaged Navier–Stokes (RANS) or LES models, which are able to resolve flows around complex structures. Furthermore, high qualitative, time resolved reference data to verify dispersion models for heavy gas dispersion scenarios in complex environments is still lacking. This knowledge gap is tackled in this thesis.

1.2 Contribution of this Thesis

This thesis presents flow, neutral density and heavy gas dispersion measurements performed in three model configurations with increasing complexity. Measurements are performed in a very idealistic model geometry, which just consists of a large area source flush with the ground without obstacles, sections of an idealized industrial park and a complex industrial chemical park. Focus of the measurements and the analysis are near the surface up to a height of 2 m.

The heavy gas dispersion feasibility study is approached by first addressing the modelling and technical aspects of performing heavy gas dispersions in a boundary layer wind tunnel. Suitable atmospheric boundary layer flows similar to nature and with a large geometric scale are generated and tested. Model geometries that are suitable to represent specific dispersion scenarios or are aimed at answering research questions are planned and constructed. Furthermore, the dispersion scenarios are carefully planned to achieve a substantial heavy gas effect and to successfully model heavy gas dispersions.

The following research questions are discussed and answered:

1. *What is the influence of a change of the boundary layer flow on the flow and the dispersion of a neutral density and heavy gas inside a build up model area?* Two different boundary layer inflows are used to investigate the influence of the atmospheric boundary layer on the dispersion of a neutral density and heavy gas dispersion inside the idealized industrial model.

2. *How can heavy gas dispersions be evaluated statistically? Is the arithmetic mean an adequate statistical measure for heavy gas dispersions?* Most past and recent investigations of either field measurements or numerical modellings of gas dispersions often use the mean concentration to determine the risk of gas dispersions. However the arithmetic mean lacks a critical view on instantaneous concentrations, which are important in case of a release of flammable materials.

3. *Is it possible to characterise model regions by the local concentration distribution and distinguish different regions in regards to a potential heavy gas effect? Is there a measure to discern areas with direct heavy gas influence and without?* A heavy gas dispersion behaves differently to a neutral density gas dispersion. It can be assumed that this is also visible in the local concentration distribution. This

change in the local concentration distribution might be a possible way to find regions in the dispersion area where a heavy gas effect is apparent and find regions with a higher risk.

4. *What is the influence of individual roughness elements on the flow and the heavy gas dispersion?*

The dispersion of heavy gas clouds in a horizontal homogenous rough wind tunnel boundary layer is potentially subjected to the influence of singular roughness elements, which might perturb the flow and increase the entrainment of fresh air into the heavy gas cloud. A release scenario of a heavy gas release in a homogenous rough boundary layer is investigated with and without individual roughness elements in the heavy gas cloud. Furthermore, flow measurements are performed to investigate the effect of the absence of roughness elements on the flow.

1.2.1 Structure of the Thesis

After introducing and motivating the research work and posing relevant research questions in this chapter, the following chapter following Chapter 2 gives an insight into the history of heavy gas dispersion experiments. The aspects and findings of various major field and wind tunnel campaigns of heavy gas dispersions are presented and discussed. Shortcomings and technical drawbacks are also listed and addressed shortly. In Chapter 3 the theoretical background for turbulence theory, the atmospheric boundary layer and an insight into the physical modelling of heavy gas releases are given. Chapter 4 presents the experimental setup, including the model geometries, measurement techniques as well as the boundary layer wind tunnel. The used boundary layer flows are also presented and discussed. An analysis of the technical and modelling aspects, as well as the assessment of the research questions follow in the Chapters 5 and 6, respectively. A summary of the key findings and a brief outlook are given in Chapter 7.

Chapter 2

Heavy Gas Dispersion Experiments in the Past

As described in Section 1.1 the need for a better understanding of the physics of heavy gas dispersion was driven by the increasing use and transport of LNG and public health concerns due to large accidents (Meroney and Neff, 1979 and Havens, 1992). The following description and listing of the heavy gas dispersion experiments in the past is most certainly not complete but covers most of the major and impactful heavy gas field studies and wind tunnel experiments of the past.

China Lake

One of the first major heavy gas dispersion field campaigns was performed at the Naval Weapons Center, China Lake, California by the U.S. Coast Guard in the 1970s (Schneider et al., 1980). The main motivation of the China Lake test trials was to study the behaviour of LNG and other flammable, liquefied gases in aspects of marine safety. An emphasis was put on spills of LNG and Liquefied Petroleum Gas (LPG) on water. After several tests vapour cloud detonation was ruled out as a likely outcome of ship collisions. So the focus shifted to pool and cloud fires, the flame size and their thermal emissive power.

Another major aspect of the field trials were four vapour dispersion tests. These tests were, apart of the lack of an intentional ignition of the cloud, identical to the previous vapour cloud fire tests and were aimed at investigating the dispersion of the gas (Department of Energy, 1979). Several different types of sensors were tested to measure the extent and concentration of the vapour cloud.

These early measurements were very valuable for planning and designing future field tests and also gave insights into the potential dangers of LNG spills. Some major findings were: without high energy initiators no high flame speeds or overpressure occurred and fireball burnings and detonations are not very likely to occur in case of LNG spills. However, due to several constraints like the limited amount of tests (four), the strongly varying wind speed ($U_{2m} = 6.7 \text{ m/s}$, 5.1 m/s , 12.4 m/s and 4.9 m/s), the varying wind direction (214° , 260° , 256° and 224°) and no data about the boil-off rates, i.e. the source flow rate, no general information on the dispersion process or general safety distances can be deducted from the measurement data (Meroney and Neff, 1979). Furthermore only sparse or coarse information about the meteorological variables and local terrain (e.g. the roughness length) are available (Meroney and Neff, 1977). Nonetheless, Meroney and Neff (1977) determined distances of over 150 m over open desert terrain where measured concentrations remained above the lower flammability limit (LFL) of methane.

The China Lake field tests were accompanied by wind tunnel dispersion tests performed at Colorado State University (Meroney and Neff, 1979). Two models of the China Lake topography with a scale of 1:85 and 1:170 were used for dispersion experiments. Since no profile measurements for the field measurements were available only very raw approximations of the local boundary layer flow were possible (Meroney and Neff, 1982). For the roughness length z_0 a range from 0.01 m to 0.15 m is given which is expected above rural areas (Counihan, 1975). The model values in the wind tunnel model uses a roughness length of 0.017 m, which is at the lower end of the rural area range. Other unknown boundary layer parameters were approximated as well and then matched in the wind tunnel model. The approximated and known parameters of the full-scale source were scaled down by matching the Froude number and then realised inside the wind tunnel.

Meroney and Neff (1982) found that the results from the wind tunnel measurements and the field measurements generally fit quite poorly. The values from the field and wind tunnel range over several orders of magnitude. Meroney and Neff (1982) attribute these large differences to several factors: Errors, shifts and fluctuations in the determined mean wind directions ($\pm 50^\circ$) in the field; changes in the wind speed (± 1.8 m/s); issues with the sensors, peak fluctuations too rapid and peak concentrations too large for the sensors.

However, with multiple plume-release replications Meroney and Neff (1982) were able to reproduce peak concentrations within a small range ($\pm 5\%$). Regarding ignition risks the peak concentration is of major importance, since the flammability depends on the instantaneous concentrations.

Disregarding the issues of the inaccurate field measurements, insufficient number of field data points and mostly unknown boundary conditions when the wind field conditions were nearly stationary the resulting dispersion structure was well reproduced by the wind tunnel model. Furthermore, measurements at both scales produced similar concentration variations when scaled by the densimetric Froude number (Meroney and Neff, 1982). This proved the general concept of the field study and wind tunnel comparison. Two heavy gas dispersion campaigns 'Burro' and 'Coyote' of the US Department of Energy followed the previous field tests in the subsequent years at China Lake (Koopman et al., 1982 and Havens, 1992).

Thorney Island

From 1982 - 1984 one of the most influential field campaigns, the Thorney Island trials, were performed. The trials were separated into three phases. In phase one 15 instantaneous releases of 1320 m^3 - 2100 m^3 of Freon-12 were performed. The targets of phase one were to generate measurement data of heavy gas releases to verify heavy gas dispersion models and to investigate the turbulence spectra inside and outside of the heavy gas cloud. Furthermore, scaling factors for the dispersion should be determined. In phase two 10 instantaneous releases of similar sizes (1400 m^3 - 2050 m^3) were performed. However, in phase two the dispersion area was not devoid of obstacles. To investigate the influence of simple obstacles on the dispersion of the heavy gas cloud, three different kind of obstacles were placed in the vicinity of the source. The impact of a fence, a permeable fence and buildings were investigated. In phase three three continuous releases of Freon-12 (approximately $4.2 \text{ m}^3/\text{s}$) were investigated (McQuaid et al., 1985).

Meteorological boundary conditions are well documented for the different Thorney Island trials. The wind speed and wind direction were measured at multiple locations close to the ground and in

different heights above ground. This allows for a much clearer picture of the changes and fluctuations of the wind during the releases. Further wind measurements were also performed inside and outside of the gas plumes. The atmospheric stability is determined from observation, solar radiation, the vertical temperature gradient, standard deviation of the horizontal wind direction fluctuations and Richardson number. Stability during the three trials ranged from neutral to moderately stable (Pasquill, 1961).

The measurement data from the Thorney Island trials has been used to verify numerous wind tunnel dispersion measurement campaigns (Hall and Waters, 1985, van Heugten and Duijm, 1985 & König-Langlo and Schatzmann, 1991) or CFD models (Batt et al., 2016) in the last 40 years. More focus will be put on the work of König-Langlo (1987) and König-Langlo and Schatzmann (1991).

König-Langlo (1987) repeated several heavy gas releases of the Thorney Island gas dispersion experiments by releasing sulphur hexafluoride (SF_6) in a boundary layer wind tunnel of the University of Hamburg. Thermodynamic effects as well as changes in the terrain and atmospheric stability were neglected. All similarity parameters except the Reynolds number were matched. The Thorney Island boundary layer conditions were not modelled. Within the variability of the field measurements, which are subject to meteorological variability, the wind tunnel measurements well repeated the results of the field measurements. In one setup with a relatively low density excess it was found that the heavy gas cloud inside the wind tunnel moves too slow compared to the field measurements. This has also been found by Meroney (1982).

König-Langlo (1987) also performed experiments of systematic continuous releases in the wind tunnel without obstacles and was able to calculate maximum LFL as a function of release rate and density of the released heavy gas. The maximum LFLs derived from wind tunnel measurements well agree with data from field measurements of the TÜV Norddeutschland (Heinrich and Gerhold, 1986) and Maplin Sands (Hirst and Eyre, 1983). Furthermore in case of an instantaneous release a change in the density excess of the heavy gas only marginally affects local peak concentrations. However, the cloud speed, arrival and departure time are not independent of the density excess.

In case of continuous releases in open terrain the effect of a decreased excess density leads to higher concentrations (König-Langlo, 1987). This means that in most cases at measurement points with the same dimensionless distance to the source the measured concentrations are independent of the initial density. Measurements points close to the source, however, show a dependency on the density.

König-Langlo (1987) also systematically investigated the influence of the reference wind speed on the maximum LFLs. In case of low wind speeds, the transport of the gas cloud is not well supported by advection and relies on gravity induced movement. This leads to low LFLs. With an increasing wind speed the advection of the gas cloud is stronger and the LFLs increase in lee of the source. At even higher wind speeds, the gravity influence grows smaller and advection dominates. The higher wind speed leads to higher turbulent mixing and the lower flammability limits decrease again. This means that larger releases have their maximum lower flammability limits at higher wind speeds than smaller releases.

In the wind tunnel measurement campaign of König-Langlo (1987) heavy gas releases were also performed in simple geometries like fences, street canyons or street crossings. The results and findings of König-Langlo (1987) are very valuable and resulted in a Verein Deutscher Ingenieure (VDI) guideline (VDI, 1990) which defines a standardized and verified calculation method heavy gas dispersion scenarios.

Kit Fox

In 1995, the Kit Fox dense gas field experiment was carried out in Nevada, USA. The Kit Fox dense gas experiment was part of the Petroleum Environmental Research Forum (PERF) atmospheric dispersion modelling study (Hanna and Steinberg, 2001). Wind tunnel experiments precluding and accompanying the Kit Fox experiments were also part of PERF project. The wind tunnel studies investigated the efficient design of roughness elements, how to represent an industrial site with roughness elements and how dense gas plumes are entrained in neutral and stable atmospheric conditions (Snyder, 1995, Petersen and Cochran, 1995, Briggs et al., 2001 and Robins et al., 2001).

The main goal of the Kit Fox dense gas field experiment was to investigate the effect of a relatively large roughness typical of industrial process plants on dense gas clouds (Hanna and Chang, 2001). During the field campaign 52 short-duration carbon dioxide (CO₂) gas releases were performed over a rough surface in neutral to stable atmospheric conditions. Two kinds of releases were realised, continuous releases with release times of two to seven minutes and short transient puffs with release times of 20 seconds. To simulate the effect of an industrial process plant thousands of flat plywood billboards with two different sizes were installed. In the inner part (approximately 40 m by 85 m) of the measurement area large 2.4 m square elements were installed and smaller elements (0.2 m high and 0.8 m wide) in the outer parts (approximately 100 m by 300 m). With this an industrial environment with a scale of 1/10 was artificially modelled. Wind profile measurements suggest that the artificially introduced roughness elements increased the roughness length of the desert from 0.0002 m to 0.12 - 0.24 m in the inner part of the measurement area. The atmospheric boundary conditions were monitored at five different heights and positions. The CO₂ concentrations were measured with a frequency of 1 Hz at 84 positions.

The Kit Fox measurement data is used for the verification and comparison of dispersion models, e.g. the HEGADAS 3+ model (Hanna and Chang, 2001). The data is very valuable for a better understanding of the increased entrainment due to the higher turbulence of the enhanced roughness and the impact of the increased entrainment on the cloud height and peak near-ground concentrations. However, it is disputable that the representation of the industrial environment is realistic. The model of idealistic roughness elements only aims to recreate the effect on the boundary layer and the flow, but lacks the aspects of a real industrial environment. In a real industrial environment buildings could potentially completely block the flow or channel it into a single street canyon. Depressions in the ground or small dikes which are very common in industrial environments may have severe impacts on the dispersion of a heavy gas cloud and influence hazard ranges.

Jack Rabbit

Motivated by three major chlorine accidents, where 30 to 60 tons were released from railcars, two major field measurement campaigns, Jack Rabbit 1 and 2, were performed at Dugway Proving Ground in Utah, USA (Fox, 2011 and Nicholson et al., 2017). In the Jack Rabbit 1 field experiments one and two tons of chlorine and anhydrous ammonia were released in 10 individual releases (5 for each material). The target of Jack Rabbit 1 was to develop, test and evaluate the physiochemical characteristics of a disseminated gas and aerosol cloud. Jack Rabbit 1 was also aimed to evaluate instruments, test methods and strategies for subsequent industrial-scale releases (Fox, 2011). The meteorological boundary conditions were observed by an extensive network of instruments with several profile measurements of

the local atmospheric boundary layer. Concentration measurements were performed up to a distance of 2.5 km from the source and at heights of 1 m, 3 m and 6 m above ground. The Chlorine releases of Jack Rabbit 1 are described below as an example.

The chlorine release trials were mostly performed at low mean wind speeds between 0.6 m/s and 1.6 m/s (2 m measurement height), with one outlier release with a mean wind speed of 6.2 m/s. The release site was located in a circular 50 m wide and 2 m deep depression. The observed mass release rate is in the range of 30 kg/s to 40 kg/s. With this the release durations are estimated to be approximately 23 seconds for the one ton releases and 60 seconds for the two ton releases. After the main release a short second phase with a reduced release rate was observed.

For the low wind speed releases the chlorine cloud persisted in the depression for 30 to 60 minutes after the release was stopped and was only slowly entrained into the flow above the depression. At 6.2 m/s mean wind speed the gas cloud had no significant persistence in the depression and was quickly advected. The release at the lowest mean wind speed case did not result in the highest peak concentrations downwind because of the reduction of the downwind transport and turbulent mixing due to the persistent dense gas cloud. Furthermore, Rapid Phase Transitions (RPT) eruptions were observed which present an additional chlorine spill hazard. Another finding was that source phenomena are nonlinear with increasing release volumes.

Jack Rabbit 2 expanded the Jack Rabbit 1 trials with larger scale releases. In phase I up to nine tons of chlorine releases were performed, in phase II up to 20 tons were released in nine trials (Fig. 2.1). The aim of Jack Rabbit 2 was to fill critical knowledge gaps in regards to RPT, mitigation strategies for the public, upwind transport and to improve the understanding of large-scale release scenarios (Nicholson et al., 2017). Jack Rabbit 1 and 2 also aimed to create reference data for dense gas releases for dispersion model verification.



Figure 2.1: Chlorine release during the Jack Rabbit II trials. Image courtesy: Tom Spicer (Spicer and Smith, 2021).

While Jack Rabbit 1 was a release without any surrounding obstacles except for the release into a depression, Jack Rabbit 2 aimed to investigate the impact of a mock urban environment on the heavy gas dispersion. For this dozens of CONEX containers with a height of 2.44 m were placed in 13 rows around the release site.

Jack Rabbit 1 and 2 provide a very extensive data set with a multitude of data regarding the dense gas releases ranging from instantaneous concentration measurements over dosage measurements,

stationary video footage and drone footage, in-depth measurements of the meteorological state of the atmosphere, investigations of damage due to chlorine inside buildings and cars and much more.

The atmospheric boundary conditions were monitored in great detail at several locations and with three profile measurements. Flow measurements inside the mock urban environment were also performed but not during the chlorine releases.

MODITIC

From 2012 to 2016 the 'Modelling the Dispersion of Toxic Industrial Chemicals in Urban Environments' (MODITIC)-project systematically investigated the release and transport of neutral density and heavy gases in complex urban environments (Robins et al., 2016). Its aim was to improve the understanding of the dominating physical processes involved and further improve current modelling techniques. The MODITIC-project also involved numerical simulations, experiments on chemical reactivity and environmental impact but only the wind tunnel dispersion experiments will be referred in the following.

The wind tunnel experiments were performed in the EnFlo boundary layer wind tunnel at the University of Surrey, UK. The EnFlo wind tunnel was specifically designed to simulate flow and dispersion processes in the atmospheric boundary layer, in particular in dispersion scenarios where density differences play a major role. The wind tunnel has the ability to heat and cool the flow and the tunnel surfaces and operate at low wind speeds ranging between 0.3 m/s and 3 m/s (Robins et al., 2016).

In the MODITIC-project six dispersion scenarios with increasing complexity ranging from a flat surface over a two-dimensional hill, a simple array of obstacles to an urban area (inner part of Paris) were performed. Focus of this description will be put on the results from the Paris model. Released gases are CO₂, air and mixtures of both with propane as a tracer. Inflow boundary layer conditions are presented but are not compared or checked with a reference like VDI (2000). The regions where the dispersion was studied were generally left free of obstacles and additional surface roughness.

For the most complex model the central area of Paris was constructed with a scale of 1:350. The model consisted out of almost 100 flat roofed blocks. The building heights ranged from 10 mm to over 100 mm in model-scale. Releases were performed with air, an air/CO₂ mixture and CO₂ and three associated inflow directions. The source diameter was 0.1 m. Furthermore, a wide range of emission rates of air (300 l/h to 3000 l/h), air/CO₂ mixtures with varying mixing ratios (240 l/h to 3000 l/h) and CO₂ (60 l/h to 3000 l/h) were released at varying reference wind speeds ranging from 0.8 m/s to 2 m/s, whereas the majority of measurements was performed at a reference wind speed of 1 m/s. The different variations of density, flow rates, wind directions create a sizeable data set. Concentrations measurements were mostly taken at street level at a full-scale height of 3.5 m, complemented with several lateral and vertical profiles. Short term releases, i.e. puff releases, were also simulated and measured.

Special focus was put into the 3000 l/h release scenario, where a very strong dense gas effect was found. The CO₂ gas plume was almost confined within the street canyons. Furthermore, a significant upstream and lateral spread was observed. The observed CO₂ plume was found to be much shallower than the air plume (Robins et al., 2016).

The very high model-scale release rates of 3000 l/h beg the question if the release scenario is still realistic in full-scale. By scaling the release scenario up with the geometric scale of 1:350 and conserving the densimetric Froude number the full-scale scenario has a release rate of approximately 2000 m³/s.

Such a release is unrealistic and bears no semblance to any real world accidents. This is also shortly discussed by the experimenters of Robins et al. (2016).

Over the last 40 to 50 year major advances in the modelling and measuring of heavy gas dispersions have been made. It was proven that heavy gas dispersions in boundary layer wind tunnels are able to accurately model full-scale heavy gas dispersions and can provide important reference data with quasi-stationary boundary conditions for the verification of dispersion models. Valuable insights and finding of the driving factors of heavy gas dispersion were confirmed with a combination of field experiments and wind tunnel measurement campaigns. Knowledge gaps, however, still exist and new generations of dispersion models need high quality reference data sets. Especially reference data for heavy gas dispersions in complex environments are still sparse. Hanna et al. (2021) state that the effects of terrain and large obstacles on the dispersion of TICs are still uncertain, since the majority of field experiments have been performed over flat terrain.

Chapter 3

Theoretical Background

In this section a brief introduction into turbulence theory, the fundamentals of atmospheric boundary layer flows and the physical modelling of heavy gas dispersion will be given. For a deeper insight the reader is referred to Tennekes and Lumley (1972), Snyder (1981) and Britter and McQuiad (1988).

3.1 Turbulence Theory

The following description of turbulence is inspired by Tennekes and Lumley (1972). Turbulence can be seen in almost all facets of life. Turbulent flows can be observed in the exhaust of a factory smoke stack or a car exhaust, in water currents in rivers and in the planetary boundary layer (unless very stable conditions occur) and in flows of liquids and gases in pipelines.

Although everyone has seen turbulence in many different forms, no exact and formal definition can be given. Some of the characteristics of turbulent flows Tennekes and Lumley (1972) list are:

Irregularity Turbulent flows are random and virtually unpredictable. To describe turbulent flows one has to rely on statistical methods.

Diffusivity Turbulence effectively mixes momentum and scalar quantities like temperature or mass within a fluid. Turbulent mixing is much bigger than molecular mixing.

Three-dimensionality Turbulent motion is rotational, three dimensional and highly variable in space and time. Turbulence is also characterized by strong variations of vorticity.

Dissipation Turbulent flows constantly lose energy to heat. Bigger eddies get broken up into smaller and smaller eddies until viscosity becomes dominant. Turbulence needs a constant supply of energy to stay turbulent. Without the turbulence dies and the flow ultimately relaminarizes.

Turbulence is a feature of the flow, not a feature of the fluid. If the Reynolds number of the turbulence is large enough, most dynamics of the turbulence is the same in all (near) Newtonian fluids, regardless if the fluid is a gas or a liquid. The characteristics of turbulence depend on the initial and boundary conditions and to a smaller degree on the molecular properties of the fluid. Flows always become turbulent at sufficiently high Reynolds numbers. The Reynolds number describes the ratio between inertial forces and viscous forces, acting in the fluid. It is defined as:

$$Re = \frac{\textit{inertial forces}}{\textit{viscous forces}} = \frac{U_{ref} \cdot L_{ref}}{\nu}, \quad (3.1)$$

where U_R and L_R are characteristic velocity and length scales of the flow and ν is the kinematic viscosity of the fluid.

3.1.1 Reynolds Number Independence

Townsend (1956) introduced the concept of Reynolds number similarity of fluid flows. "In absence of thermal and Coriolis effects and for a geometrically similar flow with nondimensionalized boundary conditions, the flow structure is similar at all sufficiently high Reynolds numbers." If the Reynolds number is sufficiently large most non-dimensional mean-value functions depend only on non-dimensional time and space variables and not on the Reynolds number (Snyder, 1981). There are however exceptions to this: if one is interested in the very small-scale structure to investigate viscous dissipation of energy or one investigates in very close proximity to walls where viscous effects become dominating (Snyder, 1981). An exact value where Reynolds numbers are 'sufficiently high' can not be given generally. It depends on several conditions, e.g. the overall model geometry, the roughness of the surfaces, the desired accuracy and the model fluid. Especially in case of flows around round-shaped structures Reynolds number independence at low wind speeds is difficult to achieve. At low wind speeds the position of the flow separation point of round-shaped structures can change with a change of the wind speed, which results in a change of the flow around and behind the structure. Reynolds number independence in the presence of obstacles is easier to achieve with structures with sharp edges due to the clear defined flow separation points.

A graphical representation of Reynolds number independence is illustrated in Fig. 3.1. Two turbulent jets with the same boundary and flow conditions except for a different viscosity, resulting in different Reynolds numbers, are depicted. As long as the flow remains turbulent the overall shape and rough structure does not change with a change of the Reynolds number, but the fine structure and smaller scales of the turbulence changes.



Figure 3.1: Exemplary illustration of two turbulent jets. The upper jet has a higher Reynolds number compared to the lower jet. The large scale structure does not change significantly as long as the jet is turbulent. Adapted and reproduced from Snyder (1981).

3.2 Atmospheric Boundary Layer

The Atmospheric Boundary Layer (ABL), also called the friction layer, is the lowest part of the troposphere where the atmospheric motion interacts with the earth's surface. The section intentionally gives a very brief introduction into an established and well documented ABL theory. For more in-depth information follow Snyder (1981), Oke (1988) and Stull (1988).

Processes in the ABL greatly differ from the processes in the free atmosphere above the ABL. In the free atmosphere the air motion, the geostrophic wind, is driven by a balance between the horizontal pressure gradient and the Coriolis force. In the ABL a considerable influence of the earth's surface can be observed. Depending on the latitude, altitude, season, time of day or weather, the depth of the boundary layer varies greatly. Under neutrally stratified conditions it generally ranges between approx. 0.5 km and 2 km. The ABL thickness is roughly 10% to 20% of the total troposphere height.

The ABL can be divided into several sublayers. The two most important and most commonly mentioned is the surface layer and mixed layer (Fig. 3.2a). The bottom 10% of the ABL is the surface

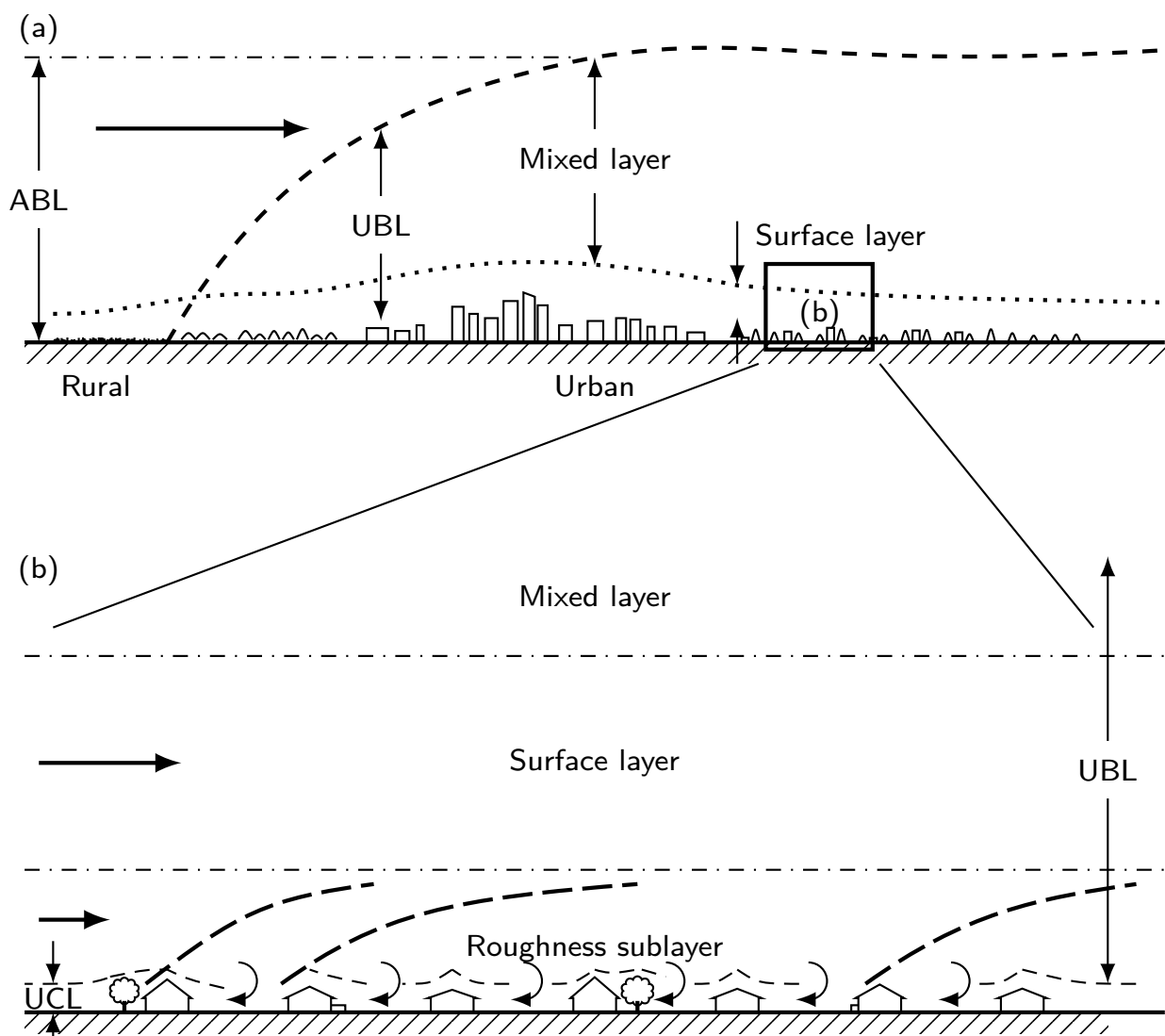


Figure 3.2: Idealized arrangement of boundary layer structures over a city (adapted after Oke, 1984)

layer. Here the direct interaction between the surface and the atmosphere takes place. The surface layer is characterised by a nearly constant level of turbulent fluxes and stress characterising exchange processes. Over the height of the mixed layer this shear stress value reduces to almost zero at the interface to the free atmosphere. The surface layer (Fig. 3.2b) contains the roughness sublayer and the viscous sublayer next to solid walls (not shown). In the presence of urban terrain, the ABL may also be called Urban Boundary Layer (UBL) and can contain an Urban Canopy Layer (UCL) (Oke, 1984) in the vicinity of dense urban terrain. The UCL extends from the surface to approximately the height of buildings. This sublayer is dominated by the influence of buildings and other flow obstacles and atmospheric motion in this layer can potentially be decoupled from the general motion in the ABL. The atmospheric motions in the roughness sublayer are still directly affected by obstacles.

Due to the diurnal cycle of surface heating and cooling the ABL changes throughout the day. Stull (1988) introduces components of the diurnal cycle of the boundary layer, the residual and the stable boundary layer, which form during the night. The residual layer is the remnant of the mixed layer, which does not interact with the surface and remains neutrally stratified. At night the layer which is in contact with the surface and subject to radiative cooling becomes the stable boundary layer. This layer is characterized by a thermally stable stratification and less and weaker turbulence. The previous definitions obviously describe an idealized version of the chaotic and constantly changing real-world atmosphere.

Due to different points of research of Snyder, 1981 (physical modelling), Oke, 1988 (urban climate and micrometeorology) and Stull, 1988 (atmospheric sciences) their definitions and subdivisions of the ABL differ corresponding to their focus on different aspects of the ABL.

3.2.1 Physical Modelling of the Atmospheric Boundary Layer

The main idea behind the physical modelling of the ABL is the geometric and physical downscaling of atmospheric processes to a size which can be modelled inside a boundary layer wind tunnel. This is mainly based on the concepts of physical similarity and Reynolds number independence (Section 3.1.1). In this section, only a brief introduction into the concept of physical modelling of ABL flows will be given. The derivation of the equations of motion and non-dimensional numbers are left out on purpose. For a more detailed approach one can follow most of the existing literature on environmental fluid dynamics or dedicated references such as the previously mentioned works of Snyder (1981) or Stull (1988).

Following Snyder (1972) the starting point for the similarity analysis are the equations for the conservation of momentum, continuity and energy. The equations of motion are nondimensionalized with appropriate reference quantities, which are defined by setting adequate boundary conditions. With this, the nondimensionalized equations of motion are in a form containing a set of dimensionless coefficients: the Rossby number Ro , the ratio of inertial forces to the Coriolis force; the densimetric Froude number Fr , the ratio of inertia to the buoyancy; the Reynolds number Re , the ratio of inertial forces to viscous forces and the Peclet number Pe , the ratio between advective and diffusive transport. Solutions to the nondimensionalized equations of motion will only be identical if the coefficients Ro , Fr , Re and Pe and the non-dimensional boundary conditions are identical.

With this, any atmospheric flow that can be described by the nondimensionalized equations, may also be modelled by any other flow which also can be described by the same set of equations and has the same non-dimensional boundary conditions.

According to Snyder (1972) achieving perfect physical similarity is not possible when the geometric scale between model and nature is greater than 10 because with this scale a matching of the Froude and Reynolds number becomes virtually impossible. Furthermore, in the physical modelling of ABL flows scales much greater than 10 are usually desired (Snyder, 1981). However, under certain circumstances some of the matching criteria might be relaxed or neglected. For example the Rossby number can be neglected when the modelled geometry has an horizontal extent less than 5 km (Snyder, 1981). In case the modelling of neutrally stratified and non-buoyant dispersion problems, the Froude number can be omitted. In turbulent flows turbulent mixing dominates over molecular mixing, so the matching of Peclet number is unimportant as long as the same fluid is used in the model and the prototype. Snyder (1981) states that the Peclet number may be neglected as a modelling criterion if the flow is Reynolds number independent.

All model geometries in this thesis were tested regarding the Reynolds number independence and all measurements were performed above the wind speed where Reynolds number independence was observed. The full-scale horizontal extent of the models is far smaller than the extent of 5 km Snyder (1981) stated. Because of this and the fully turbulent flows the matching of Rossby and Peclet number is not necessary for the experiments presented in this thesis and thus neglected. For the heavy gas dispersion experiments the Froude number had to be matched between the full-scale dispersion scenario and the wind tunnel experiment as close as possible.

3.3 Physical Modelling of Neutral Density and Heavy Gas Dispersion

The physical modelling of gas dispersion inside an atmospheric boundary layer is based on the same similarity principle as presented in Section 3.2.1. To physically model ABL processes inside a wind tunnel the geometry of the model area and the turbulent flow properties need to be scaled down to model scale. The descriptions in this section closely follow Schatzmann et al. (1986), König-Langlo (1987), VDI (1990) and Britter and McQuiad (1988).

In case of a dispersion of an inert gas with a density close to the density of the surrounding air (e.g. a neutral density dispersion) regarding the flow only the Reynolds number must be matched or the Reynolds number independence criterion must be fulfilled. The ratio of the momentum flux density of the source flow and the wind flow and the outlet Reynolds number must be equal between the model and full-scale (VDI, 2000). If these criteria are fulfilled, concentrations measurements made in the wind tunnel can be made dimensionless and scaled up to full-scale. The neutral density concentration measurements in this thesis are given as a dimensionless concentration c^* . The measured concentration is nondimensionalized with the following equation:

$$c^* = \frac{C \cdot U_{ref} \cdot L_{ref}^2}{q}, \quad (3.2)$$

where C is the measured volume concentration, U_{ref} is the reference wind speed in model, L_{ref} is the reference length and q is the source volume flow (VDI, 2000).

In case of a heavy gas dispersion, additionally the densimetric Froude number must be matched. The densimetric Froude number Fr_D describes the ratio between inertial and buoyancy forces and is

calculated with:

$$Fr_D = \frac{\text{inertial forces}}{\text{buoyancy forces}} = \frac{U_{ref}}{(\dot{V}_0 \cdot (g \cdot \frac{\rho_0 - \rho_a}{\rho_a})^2)^{\frac{1}{5}}}, \quad (3.3)$$

where U_{ref} is the reference wind speed, \dot{V}_0 is the source volume flow, g is gravity, ρ_0 is the density of the released heavy gas and ρ_a is the density of ambient air (VDI, 1990). In the event of a calm ($U_{ref} = 0$ and $Fr_D = 0$) any gas dispersion where $\rho_0 > \rho_a$ must be considered a heavy gas dispersion because the dispersion is entirely driven by the negative buoyancy forces. For values $Fr_D \gg 1$ a dispersion of a gas with a density greater than the ambient air behaves like a dispersion of a gas of neutral density. Whether a gas has to be treated as a heavy gas depends on the gas density, the release amount and the ambient wind speed. The range where a heavy gas release can be regarded as a neutral density gas released is reached between $2 < Fr_D < 10$ (VDI, 1990). Concentration measurements for the heavy gas dispersions are given in a relative concentration. The relative concentration is the ratio of the measured concentration and the initial concentration of the released gas. In contrast to measurements of dispersions of gas of neutral density, heavy gas dispersion measurements are not Reynolds number independent since they are for example influenced by a change in the reference wind speed.

3.3.1 Idealized Heavy Gas Dispersion

According to König-Langlo (1987) a heavy gas dispersion process can be divided into distinct phases where different physical forces dominate. An idealised instantaneous heavy gas release of a liquefied gas from a pressurized container is shown in Fig. 3.3. After König-Langlo (1987) an idealised heavy gas dispersion can be divided into five phases:

Storage A heavy gas is stored under pressure in a storage container (Fig. 3.3a). For this schematic it is assumed that the dense gas is stored as a liquefied gas and is thus heavily pressurized and potentially cold.

Ejection A containment breach causes the heavy gas to be released from the container (Fig. 3.3b). Due to lack of pressure the liquefied gas now undergoes a phase change by using the thermal energy of the air. Depending on the availability of thermal energy and the type of gas not necessarily all liquid is immediately turned into gas and a mixture of liquid aerosols and gas is released. This mixture has a much higher density than the dense gas alone (Britter et al., 2011). By changing the phase to a gaseous state the volume of the gas greatly increases. This happens in a very short time frame.

Buoyancy phase Due to the higher density of the cold dense gas the gas slumps down and congregates in a shallow layer near the ground (Fig. 3.3c). The internal flow caused by gravitation creates vortices near the front of the dense gas cloud. The movement of the dense gas cloud is fully dominated by the buoyancy effects of the higher density. For simplicity advection is ignored in this phase. In case of a neutral density gas, the gas would not experience any buoyancy effects and this phase would be skipped.

Intermediate phase With growing distance to the source and mixing through atmospheric turbulence the density of dense gas decreases over time and the buoyancy effects of the dense gas wane.

Gravity effects stop being dominant and the dispersion of the gas cloud is more influenced by the overall atmospheric motion. This phase is between Fig. 3.3c and d.

Advection phase Due to entrainment of air the density of the initially dense gas is now equalized with the atmosphere and no buoyancy effects are present (Fig. 3.3d). The dispersion of the gas is now behaving like a neutral density gas dispersion and the dispersion process is fully driven by atmospheric mixing and advection. This is usually called a passive dispersion scenario.

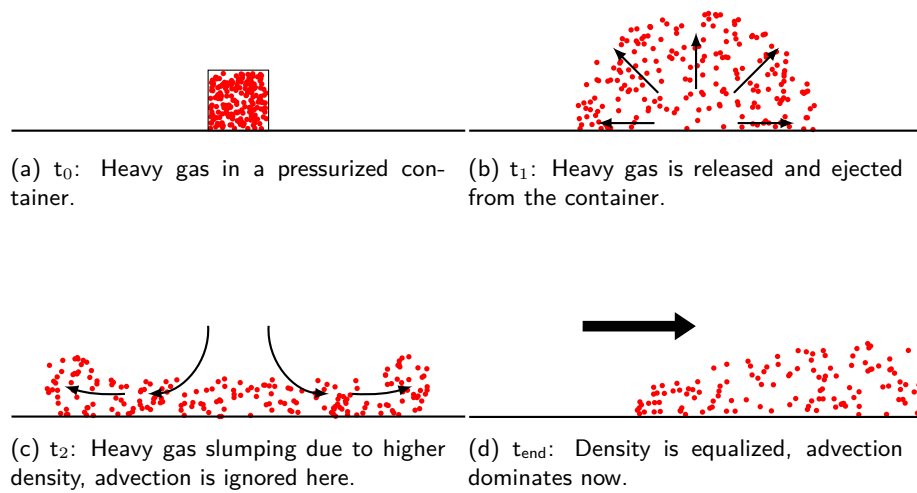


Figure 3.3: Schematic of an instantaneous heavy gas dispersion from a pressurized container.

Heavy gas dispersions can be separated into two general scenarios, depending on the release duration. Releases with a short or negligible release duration $t_r \rightarrow 0$, where the entire volume of a container is released, are called instantaneous releases. Instantaneous releases generally have a strong natural variability concerning both, the release and the subsequent dispersion process. To accurately describe such release scenarios several repetitions with quasi-stationary boundary conditions are needed. Instantaneous releases are for example caused by a hull breach of pressurized containers (Fig. 3.3). For more information on instantaneous releases follow König-Langlo and Schatzmann (1991).

The other type of release is the continuous release ($t_f \gg 0$). Here the release duration is long enough so that with quasi-stationary boundary conditions the concentration distribution in the vicinity of the release location is quasi-stationary as well. For continuous releases repetitive measurements are not needed to get a full picture of the dispersion process. However, measurements have to be long enough to show convergence and repetitive measurements are required to quantify the confidence interval of the measurement. Convergence of the measurements in this thesis was usually observed after three to five minutes of sampling (model-scale), depending on the reference wind speed. At similar wind speeds in full-scale this sampling time translates to 10 to 20 hours of sampling time. Continuous releases are usually caused by tank or pipeline leakages or ventilation of buildings. Since all dispersion experiments in this work were continuous releases the following theoretical background will focus on continuous releases as well.

3.3.2 Dimensional Analysis of Continuous Release Scenarios

The complex thermodynamic and chemical processes after the release of a heavy gas very close to the source are neglected. For the sake of the experiments it is assumed that the thermodynamic and chemical processes are already finished and the release can be characterised by a steady source volume flow \dot{V}_0 and an initial density ρ_0 .

The local relative dilution of released material $\chi = \Delta C / \Delta C_0$, where C is the local and C_0 initial concentration, is in the buoyancy and intermediate phase a function depending on the parameters shown in Eq. 3.4. By defining the initial concentration as 100%, χ can be called the local concentration.:

$$\chi = f_3(x, y, z, g, \rho_0, \mu_0, \dot{V}_0, z_R, \rho_a, \mu_a, \bar{u}_{aR}, \delta, l_1, \dots, l_n, \Theta). \quad (3.4)$$

The quantities x , y , and z are the local coordinates in reference to the coordinate system shown in Fig. 3.4. g is the acceleration due to gravity, ρ_0 and μ_0 are the initial density and viscosity of the released heavy gas. \dot{V}_0 is the source volume flow, z_R is the roughness length of the ground over where the cloud is spreading and u_{aR} is the reference wind speed at a reference height δ . The length scales l_1, \dots, l_n

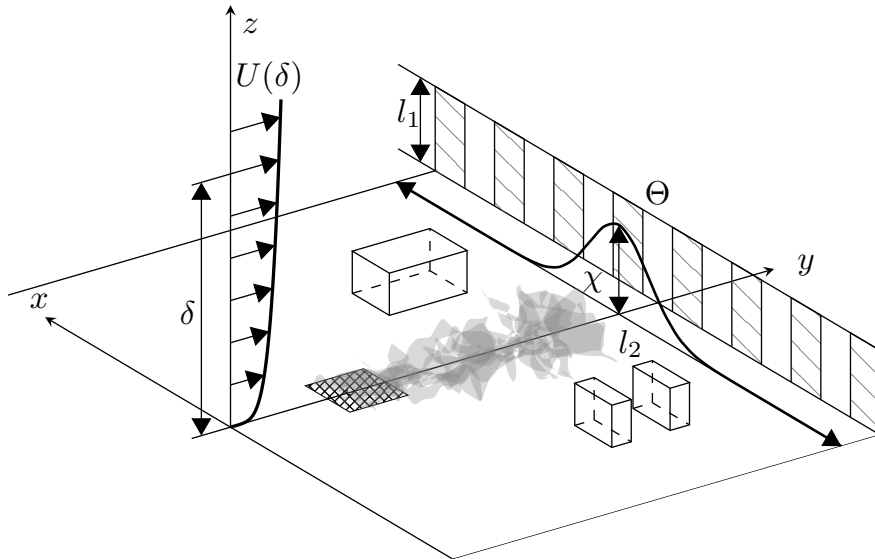


Figure 3.4: Sketch for a continuous heavy gas release. Created after König-Langlo (1987).

and the porosity Θ can be used to describe the geometry and potential obstacles in the dispersion area. In most cases of accidental releases the exact source conditions are unknown anyway, so an accurate description of the source like the source area or the exit velocity of the gas are only estimated and not considered separately.

By defining characteristic scales for a continuous release depending on the source volume flow and the weighted effective gravity $g' = g \frac{\rho_0 - \rho_a}{\rho_a}$ Eq. 3.4 can be transformed into a dimensionless form. According to König-Langlo (1987) the characteristic scales for length L_{cc} , time T_{cc} and speed U_{cc} are defined as following:

$$L_{cc} = \left(\frac{\dot{V}_0^2}{g'} \right)^{1/5} \quad T_{cc} = \left(\frac{\dot{V}_0}{g'^3} \right)^{1/5} \quad U_{cc} = (\dot{V}_0 g'^2)^{1/5} \quad (3.5)$$

By using the characteristic scales of Eq. 3.5 the dimensionless form of Eq. 3.4 loses three terms and becomes Eq. 3.6.

$$\chi = f_4\left(\frac{x}{L_{cc}}, \frac{y}{L_{cc}}, \frac{z}{L_{cc}}, \frac{\Delta\rho_0}{\rho_a}, \frac{L_{cc}U_{cc}}{\mu_0/\rho_0}, \frac{L_{cc}\bar{u}_{aR}}{\mu_a/\rho_a}, \frac{z_R}{L_{cc}}, \frac{\bar{u}_{aR}}{U_{cc}}, \frac{\delta}{L_{cc}}, \frac{l_1}{L_{cc}}, \dots, \frac{l_n}{L_{cc}}, \Theta\right) \quad (3.6)$$

In Eq. 3.6 no quantities that describe the individual problem are needed. Thus, the equation must be generally valid and is independent of the used scale. If all terms in Eq. 3.6 have the same values in nature and in the wind tunnel, the wind tunnel measurement results are directly transferable to full-scale.

Britter and McQuiad (1988) rank variables of a dense gas dispersion in regard of their impact on the dispersion. The most dominant independent variables are:

- a characteristic measure of the amount of released material, depending on the type of release, the total volume V_0 (instantaneous) or the source volume flow \dot{V}_0 (continuous)
- a characteristic density of the released material and the ambient density
- a characteristic mean cloud velocity
- a characteristic dimension of the source

Relevant variables which still have a significant impact on the dispersion, but are of lesser importance:

- the surface roughness
- the atmospheric stability
- the turbulent length scales in the atmospheric boundary layer
- the source geometry

Variables of little to no importance at full-scale:

- molecular properties as long as the Reynolds number is large (which is normally satisfied in full-scale)
- the scale of the atmospheric boundary layer

In this thesis the influence of a change of the source volume flow (Sec. 5.5), the boundary layer (Sec. 6.1), the reference wind speed (Sec. 6.3) and the surface roughness (Sec. 6.4) on the heavy gas dispersion is investigated.

Chapter 4

Experimental Setup

4.1 Boundary Layer Wind Tunnel WOTAN

The wind tunnel WOTAN is a closed test section, open-return boundary layer wind tunnel at the Environmental Wind Tunnel Laboratory of the University of Hamburg and is one of the largest boundary layer wind tunnel worldwide to model atmospheric boundary layer flows. WOTAN has a total length of 25 m and the closed test section has a size of 18 m length, 4 m width and a height of 2.75 m - 3.25 m (Fig. 4.1). The height of the test section can be adjusted to account for blockage effects of large models

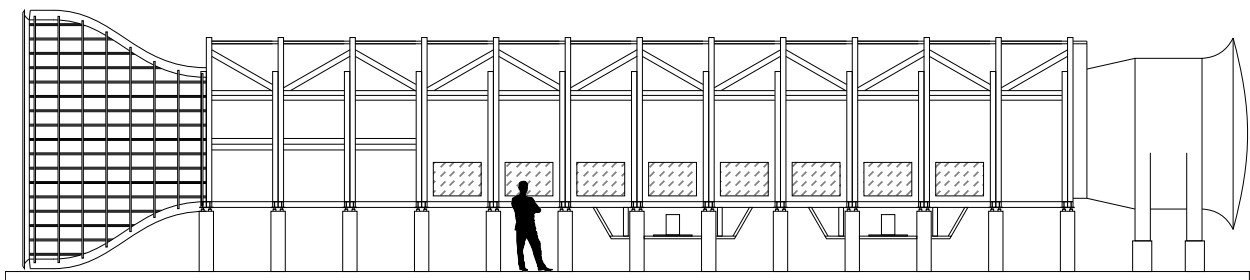


Figure 4.1: Sketch of the large boundary layer windtunnel facility WOTAN of the University of Hamburg.

inside the test section and minimize the longitudinal pressure gradient inside the wind tunnel. WOTAN is designed for modelling neutrally stratified flows. With the used setup the possible mean wind speeds at the top of the boundary layer range from 0.5 m/s to 20 m/s. Experiments in this thesis have been performed with mean wind speeds of approximately 1 m/s to 6 m/s.

Inside the test section two turn tables are installed in the floor of the wind tunnel. The turn tables allow the simulation of different inflow directions. At the end of the wind tunnel a 130 kW 14-blade axial blower with a diameter of 3.2 m is installed. This axial blower sucks air into the wind tunnel which has to pass a flow straightener at the beginning of the wind tunnel. The flow straightener reduces lateral and vertical turbulences and creates a more uniform flow. Further reductions in the turbulences are achieved by the acceleration due to the contraction of the lateral and vertical dimensions of the intake of the wind tunnel.

At the entrance to the boundary layer development section triangle shaped vortex generators are installed. The vortex generators roughly shape the flow. Further development of the boundary layer is achieved by roughness elements on the floor of the wind tunnel (Fig. 4.2). More details about the development of the boundary layers are given in Section 4.4.1.

The wind tunnel is equipped with a computer-controlled traverse system which allows a sufficiently precise (approximately 0.1 mm accuracy) three dimensional positioning of the measurement probes.

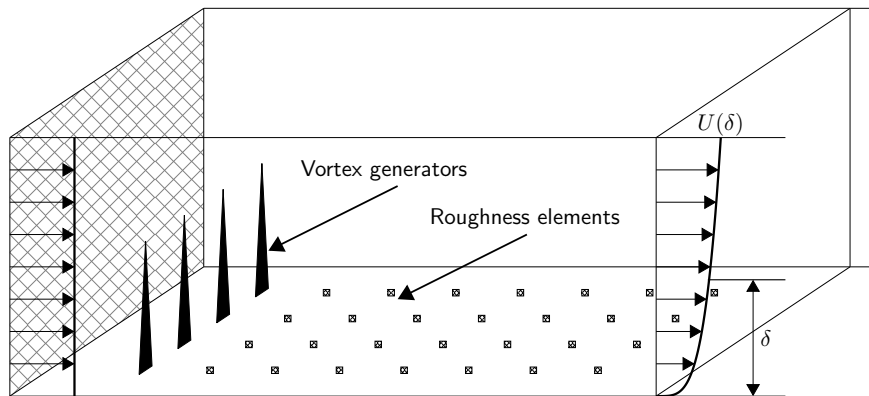


Figure 4.2: Schematic of the development section of WOTAN.

4.2 Measurement Techniques

Free-stream wind velocity

The free-stream or base wind speed was measured at the intake of the wind tunnel in the centreline at a height of 1.9 m. The measurements were performed with a wind speed and wind direction (WSWD) Ultra Sonic Anemometer (USA). Previously the reference wind speed was measured with a Prandtl tube connected to a pressure transducer. However, due to the length of tubing and the measurement setup the lower limit of measurable reference wind speed of the Prandtl tube was slightly above 1 m/s. The desired free-stream wind speeds were slightly below 1 m/s, so the traditional setup could not be used any longer.

USA measure the wind speed by measuring the flight time difference between pairs of transducers. The used WSWD USA measures the wind speed and wind direction in two dimensions. It has a temporal resolution up to 100 Hz (MESA, 2019) and can measure wind speeds from 0.1 m/s to 75 m/s. With the position of the USA in the free-stream above the influence of the vortex generators and the roughness elements the unperturbed free stream wind speed can be measured precisely. This reference mean wind speed is then scaled down to a representative reference velocity at a height below 100 m in full-scale upstream of the model area.

Laser Doppler anemometry

Boundary layer wind speed measurements and flow inside the model area were performed with a two-component Laser Doppler Anemometry (LDA) system. The LDA system is an Argon ion-gas laser. LDA systems allow a measurement of flow signals at a distance away from the measurement device without influencing the flow. In the following only a basic introduction into LDA will be given, for more details follow Albrecht et al. (2003) or Hertwig (2013).

LDA systems operate on the principle of backscattering of particles which move through an interference pattern. The necessary particles were generated with a hazer (Smoke Factory Tour Hazer) and dispersed throughout the whole wind tunnel hall to mitigate effects of a heterogeneous distribution of the fog particles and to ensure a sufficiently stable data rate. LDA systems measure absolute wind speeds and require no pre-calibration. The Argon ion-gas laser generates a laser beam which is then separated into a blue (488 nm) component and a green (514.5 nm) component. Both laser beams are

Table 4.1: Sizes of used LDA probes and their respective measurement volumes. Values of dx , dy and dz are giving for the setup of the LDA looking downward.

| | Probe diameter | Focal length | dx (mm) | dy (mm) | dz (mm) |
|-----------------|----------------|--------------|-----------|-----------|-----------|
| Configuration 1 | 26 mm | 160 mm | 0.078 | 0.078 | 1.658 |
| Configuration 2 | 85 mm | 500 mm | 0.077 | 0.077 | 1.102 |

then split up again. Inside the wind tunnel two coherent laser beams with the same wave length intersect at the focal point inside the wind tunnel and create an interference pattern. This is done with all four laser beams, two of each colour, so that two measurement volumes are spanned. The measurement volumes are at the same position with the interference pattern perpendicular to each other. Depending on the orientation of the LDA probe either the streamwise and spanwise, $U - V$ components of the wind or the streamwise and vertical $U - W$ components are measured.

Particles which move through a measurement volume scatter back the emitted laser light. This backscatter is captured by the probe. The recorded intensity of the back scatter forms a 'Doppler burst'. This 'Doppler burst' is transferred to an electrical system by a photomultiplier and further processed by a 'burst spectrum analyser'. The velocity component perpendicular to the fringe pattern is derived from the burst frequency for each particle flying through the measurement volume.

During the measurement campaign two fibre probes with different focal lengths were used (Tab. 4.1). For the boundary layer measurements, a probe with a focal distance of 160 mm was used. For measurements inside the model area a probe with a focal distance of 500 mm was used. Depending on the width of the probe and the focal length the size of the measurement volume changes. An increase of the size of the measurement volume decreases the spatial resolution of the measurement, because it increases the volume over which the individual measured velocities are averaged. However, with both LDA probes the measurement volumes were small in regard to the scale of the structures. During a UV-measurement setup the height of the measurement volumes of both LDA probes is less than 20 cm (full-scale).

Flame Ionization Detector

For the concentration measurements two Flame Ionization Detectors (FIDs) were used: one FID with a slow response rate to monitor the background concentration in the air in front of the model and one fast FID with a high temporal resolution to measure inside the model in the wind tunnel. The operation principle of FIDs is based on the detection of hydrocarbon ions during the combustion of the sampled gas in a hydrogen flame.

The background concentration was measured upwind of the model area with a FID (Model 400A, Rosemount Analytical). The concentration inside the model area was measured with a Fast-FID (HFR400, Cambustion Ltd.). Both FIDs function in the same way, but the slow response FID is located outside of the wind tunnel and sucks in air from the wind tunnel. The combustion chamber of the fast response FID is located inside the wind tunnel to reduce tubing distances and thus improve the temporal resolution and response time. For the neutral density gas dispersion experiments ethane (C_2H_6) was used as the measurement gas, whereas n-butane (C_4H_{10}) was used for the heavy gas dispersion experiments. If the

Table 4.2: Fast FIDs settings and their respective temporal resolutions.

| | Nozzle diameter | Nozzle length | Delay | Response rate |
|-----------------|-----------------|---------------|-------|---------------|
| Configuration 1 | 0.32 mm | 300 mm | 33 ms | 67 Hz |
| Configuration 2 | 0.22 mm | 200 mm | 19 ms | 176 Hz |

sampled air contains hydrocarbon positively charged carbon ions and electrons are produced (Peckham, 2006). The generation of positive ions is nearly linearly proportional to the number of carbon atoms burned in the hydrocarbon and thus to the concentration of hydrocarbons in the sampled gas.

Due to higher buildings heights and the large scale of the models in different model configurations different nozzles were used for the fast FID. The nozzles differ in length and diameter (Tab. 4.2). Changes of the nozzle diameter and the nozzle length change the response rate of the system and the delay of the signal of the measurements. The combustion chamber of the fast FID was mounted on the wind tunnel traverse. With traverse system every location in the model area could be reached with a precision of up to 1 mm.

The FID-systems are sensitive to changes in the ambient conditions like temperature or atmospheric pressure changes. Changes in the ambient conditions result in changes of the combustion chamber temperature and the pressure differential and thus the overall operation of the FID. To mitigate a drift in the signal of the FIDs, the FIDs were calibrated multiple times daily. Calibration of the FID systems differed slightly between the neutral density and heavy gas dispersion experiments. For the neutral density gas dispersion experiments three premixed gases with different concentrations of the trace gas Ethane were available. With the known concentrations of the ethane-air mix a linear voltage response calibration is performed. The calibration for the heavy gas dispersion experiments was performed by creating self-mixed mixtures of butane-CO₂. With the premixed gases an accuracy of up to 2 ppmV and with the self-mixed gases an accuracy of up to 5 ppmV was achieved.

4.3 Model configurations

Throughout the measurement campaign three different models were used to conduct flow and dispersion experiments. The models range from a simple flat open terrain scenario to a highly complex geometry. The first model is a dispersion scenario where an area source, flush with the ground, is placed in a horizontal homogenous rough boundary layer flow without obstacles (Section 4.3.1). The second model is a simple industrial environment which consists of approximately 20 cuboid-shaped buildings with a large building in the middle of the model area. From the large building in the middle of model area gases are emitted (Section 4.3.2). The most complex model is a section of a chemical industrial park. This model represents a part of the chemical park of the company BASF in Ludwigshafen, Germany. The model geometry consists of buildings of various heights and sizes as well as round shaped tanks and lowered tank pits which act as the source area (Section 4.3.3). In the following sections the three model geometries are described in detail.

4.3.1 Area Source in a Horizontally Homogenous Rough Boundary Layer

The first model is a simplified scenario at a model scale of 1:100, which just consists of a large area source (25 m by 40 m) placed in the middle of the model area (Fig. 4.3) flush with the ground. No obstacles are in the model area, except for the surface roughness required for the ABL flow modelling. The flow impacting the dispersion of the released gas is the boundary layer flow which is set up by the roughness elements and the turbulence generators in the boundary layer development section. This configuration represents an academic case and has no real world counterpart.

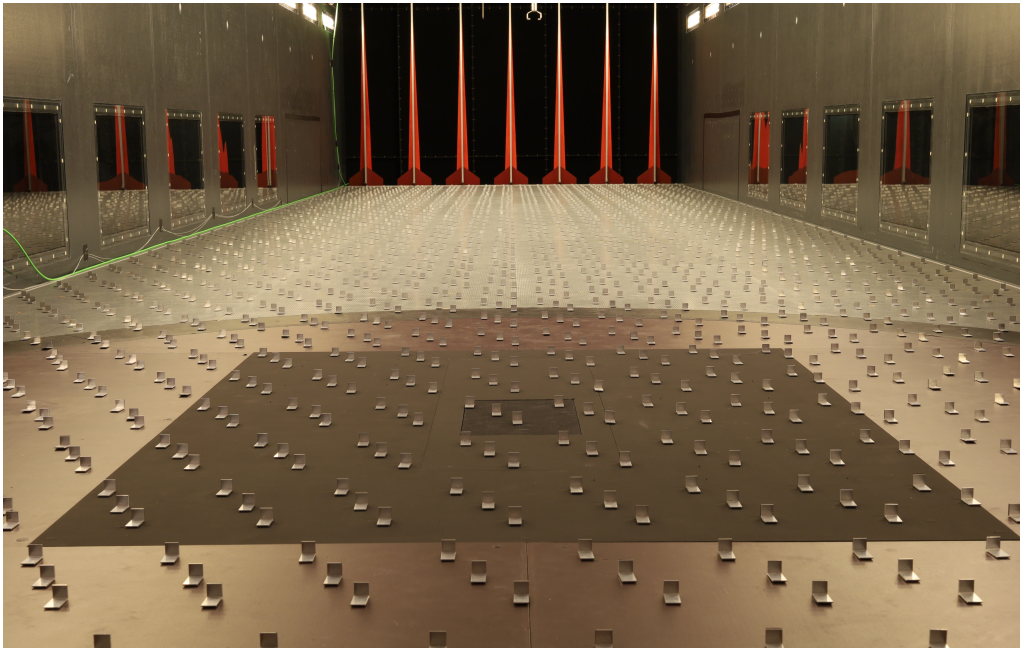


Figure 4.3: Overview of the area source model in the wind tunnel. View from the back of the wind tunnel towards to the front of the wind tunnel along the x-axis.

The main focus of gas dispersion experiments in this simple geometry was to get a better understanding of the physical processes of heavy gas dispersion without the disturbing influence of large obstacles. Measurement results from this geometry are important for the development of CFD models to test and verify the buoyancy effects of a heavy gas dispersion without the interfering influence of obstacles in the flow and the gas cloud.

The area source in this configuration shares its design with the area source of the chemical park model (Section 4.3.3) and is described in detail in Section 4.3.4.

The measurement grid is focused in a cone behind the area source to laterally and vertically capture the extent of the gas cloud. The bulk of the measurements is performed in a height of 2 m or less.

4.3.2 Idealized Industrial Park

The second model setup with an increased complexity is an idealized medium density industrial zone with a model-scale of 1:100. (Fig. 4.4). This geometry has been derived from aerial images and building data of real industrial districts. The model spans an area of 300 m by 300 m.



Figure 4.4: Idealized industrial park model in the wind tunnel. View from the back of the wind tunnel towards to the model along the x-axis.

The model consists of several cuboid-shaped buildings. The buildings have varying horizontal sizes ranging from 15 m to 60 m, but all have the same full-scale height of 15 m (Fig. 4.4 and Fig. 4.5). Distances between the buildings range between 10 m to 80 m.

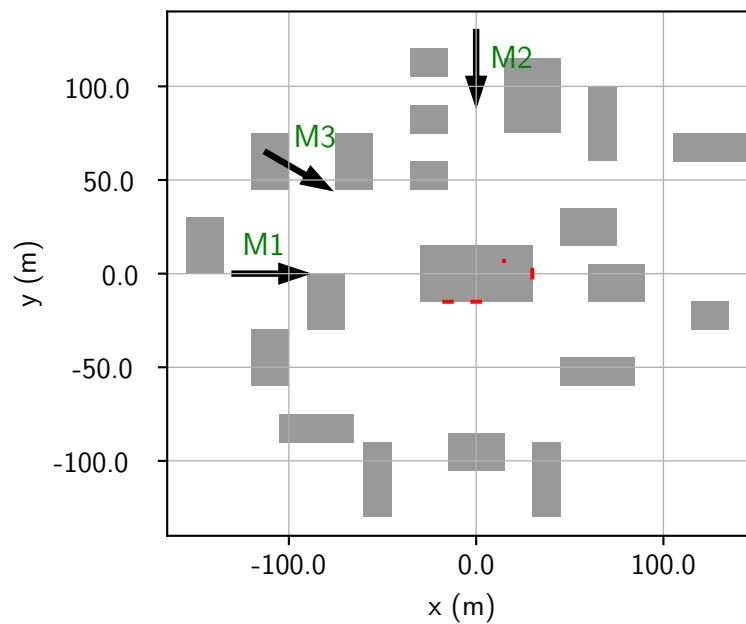


Figure 4.5: Overview of the idealized industrial environment model. The arrows indicate the three different wind directions (M1: 0°, M2: 90° and M3: 30°).

In the middle of the model geometry the main storage hall is placed. The extents of the main hall are 60 m width, 30 m length and 15 m height. The main hall in the middle of the model geometry is the largest building of the model geometry. On different points on the sides of the main hall openings are cut out. In these openings sources are installed. Gases and smoke can be released from these openings. Details on the design of the source are given in Section 4.3.4.

All buildings are made from wood and are build with a precision of up to 0.1 m in full-scale (up to 1 mm in model-scale). Due to the low wind speeds and the weight of the buildings, they do not need to be fastened to the floor and are simply placed on the ground. The model has no varying topography and is flat. The model buildings are mostly placed on a black coloured ground plate. This plate has in full-scale a width of 150 m and a length of 200 m.

Any small details like cars, vegetation, fences, alterations in the roofs or small buildings are omitted in the wind-tunnel model. Furthermore any irregularities on the ground like gutters or walkways are not regarded to keep the model as simple as possible. This simplification is essential for the CFD-modellers which are constrained by the resolution of their models.

Three inflow directions into the model are realised (black arrows in Fig. 4.5). A 0° inflow case (M1), as seen in Fig. 4.5, a 90° case (M2) and a tilted 30° case (M3). The model geometry has a blockage of approximately 3% which fulfils the blockage criteria of a maximum blockage of less than 5% for an enclosed measurement section (VDI, 2000).

4.3.3 Industrial Chemical Park

The industrial chemical park model (Fig. 4.6) is the model geometry with the highest complexity investigated in this thesis. The geometry is directly derived from a part of the BASF chemical park in

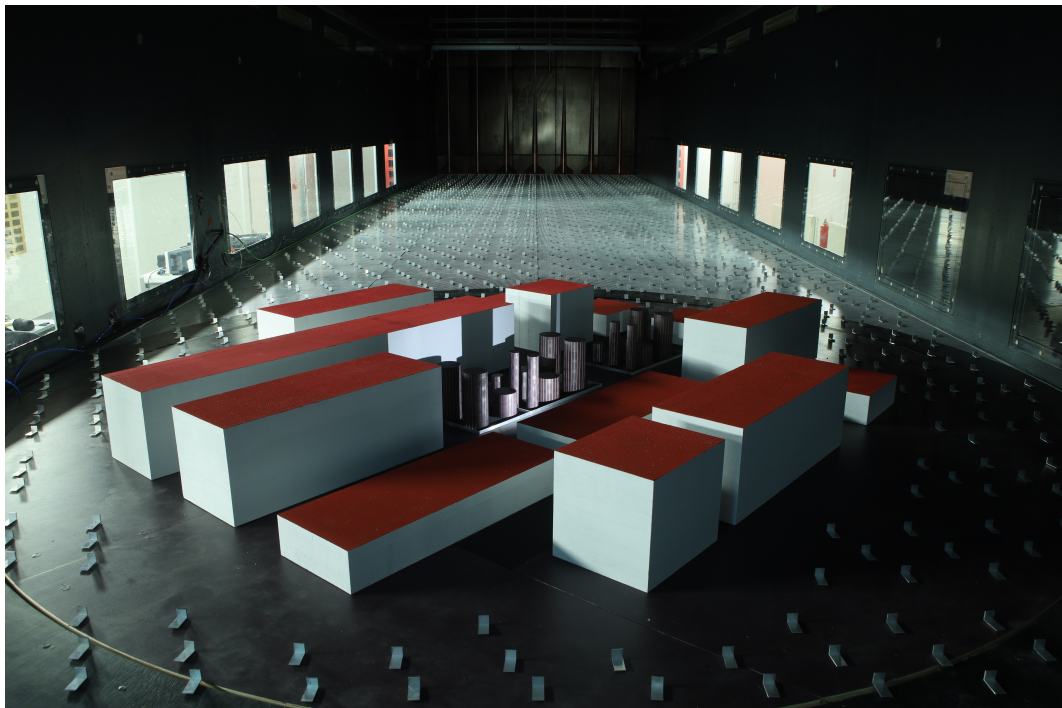


Figure 4.6: Industrial Chemical Park model in the wind tunnel. View from the back of the wind tunnel towards to the model along the x-axis.

Ludwigshafen, Germany. Data for the dimensions and building sizes have directly been provided by BASF. The location of the section of the chemical park is centred around the Benzolstreet and Butanolstreet in Ludwigshafen. The horizontal extent of the model is roughly 300 m by 300 m. The model consists of 14 cuboid shaped buildings with two different heights (10 m and 25 m) and greatly varying lengths. All cuboid shaped buildings have a width of 25 m and the lengths vary between 30 m to 150 m (Fig. 4.7). The buildings are simplifications of the buildings in the industrial chemical park. In reality the obstacles are not completely solid but rather porous and have a high amount of variability in form of tubing, exhaust stacks and various other extensions on the roofs and facades.

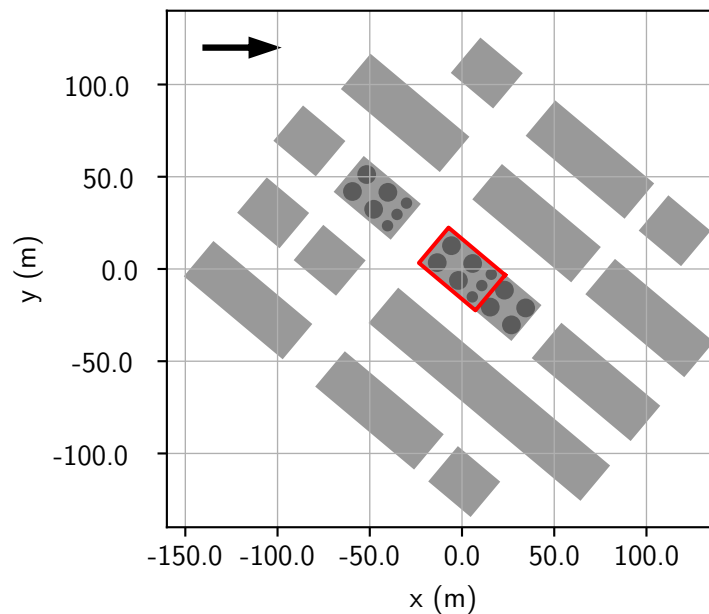


Figure 4.7: Overview of the industrial chemical park model. The red rectangle marks the source area. The black circles are the tanks. The black arrow marks the wind direction (40°).

The cuboid shaped buildings are centred around three collecting basins with several cylinders on top. Two of the three collecting basins are 2 m recessed into the ground. These two collecting basins have a horizontal extent of 25 m by 40 m. The smaller collecting basin has a horizontal size of 25 m by 25 m. All collecting basins are surrounded with thin individual sharp-edged walls which protrude 1 m up from the ground. From the collecting basin in the middle of the model geometry gases for the neutral density and heavy gas dispersion experiments are released. Further information on the source design is given in Section 4.3.4.

On top of the collecting basins cylinders are placed, which represent tanks and have two different heights of 10 m and 20 m as well as two different diameters of 4 m and 8 m. To achieve Reynolds number independence at lower wind speeds the round shaped cylinders are roughened with additional surface roughness. The industrial chemical park model has two variations with minor differences. One model (shown in Fig. 4.6 and Fig. 4.7) is the full configuration with 18 tanks on top of the three collecting basins. The other configuration only has 10 tanks on top of the three collecting basins (not shown here). In the configuration with a lower number of tanks Reynolds number independence is achieved at lower wind speeds compared to the full configuration. Therefore, this configuration is used for the heavy

gas dispersion experiments in the industrial chemical park model (Reynolds number independence test shown in Section 5.5). Measurements in the industrial chemical park model are only performed at a wind direction of 40° as shown in Figure 4.7.

Even with the wind tunnel ceiling lifted to the maximum the model geometry has a blockage of approximately 5.5%, which slightly exceeds the blockage criteria of a maximum blockage of 5% for an enclosed measurement section (VDI, 2000). Blockage of the cross-section of the wind tunnel can cause an acceleration of the flow. Due to the desired geometric scale of 1:100 this slight exceedance of the 5% blockage criteria was unavoidable with the industrial chemical park model.

4.3.4 Source Design

Idealized Industrial Park

As described in Section 4.3.2 the gas release in the idealized industrial park is performed from the main hall in the middle of model geometry. This main hall has four openings (Fig. 4.8): two openings at the long lower side (S1 and S2), one at the short right side (S3) and one opening on the top of the roof (S4). The openings on the sides of the building have a full-scale size of 4 m by 4 m (S1-S3), while the opening on the roof has a size of 2 m by 2 m (S4).

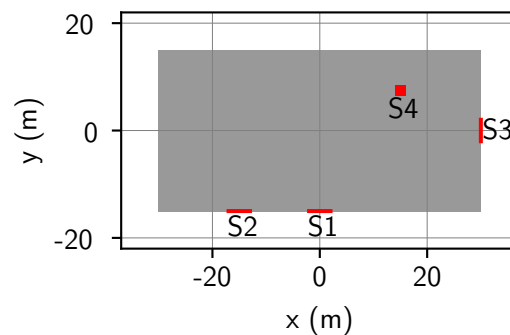


Figure 4.8: Source locations (S1-S4) on the main hall in the simple industrial park model. S1-S3 are located on the sides and S4 is located on the roof of the building. The orientation of this figure is the M1 case (also shown in Fig. 4.5).

Regardless of the different opening sizes and locations, the source mechanism in all four sources is the same. Via tubing gas is released into a cavity inside the building. This cavity is enclosed with a dense permeable filter material to ensure a release as homogeneous as possible across the entire exhaust. The filter material also inhibits fluctuations of the release rate by preventing that vortices directly enter the cavity and transport gas out of the cavity. All four sources are equipped with a solenoid valve to control the gas release.

Industrial Chemical Park

A schematic of the source design is shown in Fig. 4.9. The dimensions of the source are 40 m by 25 m (long side shown in Fig. 4.9). Due to the large size of the source a sophisticated design was necessary to

ensure a homogenous release over the complete surface of the source. Gas is supplied to the source via

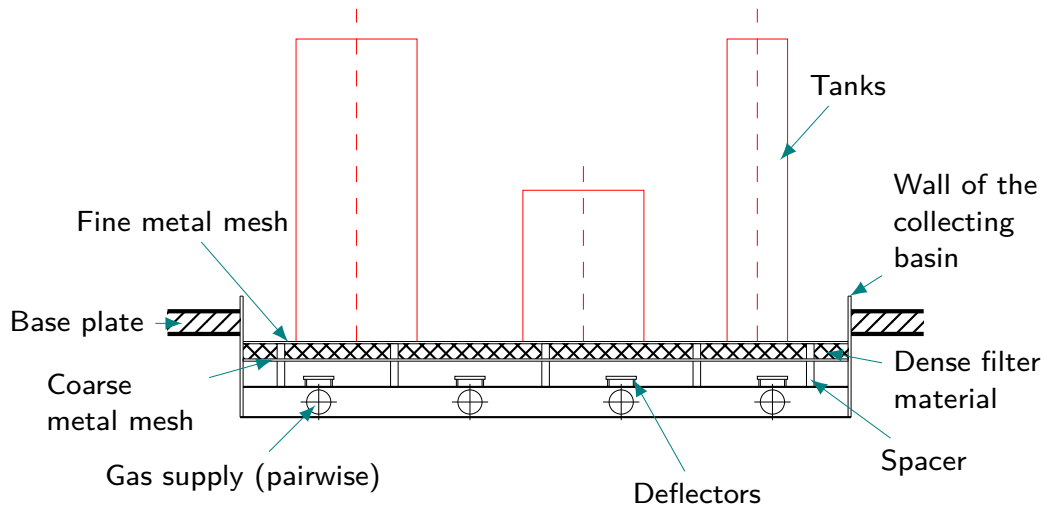


Figure 4.9: Source design for the industrial chemical park model. Differences of source design between the area source without obstacles and the industrial chemical park are listed in the text in Section 4.3.4.

eight intakes at the bottom of the source. Each side of the source has four intakes and both sides are supplied pairwise to ensure a release as symmetric as possible. The released gas is deflected by deflectors on the bottom of the source and fills a cavity in the source. The purpose of the deflectors is to prevent the formation of vertical jets, to slow down the released gas and ensure a uniform filling of the cavity and a release from the source as homogeneous as possible.

Due to the pressure of the released gas inside the cavity the gas slowly rises out of the cavity. The cavity is shielded from influence from the outside by three layers of flow resistance. A combination of a fine metal mesh on the top, dense filter material and a coarse metal mesh on the bottom minimizes the impact of pressure changes due to turbulence in the wind tunnel on the release of gas from the source.

By performing gas dispersion visualisation experiments (Fig. 6.26 in Section 6.4) and measuring lateral profiles (Fig. D.1 in Chapter D) a sufficiently homogenous release was verified experimentally.

The source used in the area source without obstacles model and in the industrial chemical park model is in essence the same. The main difference is that the area source in the area source without obstacles model is not recessed into the ground and not surrounded by a one metre high wall. The source in the area source without obstacles model is flush with the surrounding base plate.

4.4 Modelled Wind Tunnel Boundary Layer Flows

In this chapter the physical modelling of two wind tunnel boundary layer flows similar to atmospheric boundary layer flows is presented. The aim was to generate boundary layer flows which are self-consistent, in agreement with guidelines for physical modelling of ABL flows (VDI, 2000) and have a geometric scale as large as possible. A geometric scale as big as possible is desired to achieve favourable conditions for the investigation of heavy gas dispersion. A big geometric scale allows to reach smaller densimetric Froude numbers while still maintaining realistic source volume flow conditions at full-scale (Sec 5.1).

The modelled wind tunnel boundary layers do not represent any specific atmospheric boundary layers of a particular location, but rather a boundary layer flow above a specific type of terrain. One of the

wind tunnel boundary layers aims to represent an atmospheric boundary layer above grass- or farmlands and the other modelled wind tunnel boundary layer is similar to an atmospheric boundary layer which can be expected over a suburban area. Following the definitions from VDI (2000) the modelled rural boundary layer can be described as a moderately rough boundary layer and the suburban boundary layer as a rough boundary layer. Both wind tunnel boundary layer flows are modelled with a neutral atmospheric stratification.

4.4.1 Boundary Layer Development

Target of the boundary layer development was to create two consistent wind boundary layers with a scale of 1:100. As described in Section 4.1 the wind boundary layers are modelled in the boundary layer wind tunnel WOTAN with vortex generators and roughness elements. Vortex generators and roughness elements are available in various sizes and shapes and can be arranged and combined in countless configurations. By changing the vortex generators or the roughness elements, the properties of the modelled boundary layer change. To achieve suitable configurations for the boundary layers more than 40 different combinations of vortex generators and roughness elements were tested.

Ideas and Suggestions for Future Boundary Layer Development

This section is a collection of potential findings and insights in regard to the development of new configurations for the creation of wind tunnel boundary layers. The development of a new configuration is mostly driven by successive empirical improvements of existing spire and roughness configurations. The following statements to the influence of certain design decisions of the spire and roughness element configuration are in no means definitive and are merely broad assumptions and ideas, which may prove to be of help for future boundary layer development. Furthermore the potential findings are all based on experiments inside the WOTAN wind tunnel and are not necessarily transferable to other wind tunnels. Heights mentioned in this section are in model-scale.

- A general finding was that a change in the roughness elements usually influences the lower parts of the boundary layer (0.3 to 0.4 m). However only small to medium roughness elements were used. Larger roughness elements could potentially affect higher parts of the boundary layer. Changes in the foot of the vortex generators also only affected lower parts of the boundary layer and were of minor effect or negligible. Changing the vortex generators influenced the complete modelled boundary layer flow.
- Increasing the size of the roughness elements has a very strong effect on the lower parts of the boundary layer (0.3 to 0.4 m). Turbulence intensities increase and mean wind speeds slightly decreases. Changes in the orientation of the roughness elements, e.g. parallel or perpendicular to the wind, can have a significant influence on the turbulence intensities in the respective direction. This can be useful if only one component of the turbulence intensities does not match the reference values.
- For the case of the present moderately rough boundary layer an increase of approximately 30% in the density of the roughness elements showed a little increase in turbulence intensities in the lowest part of the boundary layer (up to 0.2 m). Depending on the already present density of

roughness elements a further increase in density might show only minor effects. However, a very strong increase in density of roughness elements might trigger a tipping point for the flow and might cause a skimming flow.

- Even minor changes in the shape, size or position of the vortex generators can have a strong influence on the overall shape of the wind boundary layer. Very large and wide (triangle and rectangular) vortex generators greatly increase the turbulence intensities and reduce the mean wind speeds in the entirety of the boundary layer. By also reducing the number of vortex generators a slight increase in the L_{ux} was achieved. However by substantially increasing the size of vortex generators and also changing the shape to a rectangular mostly resulted in an unbalance and inconsistency between the lower and upper parts of the boundary layer. To fix this imbalance matching roughness elements need to be chosen. Accurately predicting the influence of a change in the shape or size of the vortex generators is very difficult and would require more thorough testing and variation.
- A change in the boundary layer can also be achieved by varying the position of the vortex generators. By reducing or increasing the spacings between the vortex generators and the walls of the wind tunnel lateral inhomogeneities in the mean wind speeds can be alleviated. However, changes in the spacings need to be done very carefully and in small steps because a change in the spacings can also influence the turbulence intensities and the overall wind profile.

In the following the moderate rough boundary layer (MRBL) (Section 4.4.2) and the rough boundary layer (RBL) (Section 4.4.3) are documented and discussed. The parameters of the modelled wind tunnel boundary layers are evaluated for consistency and compared to the corresponding VDI (2000). All given heights are above ground and are in full-scale.

Measurement Uncertainty

Any kind of measurement is prone to some degree of uncertainty. The operation of measurement devices like for example the FID can be influenced by atmospheric boundary conditions like humidity, pressure and temperature. The location of the used boundary layer wind tunnel WOTAN is in a basement so temperature and humidity fluctuations are dampened, but still have a significant effect on the calibration of the instruments and the measurements. To alleviate the issue of variations in the atmospheric boundary conditions multiple calibrations have been performed in the course of a day. The temperature and humidity in the wind tunnel hall have an influence on the efficiency of the aerosol seeding for the LDA measurements, which has a significant effect on the data rate of the measurements. The mass flow controllers, which are used to control the flow rate of the calibration and measurement gases, also add further uncertainty to the calibration and operation of the FIDs.

Another known factor, which has an influence on the measurement uncertainty, is the positioning of the probe. Small step errors or a slight offset in the initial positioning of the reference coordinate system (for example the height above ground) can lead to minor offsets in the measurement position. Especially in the presence of strong gradients (velocity or concentration) the mispositioning can lead to an increase in measurement uncertainty.

The limited averaging time of the measurements also causes measurement uncertainty. Due to the instationarity of turbulent flows measurements have to be performed over a sufficiently long enough sampling period to achieve a representative mean value. If the time of sampling is not long enough it is possible that low frequency events are not captured sufficiently. To determine a suitable averaging time for the measurements, convergence tests have been performed (Fig. A.5 and Fig. A.6 in Appendix A). From these tests, an averaging time of 3 minutes for the flow and neutral density gas dispersion measurements and an averaging time of 5 minutes for the heavy gas dispersion measurements has been determined. Due to the different reference wind speeds, the 3 minutes represent approximately 30 hours in full-scale and the 5 minutes of the heavy gas concentrations measurements represent approximately 8 hours in full-scale at full-scale wind speed of 1 m/s.

The total measurement uncertainty is a combination of the previously listed known and other unknown measurement uncertainties. The exact total measurement uncertainty is not known. With repetition measurements at multiple critical positions for flow, neutral density and heavy gas dispersion measurements in all model geometries and boundary layers, the total measurement uncertainty or confidence interval is estimated. Measurement uncertainties for the boundary layers are presented in Sec. 4.4.2 and 4.4.3 are shown in Tab. 4.3. Measurement uncertainties for other variables are included in the specific plots where the variables are presented.

Table 4.3: Measurement uncertainty for specific variables in the boundary layer. The values have been determined by calculating the total range of the repetition measurements. The presented values are the positive and negative variations around the mean.

| Parameter | MRBL | RBL |
|-----------------------------|---------------|--------------|
| U_{mean}/U_{ref} | $\pm 0.03\%$ | $\pm 0.03\%$ |
| $\overline{u'w'}/U_{ref}^2$ | ± 0.00015 | ± 0.0002 |
| $I_{u,v,w}$ | ± 0.01 | ± 0.01 |
| L_{ux} | ± 10 m | ± 10 m |

4.4.2 Moderate Rough Boundary Layer

As mentioned before the modelled atmospheric boundary layer is not represented by a specific boundary layer but rather an idealized boundary layer which is characterized by a suburban surface roughness. The properties of the modelled boundary layer are based on guidelines originating from physical modelling of atmospheric boundary layer flows (VDI, 2000). These guidelines split representative surface roughness features into roughness classes and characterise the respective classes by their boundary layer properties.

In case of the rural boundary layer the atmospheric flow is influenced by a moderately rough surface roughness. The roughness is achieved by a combination of roughness elements and vortex generators (see Fig. B.1 and B.2 in Appendix B). A vertical wind profile which is modelled with this configuration is shown in Fig. 4.10. This vertical wind profile is measured approximately two metres before the end of the flow development section and up-wind of the model area in the middle of the wind tunnel (measurement position $x = -1700$ mm, $y = 0$ mm). Fig. 4.10 shows the dimensionless wind speed of

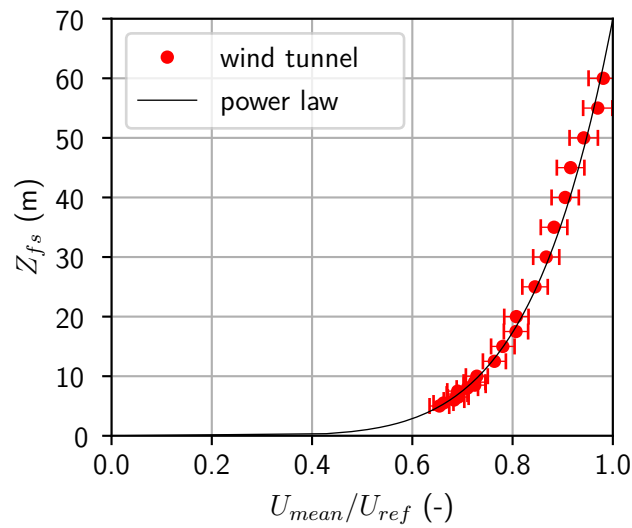


Figure 4.10: Vertical profile of the mean U wind speed (streamwise velocity) at the end of the boundary layer development section in front of the model area. Wind tunnel measurements in red and a power-law fit with $\alpha = 0.17$ in black. The confidence interval of the velocity measurements is represented by the red bars.

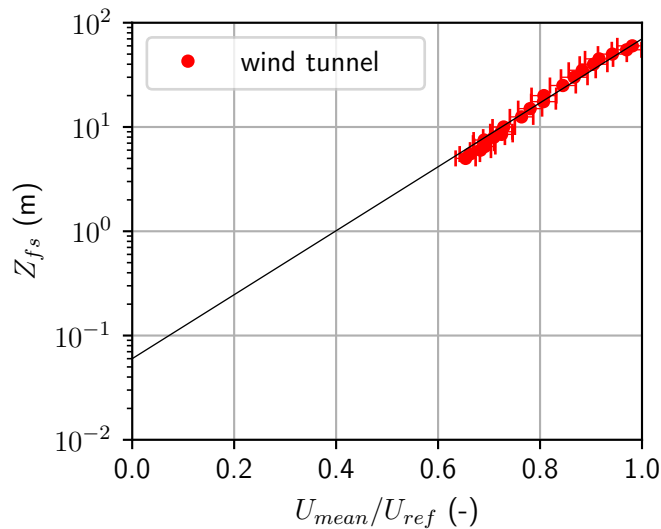


Figure 4.11: Vertical profile of the mean U wind speed (streamwise velocity) at the end of the boundary layer development section in front of the model area in a semi-logarithmic scale. Wind tunnel measurements are in red and the logarithmic fit for the roughness length ($z_0 = 0.06$ m) is depicted in black. The confidence interval of the velocity measurements is represented by the red bars.

the main flow in dependency of the full-scale height. Fig. 4.11 shows the same vertical wind profile but in a semi logarithmic scale.

The vertical wind profile is nondimensionalized with a reference wind speed taken at a height of 1.9 m and referenced to a height of 70 m.

The vertical profile of the mean U -wind speed can be approximated with the power-law function:

$$\frac{\bar{U}(z)}{U_{ref}} = \left(\frac{z - d_0}{z_{ref} - d_0} \right)^\alpha, \quad (4.1)$$

where $\bar{U}(z)$ is the time average of U at a height z , d_0 is the displacement height, z_{ref} is the reference height, U_{ref} is the mean wind speed at the reference height and α is the power-law parameter or profile exponent. With an exponential fit to the vertical profile of the measured U -wind speed in Fig. 4.10 the profile exponent α (Eq. 4.1) is derived. Using wind speed measurements in a height range from 8 m to 50 m (full-scale) a profile exponent of 0.17 ± 0.01 is derived. A wind profile derived with this profile exponent and the power law in Eq. 4.1 is also shown in Fig. 4.10. Following the roughness class definitions from VDI (2000), a profile exponent of 0.17 lies in the moderately rough class from 0.12 - 0.18.

A vertical profile of the mean vertical turbulent momentum flux of the u velocity component in the modelled boundary layer is shown in Fig. 4.12. These measurements are also taken upwind of the model area (Measurement position $x = -1700$ mm, $y = 0$ mm). The confidence interval for the vertical momentum fluxes are estimated with $\pm 10\%$. Measurements taken below 8 m are not used for profile analysis because of the interference by individual roughness elements and indicated with an empty circle. Measurements below 8 m are in proximity to the roughness elements. A minimum distance of four times the height of one roughness element to the obstacles is used here. In this configuration roughness elements with a full-scale height of 2 m (2 cm model-scale) are used. The shaded area marks the vertical turbulent momentum flux at 8 m height $\pm 10\%$ deviation from that value. The vertical turbulent momentum fluxes remain approximately constant up to 50 m height. This layer of roughly

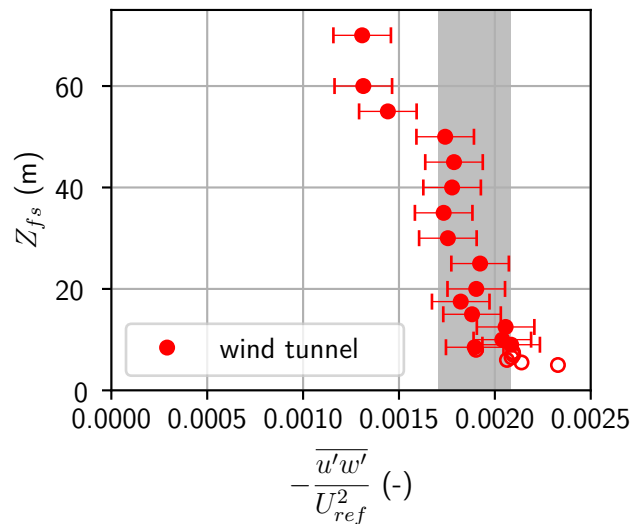


Figure 4.12: Vertical turbulent momentum fluxes measured at the end of the boundary layer development section in front of the model area. Measurement points below a height of 8 m are not considered due their vicinity to the roughness elements and are therefore indicated by empty circles. The confidence interval of the turbulent momentum fluxes is represented by the red bars.

constant vertical turbulent momentum fluxes indicates the height of the Prandtl layer at full-scale. Above

the Prandtl layer the vertical turbulent momentum fluxes decrease with increasing height. Thus, the Prandtl layer of the modelled boundary layer extends up to a height of 45 - 50 m.

Following the approach of deriving the profile exponent the roughness length of the boundary layer is derived in a similar manner. The data is fitted by a semi logarithmic relationship (Fig. 4.11). The linear fit is only applied to points which lie inside the Prandtl layer. In case of this boundary layer this means U wind speed measurements are taken from a height of 8 m to 50 m. The measurements below 8 m are again omitted due to the potential influence of the roughness elements on the flow measurements. The intersection between the y-axis and the linear fit gives the value for the roughness length of the modelled boundary layer. For this boundary layer the roughness length is $0.06 \text{ m} \pm 0.01 \text{ m}$. The uncertainty in the roughness length was derived by performing the linear fit on repetition measurements and measurements taken at a slightly different lateral position (not shown here).

Following the roughness classifications of the VDI (2000), the derived roughness length lies in the class of moderately rough terrain. The proposed roughness lengths for moderately rough terrain ranges from $5 \cdot 10^{-3} \text{ m}$ to $1 \cdot 10^{-1} \text{ m}$ and the derived roughness length is at $6 \cdot 10^{-2} \text{ m} \pm 2 \cdot 10^{-2} \text{ m}$. With this profile exponent and roughness length the modelled boundary layer is at the upper range of the moderately rough class which can be associated with a rural terrain.

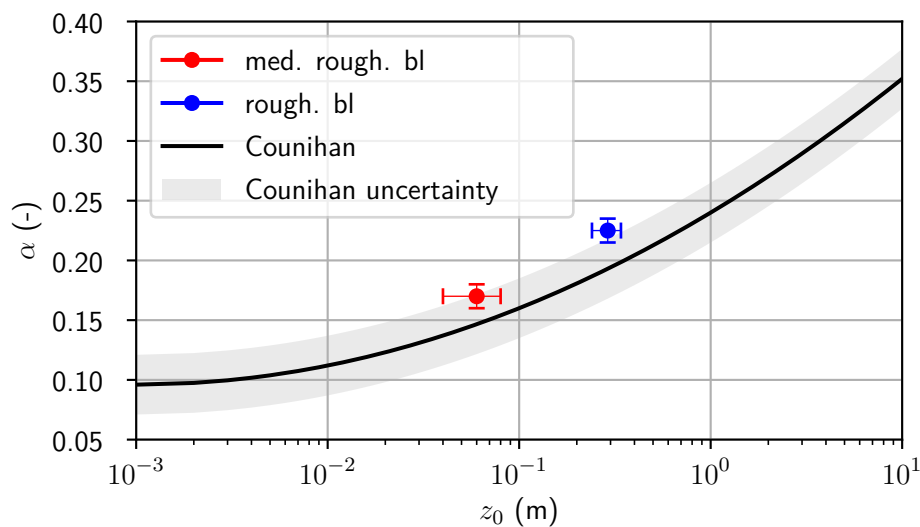


Figure 4.13: Functional relation between the profile exponent α and the roughness length z_0 of the moderately rough (red) and rough (blue) boundary layer in comparison to Counihan (1975). The confidence interval of the profile exponents and the the roughness lengths are represented by the respective bars.

Panofsky (1974), Counihan (1975) and others formulated functional relationships between the profile exponent α and the roughness length z_0 in atmospheric boundary layers (Fig. 4.13). These functional relationships were derived from field data. For better visibility the measurements of the field campaigns are not included. The shaded area in Fig. 4.13 indicates the range of the measured field data. To find the measurement values for the field campaign measurements follow Counihan (1975).

The profile exponent and roughness length of the modelled boundary layer diverges slightly from the proposed relation between profile exponent and roughness length of Counihan (1975) but still lies in the uncertainty range of the relation (Fig. 4.13).

Regarding specifications made by the Plate (1982) and VDI (2000) the minimum roughness Reynolds number is:

$$Re_* = \frac{u_* \cdot z_0}{\nu} > 5, \quad (4.2)$$

with the friction velocity u_* , the roughness length z_0 and the kinematic viscosity of air ν . For values of $u_* = 0.28 \frac{m}{s}$, $z_0 = 0.066 \cdot 10^{-2} m$ and $\nu = 14.9 \cdot 10^{-6} \frac{m^2}{s}$, the Eq. 4.2 yields a roughness Reynolds number of 12.4 at model-scale. Thus, the requirement of a roughness Reynolds number above five is fulfilled (VDI, 2000).

Another characteristic of boundary layer flows is the turbulence intensity. For the moderately rough boundary layer the vertical profiles of the turbulence intensities for the u , v and w components of the flow are shown in Fig. 4.14. The vertical turbulence intensities profiles derived from the same measurements as the mean wind profiles (Measurement position $x = -1700 mm$, $y = 0 mm$). The turbulence intensity

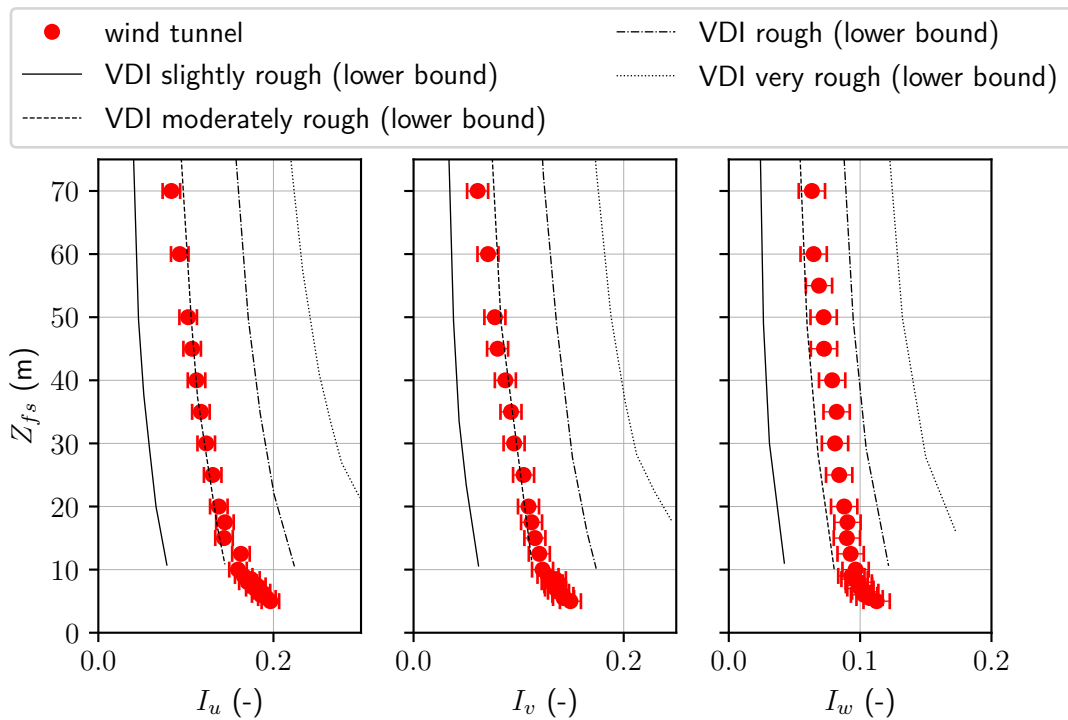


Figure 4.14: Vertical profiles of the turbulence intensities of the u , v and w components of the flow. Measurements performed at the end of the boundary layer development section in front of the model area. Reference curves are from VDI (2000). The confidence interval of the values for the turbulence intensity are represented by the red bars.

$I_i(z)$ is defined as the ratio between the standard deviation of a wind velocity component σ_i and the mean wind speed $\bar{U}(z)$

$$I_i(z) = \frac{\sigma_i}{\bar{U}(z)}; i = u, v, w \quad (4.3)$$

whereas u, v, w describe the wind components in streamwise, lateral and vertical directions. Following the definitions of the VDI (2000) for the values of the roughness classes, the values of the turbulence

intensity lie on the lower bound of the moderately rough roughness class. The vertical profiles for the turbulence intensities of all three velocity components agree well in their shape and values with the proposed lower bound of the moderately rough reference curve.

Another important property of a modelled boundary layer flow are integral length scales of the turbulent structures embedded in the mean flow. The integral length scales describe the mean extent of the dominant turbulent eddies in the flow. The integral length scale is calculated by performing temporal autocorrelations on single point measurements in the flow. The temporal autocorrelation function of the u -velocity fluctuations is defined by

$$\rho_u(\tau) = \frac{\overline{u'(t)u'(t+\tau)}}{\sigma_u^2}, \quad (4.4)$$

where τ is the lag between both time series and σ_u the standard deviation of the main wind component u . With the integral over Eq. 4.4 the integral time scale is calculated with

$$T_u = \int_0^{\infty} \rho_u(\tau) d\tau. \quad (4.5)$$

By utilizing the Taylor's 'frozen turbulence' hypotheses (Taylor, 1938) the temporal integral time scale can be transformed to a spatial integral length scale. In case of the integral length scale of the mean flow in x direction the following is used:

$$L_{ux} = T_u \cdot \bar{U} \quad (4.6)$$

In Eq. 4.6 \bar{U} denotes the time-averaged mean wind speed of the flow at measurement height. The calculation for the other spatial dimensions L_{uy} and L_{uz} of the eddies transported of the main flow is performed in an analogue fashion.

The integral length scales are influenced by the surface roughness. With an increasingly rough ground the flow becomes more turbulent and the eddies with the highest energy become smaller. An increase in height allows bigger eddies to exist and the integral length scale increases. Counihan (1975) derived a functional relation between the integral length scales, ground roughness and the measurement height from field measurements. A vertical profile of integral length scales derived from wind tunnel measurements is shown in Fig. 4.15 and compared to the functional relations of Counihan (1975) for four different roughness values z_0 of 0.01 m, 0.1 m, 1 m and 10 m. The functional relations derived by Counihan (1975) are valid for heights from 10 m to 250 m. In Fig. 4.15 it is shown that the values for the integral length scales fall in the corridor between the theoretical relation of roughness lengths of 10 m and 1 m. The values for the integral length scales of the modelled boundary layer lie between 30 m and 60 m. Thus, the eddies with the highest energy are smaller than desired. For the roughness length of the modelled boundary layer $0.06 \text{ m} \pm 0.02 \text{ m}$ values for integral length scales of 100 m to 150 m would be expected following the functional relation of Counihan (1975). However, a boundary layer flow with integral length scales of $> 100 \text{ m}$ is impossible to generate in WOTAN at a scale of 1:100. Integral length scales of 100 m at full-scale would require eddies with a size of more than 1 m (model-scale) in the wind tunnel. This is not feasible because of the limited size of the wind tunnel and the limiting

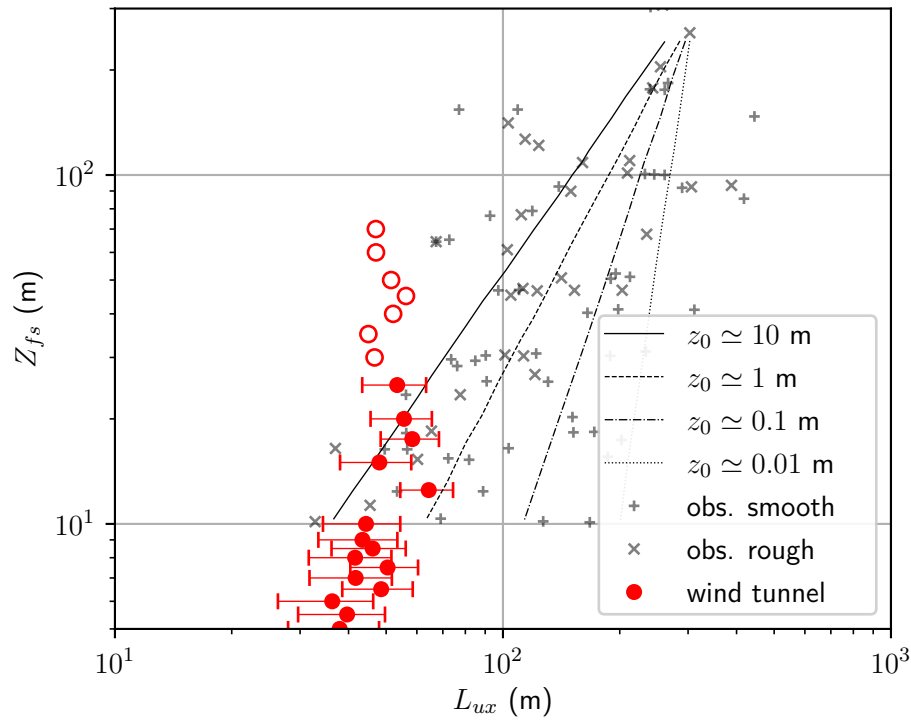


Figure 4.15: Vertical profile of the integral length scale of the mean flow in x direction (red dots). Field measurements from Counihan (1975). Obs. is short for observations. Plusses represent field measurements above smooth terrain with roughness lengths between 0.01 m and 0.1 m. Crosses represent field measurement above rough terrain with roughness lengths between 1 m and 10 m. The confidence interval of the values for the integral length scales is represented by the red bars.

thickness of the modelled boundary layer. With the used vortex generators and roughness elements a boundary layer with a thickness of approximately 80 m was modelled.

Although the values of the integral length scales do not fit with the functional relation of Counihan (1975) the trend of the length scales fits rather well up to a height of approximately 35 m to 45 m. Up to that height an increase in measurement height also represents an increase in the values of the integral length scale. Measurement locations above 45 m are indicated with empty circles in Fig. 4.15. Integral length scales derived from measurements taken above approximately 35 m to 45 m deviate from that trend. This can potentially be explained by the edge of the modelled of the Prandtl layer at approximately 45 m.

The spectral distribution of turbulent kinetic energy is an additional property of boundary layer flows which can be investigated to check if a modelled wind tunnel boundary layer flow has turbulence structures similar to energy density spectra measured in field experiments. Fig. 4.16 shows 1D auto-spectral energy densities S_{ii} for the u , v and w wind velocity components in comparison to empirical relationships for neutrally stratified boundary layer flows (Erdmann, 2017). The calculation of the turbulent energy spectra closely follows the method of Hertwig (2013).

The spectra shown in Fig. 4.16 are calculated from wind velocity measurements at a height of 30 m in front of the inflow area of the model (Measurement position $x = -1700$ mm, $y = 0$ mm). The spectra are presented in dependence on the dimensionless frequency. Values on the left side represent the low

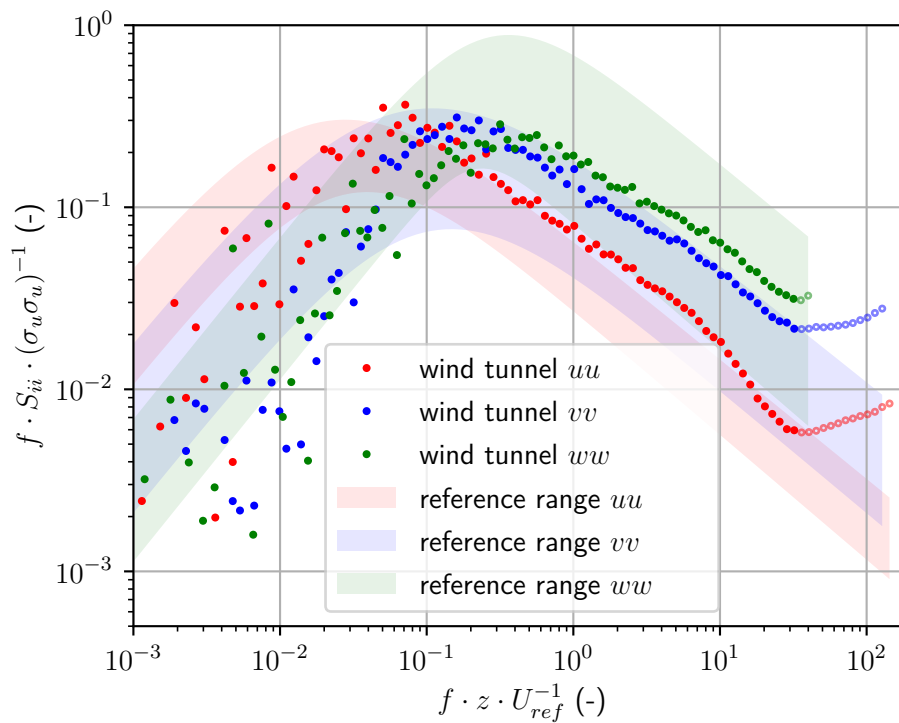


Figure 4.16: Normalized spectral distribution of turbulent energy at 30 m above the ground. Measurements performed at the end of the boundary layer development section in front of the model area. Reference range from Erdmann (2017).

frequency turbulence and values on the right side represent turbulence with a high frequency. Values of the spectra at high frequencies which are affected by aliasing are indicated with an empty circle (right side of the plot).

The frequency is made dimensionless with the mean wind speed of the u -component of the flow and the height of the measurement above ground. Following VDI (2000) the spectral distribution of the turbulent kinetic energy is made non dimensional with the standard deviation of the fluctuations of the main wind component. The shaded reference ranges for the energy density spectra are derived by Erdmann (2017). These reference ranges combine several reference spectra from von Karman (1948), Kaimal et al. (1972), Simiu and Scanlan (1978), ESDU-85020 (1985) and Kaimal (1994).

Fig. 4.16 shows turbulent energy density spectra for all three wind velocity components u , v and w at a height of 30 m. Overall the measured turbulent energy spectra show a good agreement with the reference ranges provided by Erdmann (2017). In case of the u -component the spectrum is slightly shifted to higher frequencies but the shape of the spectra fits well with the reference ranges. For the other velocity components v and w the shape and position of the spectra are in good agreement with the reference. In general the height of the energy peak compares quite well with the reference spectra. However all velocity components show an underrepresentation of the turbulent energy at the lower frequencies, which correspond to large turbulent structures. At dimensionless frequencies of 2 - 10 the effects of aliasing can be observed. Due to aliasing the measured energy density increases again. The measurements of the u and v -component are performed with a data rate of approximately 4 kHz, whereas for the w only measurements with a data rate of approximately 600 Hz were available.

Summing up, the modelled wind tunnel boundary layer shows in general a good agreement with the reference values provided by VDI (2000), Counihan (1975) and Erdmann (2017). The wind profile, turbulence intensities and vertical momentum fluxes agree very well with the references. However the comparison of the integral length scales and the turbulent energy spectrum with the reference show that the 1:100 geometric scale is stretching the limits of physical modelling in the used wind tunnel. The larger scales of the turbulence are underrepresented due to the limiting size of the wind tunnel and the height of the modelled boundary layer.

Further quality control of the modelled moderately rough boundary layer is shown in the Appendix A. The moderately rough boundary layer shows lateral homogeneity of U_{mean} up to a distance of 100 m (full-scale) from the middle of the wind tunnel (Fig. A.1). Around $Y_{fs} = -100$ m U_{mean} begins to deviate. However, the majority of measurements are performed around the centre line of the wind tunnel. A Reynolds number independence test performed in the moderately rough boundary layer is shown in Fig. A.2. The ratio between the measured wind speed and the reference wind speed remains constant within the measurement uncertainty for reference wind speeds between 1 m/s and 5 m/s. So, Reynolds number independence of the moderately rough boundary layer flow is achieved with a minimum reference wind speed of more than 1 m/s.

4.4.3 Rough Boundary Layer

The second modelled atmospheric wind boundary layer aims to represent a wind boundary layer in an suburban environment. Again no real measurements which represent a specific city or area are used as reference. The properties of the modelled boundary layer are also again based on roughness classes which are defined by the guidelines of VDI (2000). The derivation of the rough boundary layer parameters follows in an analogue fashion as presented in Sec. 4.4.2.

In case of this boundary layer the wind flow is influenced by a rough surface roughness. This is again achieved by a combination of roughness elements and vortex generators (see Fig. B.3 and B.4 in Appendix B). In comparison to the boundary layer setup for the moderately rough boundary layer a greater number and bigger roughness elements are used.

A vertical wind profile measured in this configuration is shown in Fig. 4.17. This vertical wind profile is measured approximately two metres before the end of the development section of the wind tunnel (Measurement position: $x = -1700$ mm, $y = 0$ mm). The vertical wind profile shown in Fig. 4.17 is presented as dimensionless wind and as a function of the full-scale height above ground. The dimensionless wind speed is calculated with the reference wind speed measured at the beginning of the wind tunnel (refer to USA in Sec. 4.2). The same vertical wind profile is shown in a semi logarithmic scale in Fig. 4.18.

Following the same procedures as described in Section 4.4.2 the profile exponent α is derived from the vertical profile. Using measurements of full-scale heights from 10 m to 45 m a profile exponent of 0.23 ± 0.01 is derived. With this profile exponent and the power law (Eq. 4.1) a vertical wind profile is derived and shown in Fig. 4.17. According to the roughness class definitions from VDI (2000), a profile exponent of 0.23 lies at the upper end of the rough roughness class from 0.18 – 0.24.

A vertical profile of the mean vertical turbulent momentum flux of the u velocity component in the rough boundary layer is shown in Fig. 4.19. These measurements are taken at the same position as the

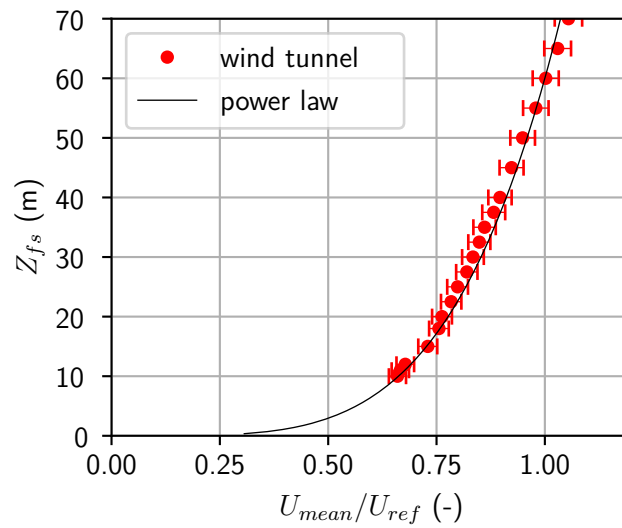


Figure 4.17: Vertical profile of the mean U wind speed (streamwise velocity) at the end of the boundary layer development section in front of the model area. Wind tunnel measurements in red and a power-law fit with $\alpha = 0.23$ in black. The confidence interval of the velocity measurements is represented by the red bars.

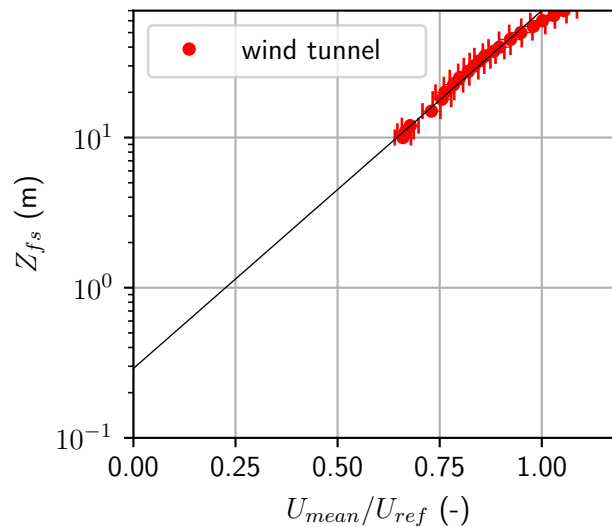


Figure 4.18: Vertical profile of the mean U wind speed (streamwise velocity) at the end of the boundary layer development section in front of the model area in a semi-logarithmic scale. Wind tunnel measurements in red and the logarithmic fit for the roughness length $z_0 = 0.29$ m in black. The confidence interval of the velocity measurements is represented by the red bars.

vertical wind profile. The confidence interval for the vertical turbulent momentum flux is approximated with $\pm 10\%$. Similar to the moderately rough boundary layer, measurements close to the roughness elements are not regarded and indicated with an empty circle. In this configuration the biggest roughness elements have a height of 5 cm (5 m in full-scale), so measurements below 20 m are excluded. The shaded area marks the vertical turbulent momentum flux at 20 m height $\pm 10\%$ deviation. The vertical

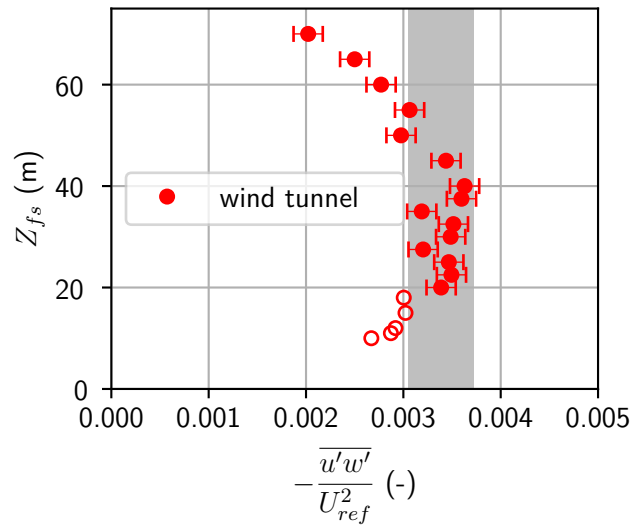


Figure 4.19: Vertical turbulent momentum fluxes measured at the end of the boundary layer development section in front of the model area. Measurement points below a height of 20 m are not considered due their vicinity to the roughness elements and are therefore indicated by empty circles. The confidence interval of the turbulent momentum fluxes is represented by the red bars.

momentum fluxes stay approximately constant for a height of up to 45 m and indicate a Prandtl layer height of 45 m.

By following the same procedure as in Section 4.4.2, the roughness length of the modelled boundary layer is derived by performing a linear fit to the vertical wind profile on a semi logarithmic scale (Fig. 4.18). From the linear fit a roughness length $z_0 = 0.29 \text{ m} \pm 0.05 \text{ m}$ is derived. Similarly as for the moderate rough boundary layer the uncertainty for the roughness length is derived by performing the linear fit on repetition measurements and measurements in a different lateral position.

Again following the roughness class definitions of the VDI (2000), the derived roughness length lies in the range of the class of rough terrain. The proposed range for the rough terrain class ranges from 0.1 m to 0.5 m. With a roughness length of $0.29 \text{ m} \pm 0.05 \text{ m}$ the modelled boundary layer fits well into that range. With this profile exponent and roughness length the modelled boundary layer lies in the middle to upper end of the rough class. This can be associated with a suburban environment, which also represents the desired surrounding of models that will be placed inside this boundary layer.

Regarding the functional relationships formulated by Panofsky (1974) and Counihan (1975) the profile exponent and roughness length of this modelled boundary layer lies at the edge of the range of the proposed relation (Fig. 4.13). With Eq. 4.2 and $u_* = 0.345 \frac{\text{m}}{\text{s}}$, $z_0 = 0.29 \cdot 10^{-2} \text{ m}$ and $\mu = 14.9 \cdot 10^{-6} \frac{\text{m}^2}{\text{s}}$ the roughness Reynolds number is approximately 67. This fulfils the requirement of a roughness Reynolds number greater than 5.

The turbulence intensities of the rough boundary layer are shown in Fig. 4.20. For the relevant part of the modelled boundary layer, the Prandtl layer, the vertical profiles of the turbulence intensities agree well with the shapes of the reference curves of the VDI (2000). Above the Prandtl layer of the modelled boundary layer the vertical profile of I_u starts to slightly deviate from the proposed reference curves. In case of the I_v the deviation from the reference begins at a lower height and is slightly stronger. The

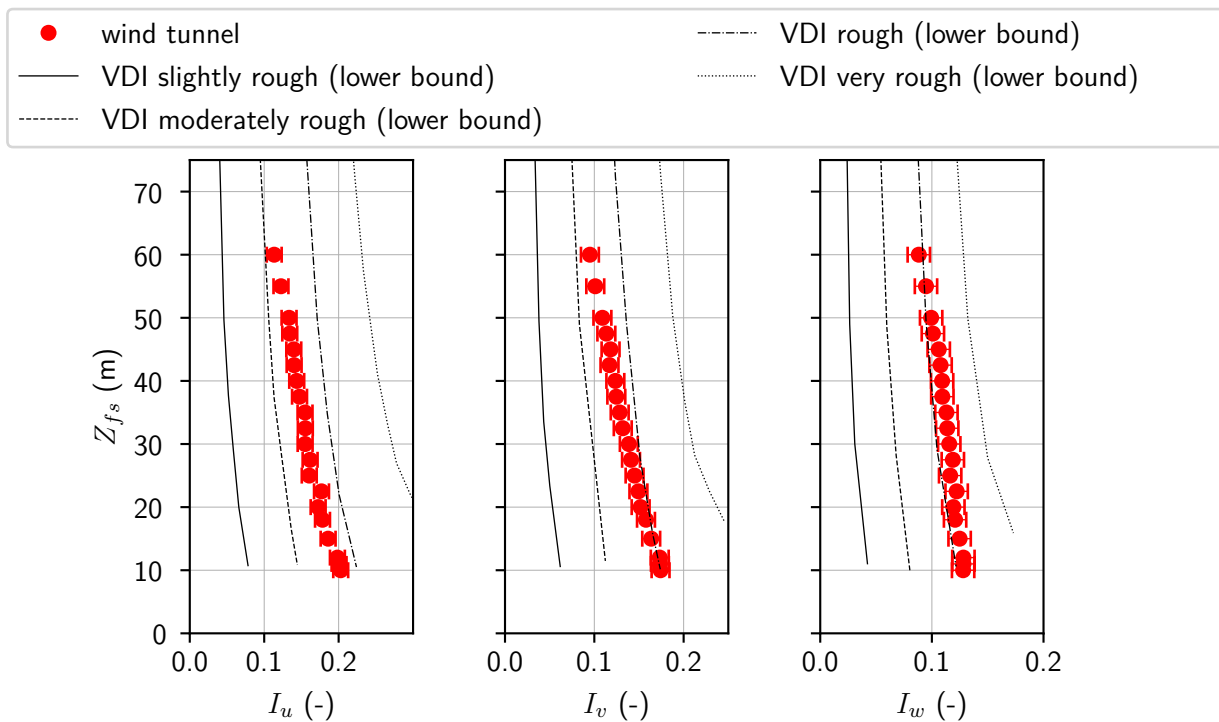


Figure 4.20: Vertical profiles of the turbulence intensities of the u , v and w -components of the flow. Measurements performed at the end of the boundary layer development section in front of the model area. Reference curves are from VDI (2000). The confidence interval of the values for the turbulence intensities is represented by the red bars.

shape of the measured I_w shows an overall good agreement with the reference and similarly begins to slightly deviate above the Prandtl layer. In general, it can be observed that measured ratios between the velocity components (u , v and w) deviate compared to the ratios between the components which have been proposed by Panofsky (1974) and Arya (1982). However, the ratios between the components remain comparatively stable over the height of the Prandtl layer. It has to be noted that the ratios (Panofsky, 1974 and Arya, 1982) between the individual components of the turbulence intensities have been derived for rural terrain. Furthermore, it can be noted that in case of wind tunnel measurements in the WOTAN boundary layer tunnel the turbulence intensities of the v and w -components are often higher compared to the reference (for example in rough boundary layers of Hertwig, 2013 and Harms, 2010).

In Fig. 4.21 the integral length scales of the modelled boundary layer are shown. Similar to the moderately rough boundary layer (Section 4.4.2) an increase in measurement height translates to a slight increase of size of the eddies. The measured integral length scales lie on the theoretical relation of the roughness length of 10 m. Similarly as for the moderate rough boundary layer the integral length scales of the eddies are approx. one order of magnitude smaller than the theoretical relation of Counihan (1975) suggests for a roughness length of $z_0 = 0.29$ m. This is again caused by the limiting size of the WOTAN wind tunnel and the height of the boundary layer.

Fig. 4.22 shows 1D auto-spectral energy densities for the u , v and w wind velocity components in comparison to empirical relationships for neutrally stratified boundary layer flows (Erdmann, 2017).

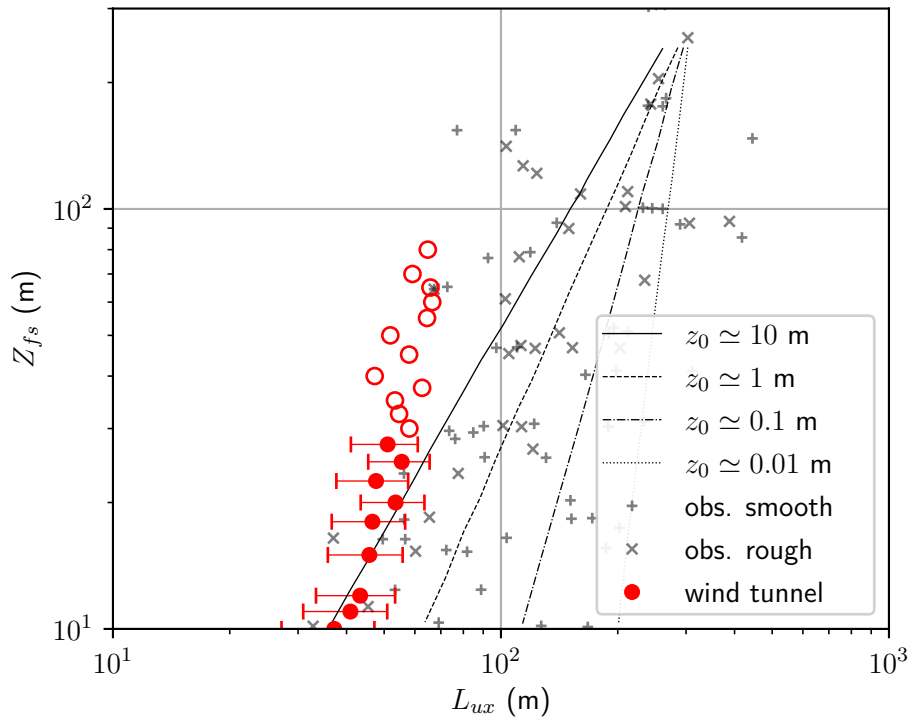


Figure 4.21: Vertical profile of the integral length scale of the mean flow in x direction (red dots). Field measurements from Counihan (1975). Obs. is short for observations. Plusses represent field measurements above smooth terrain with roughness lengths between 0.01 m and 0.1 m. Crosses represent field measurement above rough terrain with roughness lengths between 1 m and 10 m. The confidence interval of the values for the integral length scales is represented by the red bars.

The spectral distribution of the turbulent kinetic energy is made non dimensional with the standard deviation of the fluctuations of the main wind component. Fig. 4.22 show the spectral energy densities in a measurement height of 15 m at the end of the boundary layer development section.

In case of the turbulent energy spectra in a height of 15 m (Fig. 4.22) all wind components agree well with the shape of the reference spectra. However the position of the maximum of the turbulent energy of the u -component is shifted to slightly higher frequencies compared to the reference. This behaviour is not observed in the spectrum of the v and w -component of the flow. Here the measured turbulent energy spectra lie well in the reference ranges. It can be observed that the maximum of the turbulent energy of the w -component is shifted to slightly lower frequencies, but is still in the proposed reference range. Compared to the measured spectra in the moderately rough boundary layer the energy of the larger turbulent structures in the rough boundary layer show a better agreement with the references.

It can be observed that the decrease of the turbulent energy with increasing frequency deviates from the $-2/3$ slope. Due to the multiplication of the turbulent energy density with the frequency the characteristic $-5/3$ slope (Kolmogorov, 1991) turns into a $-2/3$ slope. One potential reason for the deviation from the usual $-2/3$ slope is an increased energy production in the presence of the strong wind speed gradient in the boundary layer.

At high dimensionless frequencies, above $5 \cdot 10$, the effect of aliasing becomes visible in the turbulent kinetic energy densities distributions of all wind components. The effects of the aliasing are visible at

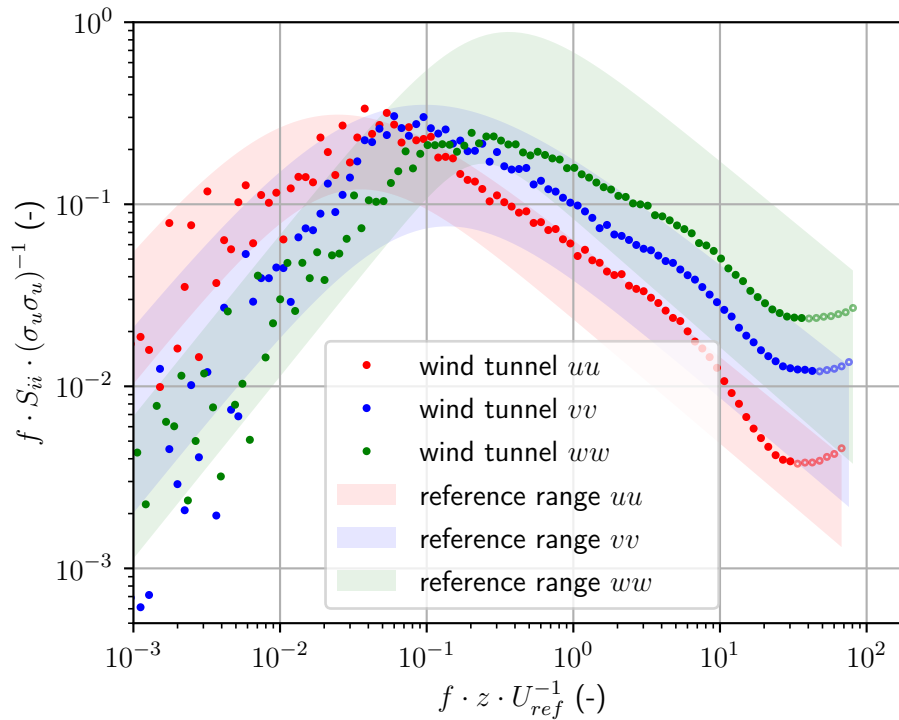


Figure 4.22: Normalized spectral distribution of turbulent energy at 15 m above the ground. Measurements performed at the end of the boundary layer development section in front of the model area. Reference range from Erdmann (2017).

slightly different dimensionless frequencies due to slightly different reference wind speeds and data rates. For example the v -component is sampled at approximately 3.3 kHz, while the u - and w -components are both measured at approximately 4 kHz.

Summing up, the rough boundary layer shows in general a good agreement with the reference data of VDI (2000), Counihan (1975) and Erdmann (2017). However, similarly to the moderately rough boundary layer (Sec. 4.4.2) the larger scales of the turbulence show differences compared to the reference data. Especially the turbulent length scales of the rough boundary layer deviate from the reference of Counihan (1975). Again, this is caused by the limited size of the wind tunnel and height of the modelled boundary layer. At a geometric scale of 1:100 turbulent structures larger than 1 m in model-scale (100 m in full-scale) are very difficult if not impossible to model in WOTAN.

Additional quality controlling of the rough boundary layer is presented in the Appendix A. The rough boundary layer shows lateral homogeneity of U_{mean} up to a distance of 50 m (full-scale) from the middle of the wind tunnel (Fig. A.3). Around $Y_{fs} = \pm 50$ m U_{mean} begins to deviate. The deviation is stronger in the negative y -direction. The majority of measurements are performed around the centre line of the wind tunnel. A Reynolds number independence test performed in the rough boundary layer is shown in Fig. A.4. The ratio between the measured wind speed and the reference wind speed remains constant within the measurement uncertainty for reference wind speeds between 1 m/s and 5 m/s. So, Reynolds number independence of the rough boundary layer flow is achieved for a reference wind speed of more than 1 m/s.

Chapter 5

Technical and Modelling Aspects

Heavy gas dispersion experiments inside boundary layer wind tunnels are subjected to several constraints and pose various challenges. In this section findings concerning technical and modelling aspects will be presented which have been found during the measurement campaign which accompanied the thesis. The findings are a combination of more general findings, which are related to the creation of realistic gas dispersion scenarios in boundary layer wind tunnels, but also of technical aspects like for example the selection of measurement locations. In the last section of this chapter an example on how to model a heavy gas dispersion scenario with a heavy gas effect is given.

5.1 Froude Number

As seen in Section 3.3 and Eq. 3.3 the densimetric Froude number (Fr_D) is influenced by three factors: the density difference between the released gas and the surrounding air, the volume flow of the release and the reference wind speed. To minimize Fr_D and maximise the heavy gas effect one wants to use a gas with a density as high as possible, use a wind speed as low as possible while still maintaining Reynolds number independence and increase the volume flow as high as acceptable to ensure sufficient similarity of the flow field. However this can not be performed freely and is heavily constrained by several controllable as well as inherently present factors. Due to the constraints it is not trivial to design a good experimental setup where a substantial heavy gas effect is present. A range of densimetric Froude numbers for a variation of the volume flow rate and the reference wind speed for a CO₂ release is shown in Fig. 5.1.

The biggest constraint to the range of the reference wind speed is the Reynolds number independence. In the case of the shown release scenario (Fig. 5.1), which also includes most of the used released scenarios in this thesis, the minimum reference wind speed to reach Reynolds number independence was experimentally verified to be approximately 1 m/s. In the models and experiments described in this thesis, reference wind speeds below 1 m/s do not fulfil the Reynolds number criterion and are not qualified for generating reference data sets. Thus the range of possible parameter combinations is constrained. This defines a lower bound for possible densimetric Froude numbers. For the presented configurations, this results in a smallest feasible Froude number using CO₂ as the released dense gas of greater than two. The range of reference wind speeds can also be constrained by the range of the operating speed of the wind tunnel (Sec. 4.1), but that does not further limit the possible densimetric Froude numbers in case of the dispersion scenarios of this thesis. If Reynolds number independence would have been achieved at lower reference wind speeds than 1 m/s, the minimum operating wind speed of WOTAN could have been changed by adjusting the pitch of the blades of the wind tunnel drive.

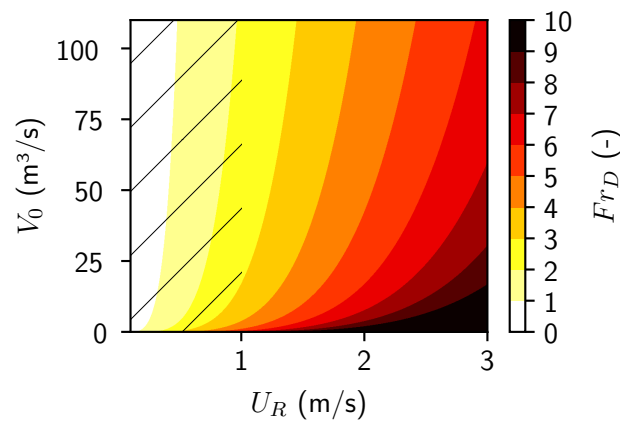


Figure 5.1: Range of densimetric Froude numbers for different values of volume flow rate and wind speed at a scale of 1:100. Assumed gas is CO_2 with a density of 1.8 kg/m^3 .

Another constraint is a limitation of the source volume flow rate. The volume flow rate can not be increased indefinitely since a high volume flow results in a high exit velocity from the source. The highest release rate presented in this thesis is approximately 2000 litres per hour in model-scale from a source with an area of 0.1 m^2 (40 cm by 25 cm). This translates into an exit velocity of less than 0.01 m/s . However if the volume flow rate is increased further and the source area is smaller, significant exit momentum might be reached. A high exit velocity from the source can counteract the heavy gas effect and can reduce the desired heavy gas effect. The influence of a source with a high volume flow on the flow further muddles the measurement results and can severely impede the ability to upscale the wind tunnel measurements to real scale. This obviously depends on the type of dispersion scenario. In case of a jet dispersion a significant exit momentum ratio from the source is present which has to be matched.

Achieving high volume flow rates is also possibly limited by technical aspects. In case of the experimental setup used for this thesis a strong throttling process was observed during very high volume flow rates. This resulted in an ice build up on the piping and the pressure regulators on the CO_2 gas bottles. The gas bottles contained pressurised liquefied CO_2 . The issue of ice build up on the tubing and the pressure regulators was solved with a gas preheater which counteracts the throttling process during the depressurization of the liquefied CO_2 .

The geometric scale of the model can improve or decrease the range of achievable densimetric Froude numbers. In case of the dispersion scenarios presented in this thesis the scale is 1:100. This scale is at the upper limit of possible geometric model-scales in the test section of WOTAN due to limitations in generating a physically similar ABL approach flow and is already showing deviation from reference data (for example in Section 4.4.2 the size of the integral length scales are too small compared to VDI, 2000). With the scale of 1:100 high release rates in model-scale still bear semblance to real world scenarios. For example a release rate of roughly 1800 l/h from a source area of 0.1 m^2 in model-scale translates into a release rate of $50 \text{ m}^3/\text{s}$ with a source area of 100 m^2 for a scale of 1:100. A volume flow rate of $50 \text{ m}^3/\text{s}$ is in the same order of magnitude as large CO_2 extinguisher systems (CEA, 2003) can provide. With a model-scale of 1:350 the range of possible densimetric Froude numbers changes drastically (Fig. 5.2). A release rate of 1800 l/h in the wind tunnel at a scale of 1:350 translates into a volume flow rate

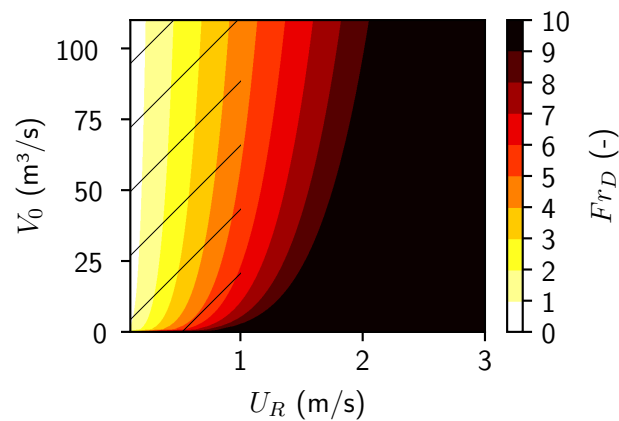


Figure 5.2: Range of densimetric Froude numbers for different values of volume flow rate and wind speed at a scale of 1:350. Assumed gas is CO₂ with a density of 1.8 kg/m³.

of around 2100 m³/s in full-scale. It is disputable if such high volume flow rates are still realistic. The range of possible densimetric Froude numbers for a scale of 1:350 for a release of CO₂ is shown in Fig. 5.2. With the same constraint to the lowest wind speed, where Reynolds number independence is still achieved (approximately 1 m/s), feasible densimetric Froude numbers are around 5. So the bigger the model-scale, the wider range of densimetric Froude numbers can be modelled.

Another factor, which can be varied, to achieve a smaller densimetric Froude number is the selection of the heavy gas which is used for the release. In all experiments presented in this thesis, CO₂ is used as the released heavy gas. CO₂ has a density of approximately 1.8 kg/m³ at room temperature, which leads to an excess density of around 0.5 ($\frac{\rho_0 - \rho_a}{\rho_a}$). Compared to other heavy gases, this is a small excess density and results in a smaller heavy gas effect. However, using CO₂ has several advantages compared to other heavy gases. Compared to other gases the health risks of CO₂ are rather low and manageable. Drowsiness and reduced mental capacity can occur at CO₂ concentrations above 1%. CO₂ becomes a health hazard when the concentration in the breathed air rises above 2% - 10% (IFA, 2021). However with a suitable ventilation of the lab environment high concentrations of CO₂ can be prevented. CO₂ is not flammable and also a relatively cheap gas and can thus be used in large quantities. A heavy gas which often has been used in the past is SF₆. SF₆ has a density of approximately 6 kg/m³ at room temperature and has an excess density of 4. SF₆ is a very stable gas, non-flammable and non-toxic. Because of these properties SF₆ is a particular suitable gas for heavy gas experiments. With SF₆ as the released heavy gas, the range of possible densimetric Froude numbers expands significantly (Fig. 5.3). With a density excess of 4 densimetric Froude numbers between one or two are easily achievable at a model scale of 1:100. However the usage of SF₆ as a heavy gas also has severe drawbacks. The biggest issue with SF₆ is that extremely corrosive compounds form when high concentrations of SF₆ are burned inside the FID. The corrosivity of the products of combustion inside the FID renders the FID unusable after just a couple of hours of measurement time (Brautmeier, 2015). Additionally, SF₆ is expensive and has one of the highest global warming potentials. Due to its chemical stability one kilogram of SF₆ has a global warming potential of 22,800 kg CO₂ over the course of 100 years (Forster et al., 2007). Because of these reasons, CO₂ was chosen as model gas for all dense gas releases in this thesis.

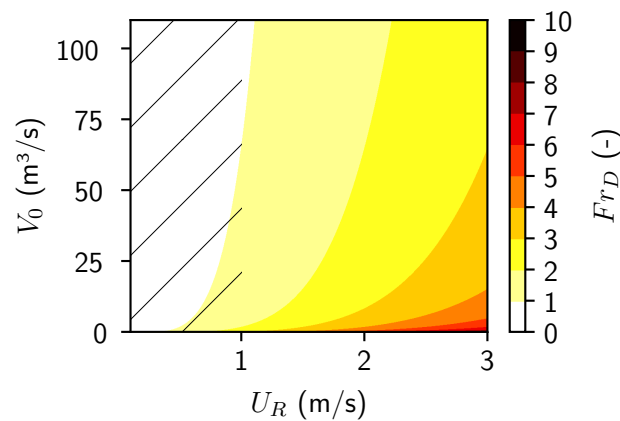


Figure 5.3: Range of densimetric Froude numbers for different values of volume flow rate and wind speed at a scale of 1:100. Assumed gas is SF₆ with a density of 6 kg/m³.

5.2 Selection of the Boundary Layer Flow

A large majority of historic heavy gas dispersion measurements, in the field and in wind tunnels, have been performed in either very smooth or smooth terrain (according to the roughness classifications from VDI, 2000). Many early wind tunnel measurement campaigns were performed as simulations of field campaigns and thus used the similar boundary layer flows compared to the field campaigns. For the field measurements it is expected that most, if not all, have been performed in locations where the ABL flows have very low to low roughness lengths (Tab. 5.1) since they are usually performed in open terrain and far away from settlements.

The field measurements in terrain with low roughness lengths were mostly performed in deserts. The roughness lengths of the Thorney Island field trials are higher compared to the rest, as it was performed on an island with a combination of mown grassland, runways and tidal flats (McQuaid et al., 1985). The Kit Fox field campaign was also performed in a desert, but there the experimenters placed wooden billboard obstacles to create an artificial roughness to simulate the roughness of an industrial site at a scale of 1:10 (Hanna and Chang, 2001). Beside the low roughness lengths many field and wind tunnel campaigns are performed with the absence of any obstacles or only replicate the orographic structure of the terrain of the desert or include single objects.

However, a couple of measurement campaigns like for example the MODITIC campaign and the Jack Rabbit 2 field trials included obstacles in their gas dispersion scenarios. The wind tunnel measurements of Robins et al. (2016) consist of measurements of simple geometries, more complex block geometries and a complex model of the inner city of Paris. The Jack Rabbit 2 field trials used a mock urban configuration consisting of more than 80 shipping containers (Spicer and Smith, 2021).

This short listing of existing heavy gas dispersion field and wind tunnel campaigns shows a knowledge and data gap for heavy gas dispersions in more rough boundary layers and also in model configurations with structures with of complexity. The project which accompanied the creation of this thesis aimed at the creation of a new near-source local scale data set of gas dispersion measurements for the development of new software tools for the simulation of accidental gas releases. For the creation of the data set

Table 5.1: Excerpt of the most important heavy gas measurement campaigns and the roughness length of the present ABL.

| Campaign name | Roughness length | Source |
|----------------------------------|---|------------------------|
| Thorney Island | $1 \cdot 10^{-2} - 2 \cdot 10^{-2} \text{ m}$ | McQuaid et al. (1985) |
| Burro and Coyote | $2 \cdot 10^{-4} \text{ m}$ | Havens (1992) |
| Maplin Sands | $4 \cdot 10^{-4} \text{ m}$ | Havens (1992) |
| Eagle, Desert Tortoise, Goldfish | $3 \cdot 10^{-4} \text{ m}$ | Havens (1992) |
| MODITIC | $8 \cdot 10^{-3} \text{ m}$ | Robins et al. (2016) |
| Jack Rabbit | $5 \cdot 10^{-2} \text{ m}$ | Hanna et al. (2012) |
| Kit Fox ERP | $1.2 \cdot 10^{-1} - 2.4 \cdot 10^{-1} \text{ m}$ | Hanna and Chang (2001) |
| Kit Fox URA | $0.1 \cdot 10^{-1} - 0.2 \cdot 10^{-1} \text{ m}$ | Hanna and Chang (2001) |

extensive measurements in the three presented configurations (Section 4.3) and two boundary layers (Section 4.4) were performed. In total, measurements were carried out at more than 2000 locations for flow measurements, 1200 for neutral density and 1000 for heavy gas dispersion measurements.

5.3 Development of the Dispersion Scenarios

Setting up a dispersion scenario including the model inside a wind tunnel needs careful planning and adjustment. Defining a clear goal or having a real dispersion scenario helps to narrow down parameters and the creation of a wind tunnel model. In this thesis, the dispersion scenarios were constructed in close cooperation with CFD modellers and safety engineers from the University of Rostock and the Bundesanstalt für Materialforschung und -prüfung (BAM). They provided valuable insights and information about realistic dispersion scenarios and articulated specific needs for the verification of the CFD models.

Similar to the MODITIC measurement campaign the dispersion scenarios presented in this thesis are designed with an increase of complexity. The first very idealistic model configuration without obstacles is aimed at the creation of neutral density and heavy gas dispersion data for the validation of CFD models without the disruptive influence of buildings. This model also served as a study to investigate the influence of individual roughness elements on the flow and the gas dispersion (Sec. 6.4). In the second model configuration, the idealized industrial park, a dispersion of gas from a CO₂ extinguishing system of a storage or manufacturing hall is investigated. The dispersion experiments are performed in two different boundary layers. The third and most complex model is a part of a chemical industrial park. In this model a dispersion from a collecting basin with various types of obstacles is investigated.

All models were manufactured with care to mitigate or prevent steps between joints. Cavities below and inside the models were sealed to prevent leakages and the accumulation of gases. The correct placement of the individual buildings were checked using the computer controlled traverse system of the wind tunnel.

5.4 Measurement Locations

As mentioned before, part of the project work, which accompanied the writing of this thesis, was the creation of a reference data set for the verification of newly developed CFD models. While creating a reference data set the measurement locations inside the models need to be determined in a way to use the measurement time as effective as possible. A grid of flow measurements with high spatial resolution over the whole model area would potentially capture most of the relevant flow features of the model configuration but would also take a lot of measurement time. Using a coarse grid for the whole model area to capture the general flow structure inside the model and using a fine measurement grid in the vicinity of the source can lead to measurement time saving and enables more variation of the source or the boundary layer inflow. This is especially important for the selection of the measurement locations of the concentration measurements. Concentration measurements obviously should be focussed in the area of dispersion and at the corresponding edges of the plume. By focussing the concentration measurements on the gas plume and its vicinity the experimenters can use the measurement time more efficiently. This, however, is not trivial and potentially needs steady reiteration of the measurement plan.

Almost all measurements presented in this thesis and measurements in the data set are carried out close to the ground. This is mainly motivated by the fact that almost all human activity is in a height of 0 m - 2 m above ground. In the case of the flow measurements this is in contrast to existing data sets like for example the CEDVAL data set (EWTL, 2006), where many measurement points are in heights above 10 m to 20 m. In the newly created data set approximately 45% of the flow measurements locations are in a height of 4 metres or less.

The locations for the heavy gas measurements presented in this thesis are close to the ground (roughly 2/3 below two metres) to sufficiently capture the heavy gas cloud. The heavy gas cloud mostly has a height of approximately two to three metres in the different model configurations. This selection of the measurement locations close to the ground and the walls is problematic for LES models based on the Monin–Obukhov similarity theory (MOST), which is not defined for measurement locations close to walls (Basu and Lacser, 2017). CFD models which are compared to this data set will probably show a lower agreement to the reference values compared to other data sets which do not focus on the lowest 2 metres.

5.5 Achieving a Heavy Gas Effect

This section presents an approach on how to perform a heavy gas dispersion experiment in a model configuration. This is exemplary shown for the industrial chemical park model (Section 4.3.3). As seen in Sec. 5.1, a reference wind speed as low as possible is desired to maximise the heavy gas effect. However, the reference wind speed can not freely be varied and is constrained by the necessary Reynolds number independence of the flow.

As a first step, a Reynolds number independence test is performed to ascertain the lowest reference wind speed where independence of flow patterns and turbulence characteristics is still achieved. Results from a corresponding Reynolds number independence test are shown in Fig. 5.4. For this, trace gas dispersion measurements were used to verify Reynolds number independence of flow and dispersion processes. At three locations critical with respect to Reynolds number dependence of flow and dispersion

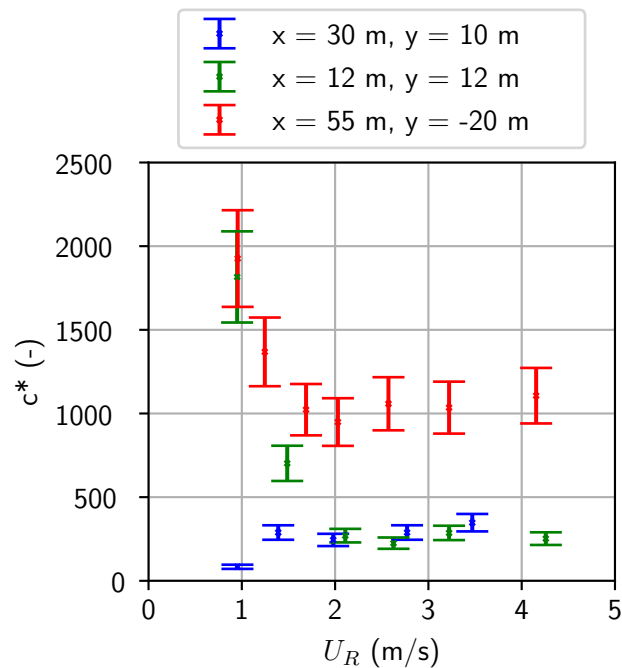


Figure 5.4: Reynolds number independence test at reference wind speeds between 1 m/s and 6 m/s for three critical locations in the industrial chemical park model with 10 tanks on top of the collecting basins. Measurement heights for all points is 2 m. The confidence interval of the concentration measurements in this figure are $\pm 15\%$.

patterns, the dimensionless concentration of a neutral density gas release is shown in relation to the reference wind speed. Reynolds number independence is achieved when the dimensionless concentration (Eq. 3.2) does not change with a change of the reference wind speed. The three locations are selected to represent different flow regimes and are in close vicinity to the cylindrical tanks, which are critical in regard to Reynolds number independence (Sec. 3.1.1). For the measurements at $x = 55$ m, $y = -20$ m and $z = 2$ m (red points) and $x = 30$ m, $y = 10$ m and $z = 2$ m (blue points) Reynolds number independence is achieved at a reference wind speed slightly below 2 m/s. The concentration measurements at $x = 12$ m, $y = 12$ m and $z = 2$ m (green points) show Reynolds number independence at reference wind speeds of approximately 2 m/s. With that, an overall minimum reference wind speed for the Reynolds number independence is assumed to be 2 m/s.

Prior to this, test modifications have been made to the original model configuration of the industrial chemical park model. Initially, the cylinders which represent tanks only had small indentations as surface roughness. This however proved to be insufficient and lead to Reynolds dependence of flow separation and corresponding changes in the flow and dispersion fields at reference wind speeds of 3 m/s. The roughness of the cylinder surfaces was increased and cylinders blocking the flow were partly removed until Reynolds number independence was achieved at reference wind speeds of approximately 2 m/s (as seen in Fig. 5.4). This lead to the model configuration with 10 tanks shown in Fig. 5.5, which then was used for the heavy gas dispersion experiments.

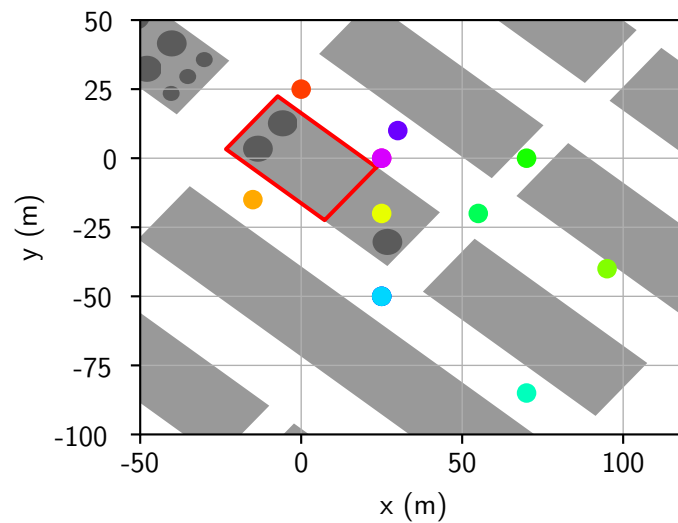


Figure 5.5: Measurement locations of the heavy gas dispersion measurements inside the industrial chemical park model configuration with 10 tanks (black circles). Wind direction is from left to right. The majority of the measurement points is in a height of one metre. The colours of the measurement points is the same as in Fig. 5.6 and Fig. 5.7.

The dispersion scenario in this configuration is a leakage of a liquefied gas from one of the tanks on top of the collecting basin (red rectangle in Fig. 5.5) which accumulates inside the collecting basin below the tank. The collected liquefied gas then slowly evaporates and disperses through the model area. With information provided from project partners working at the BAM, the assumed full-scale release rate of gas from a possible rate of evaporation is set at $2 \text{ m}^3/\text{s}$. This is a rate of evaporation which roughly can be expected from a spill of propane of a size of 100 m^2 . At a temperature of 20°C propane has roughly the same density as CO_2 .

With a volume flow rate of $2 \text{ m}^3/\text{s}$, a reference wind speed of 2 m/s and a density of approximately 1.8 kg/m^3 the release has a densimetric Froude number of approximately 9. This is at the upper edge of where a heavy gas effect can still be expected. A further reduction of the heavy gas effect is caused by the large area of the source over which the release is spread out. All this results in very low measured relative concentrations at a release rate of $2 \text{ m}^3/\text{s}$ which are shown in Fig. 5.6. Even at measurement locations very close to the source (orange and yellow) the relative concentrations do not exceed 0.5%.

To find a dispersion scenario where a heavy gas effect could be observed the release rate was doubled four times up to a release rate of approximately $50 \text{ m}^3/\text{s}$. This obviously does not represent an evaporation from a collecting basin, but could represent a downward directed leakage of a gas from one of the tanks. The measured concentrations resulting from the increase of the release rate are shown in Fig. 5.6. Measurement points on the left side of the figure need to be regarded with caution because of their very low concentrations. At very low concentrations in the given configuration of below 10 ppm the calibration accuracy of the FID can substantially influence the measurement. The accuracy of the calibration of FID is around 3 - 5 ppm. Initially, a doubling of the release rate of heavy gas results in a doubling of the relative concentrations. This relation holds true for all measurement points up to a release rate of approximately $25 \text{ m}^3/\text{s}$.

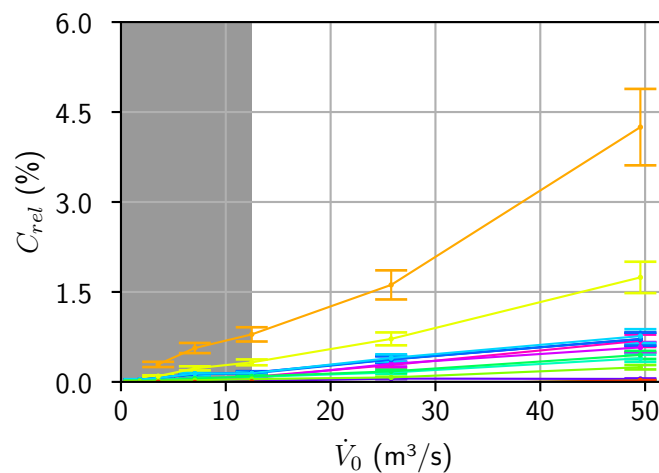


Figure 5.6: Relative concentrations measured at volume flow rates (full-scale) between $2 \text{ m}^3/\text{s}$ and $50 \text{ m}^3/\text{s}$ the measurement locations specified in Fig. 5.5. The grey box on the left side of the plot marks measurements where the uncertainty of the measurements is high due to the very low concentrations. At very low concentrations of just a few ppm the calibration of the FID has a big impact on the measured concentration. The confidence interval of the concentration measurements in this figure is approximated with $\pm 15\%$. Reference wind speed is 2 m/s .

At release rates above $25 \text{ m}^3/\text{s}$ the concentration measurements at two measurement locations (yellow and orange) show a greater increase of the relative concentration than just a doubling. This change in the behaviour is better visible in Fig. 5.7, where the measured relative concentration is divided

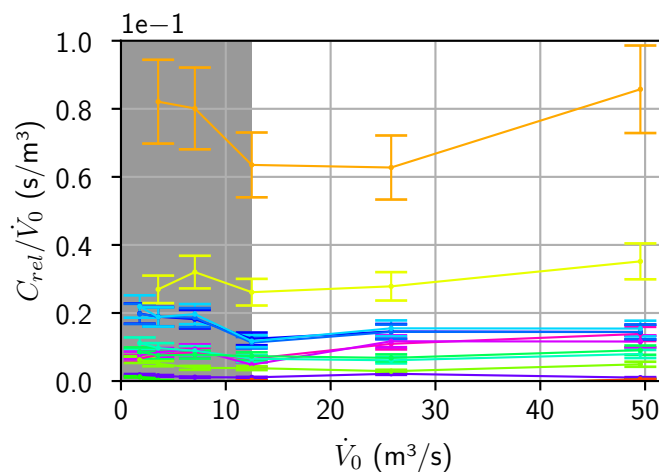


Figure 5.7: Relative concentrations divided by the volume flow rate at volume flow rates (full-scale) between $2 \text{ m}^3/\text{s}$ and $50 \text{ m}^3/\text{s}$ the measurement locations specified in Fig. 5.5. For more information read the caption of Fig. 5.6. Reference wind speed is 2 m/s .

by the release rate. Measurement points without the influence of the heavy gas effect would show a constant relation between C_{rel}/\dot{V}_0 and \dot{V}_0 . However the orange curve shows a strong increase of C_{rel}/\dot{V}_0 from $25 \text{ m}^3/\text{s}$ to $50 \text{ m}^3/\text{s}$ and the yellow curve shows a small but still significant increase from

25 m³/s to 50 m³/s. This change in the relation is not observed for the other measurement points. At reference wind speed of 2 m/s and a release rate of 25 m³/s or 50 m³/s the densimetric Froude number is approximately 5.6 or approximately 4.8 respectively. So for this explicit dispersion scenario and this selection of measurement points a heavy gas effect is starting to become relevant at densimetric Froude number of around five to six.

This example demonstrates the difficulty of achieving a significant heavy gas effect for heavy gas dispersion scenarios. At the minimum possible reference wind speeds (2 m/s) no heavy gas effect was observed for the initial scenario of the evaporation of the spillage. The scenario of the evaporation was however investigated at relatively high wind speeds which led to high densimetric Froude numbers. If the model configuration would have achieved Reynolds number independence at reference wind speeds of 1 m/s, a densimetric Froude number of approximately 4.6 at a release rate of approximately 2 m³/s could have been reached. By comparing this to the densimetric Froude number of a release rate of 50 m³/s and a reference wind speed of 2 m/s, it can be assumed that an evaporation of a spillage at lower wind speed also exhibits a dense gas effect. By using a different gas with a higher density like krypton, which has a density of 3.73 kg/m³, a densimetric Froude number around 5 could also have been achieved with a reference wind speed of 2 m/s and a release rate of 2 m³/s. Due to the high price of krypton this was however not feasible.

Chapter 6

Research Questions

6.1 Influence of the Boundary Layer Inflow on the Gas Dispersion

In this section the following research question is addressed: *What is the influence of a change of the boundary layer inflow on the flow and the dispersion of a neutral density and heavy gas inside a build up model area?* Changes in the boundary layer inflow result in differences in the local wind speed, turbulence intensities and other flow properties inside the model geometries. It however begs the question if these differences are strong enough to be visible inside the model geometry where the buildings strongly influence the flow. The investigations will be performed in the model geometry of the idealized industrial park. Flow, neutral density gas and heavy gas dispersion measurements were performed with two different wind tunnel boundary layers: a MRBL (Section 4.4.2) and a RBL (Section 4.4.3).

In the following subsections the influence of the boundary layer inflow on the flow inside the model geometry and on the neutral density and heavy gas dispersion will be presented and discussed. All heights stated in this chapter refer to height above ground.

6.1.1 Influence of a Boundary Layer Change on the Flow

To compare the influence of a boundary layer change on the flow inside the model configuration the MRBL and the RBL need to be referenced to same reference height. Regrettably the boundary layers presented in Section 4.4.2 and 4.4.3 were initially referenced to different reference heights (MRBL at 70 m and RBL at 60 m). For this subsection flow measurements in both boundary layers have been referenced to the same height of 50 m. Vertical wind profiles from the MRBL and the RBL referenced to a height of 50 m are shown in Fig. 6.1. A boundary layer flow resulting from a higher ground roughness is usually characterised by lower mean wind speeds and higher turbulence intensities. This influence on the mean U -wind speed is visible in Fig. 6.1. The turbulence intensities are higher in the rough boundary layer flow (comparing Fig. 4.14 and Fig. 4.20). To investigate the changes of the flow properties in the model, flow measurements at the same positions are compared between MRBL and RBL. The first investigated case is the 30° wind direction of the idealized industrial park model. Differences between MRBL and RBL in the horizontal mean wind speed are shown in Fig. 6.2. As shown in Fig. 6.1, the mean wind speed near the ground is lower in the RBL compared to the MRBL. The lower horizontal wind speed from the boundary layer inflow persists into the model area. At the beginning of the model area (left side of Fig. 6.2) horizontal wind speed differences are up to 20%. As the flow passes through the model area the initial differences in the horizontal wind speed become smaller and less significant.

Measurement locations where the relative difference between the two boundary layers is below the combined measurement uncertainty of both measurements ($\pm 6\%$ in case of the mean wind speed) are

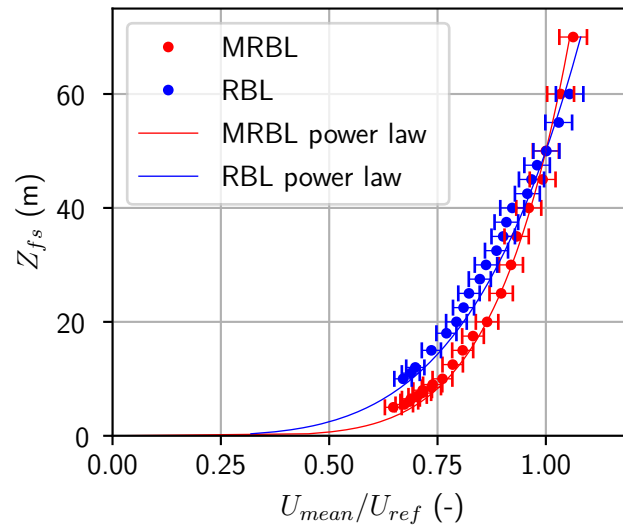


Figure 6.1: Comparison of the vertical wind profiles of the MRBL (red) and the RBL (blue). Wind tunnel measurements are represented by the dots and the power law representation of the boundary layers flows are represented by the lines. Measurement uncertainty are the bars and are listed in Tab. 4.3.

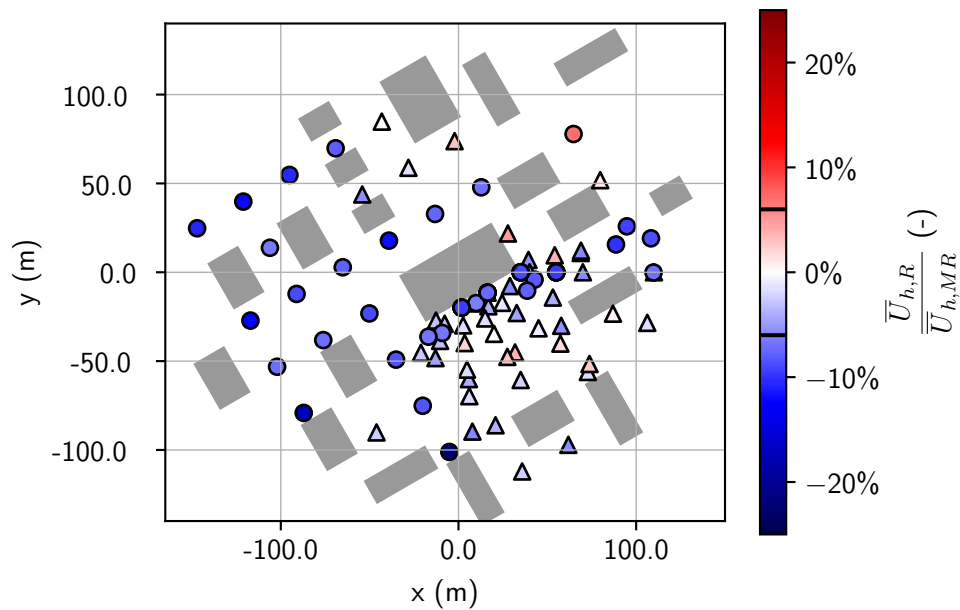


Figure 6.2: Relative difference of magnitude (horizontal wind speed) between the rough boundary layer inflow and the moderate rough boundary layer inflow. The subscript R indicates the rough boundary layer and the subscript MR indicates the moderately rough boundary layer. Blue colours indicate lower horizontal wind speed in the RBL compared to the MRBL. Wind direction is from left to right (M3). Measurement height is 2 m. Maximum measurement uncertainty ($\pm 6\%$) indicated with black lines on the colour bar. Measurement points within the range of the measurement uncertainty are indicated with triangles.

indicated with a triangle. These measurements are not inherently wrong, but have to be regarded with a higher degree of caution. General trends can still be recognized. In negative y -direction from the main

hall, in the middle of the model area the wind speed differences range between 0% - 10%. Singular measurement points indicate higher wind speeds for the RBL. This is potentially caused by local wind speeds close to 0 m/s, where small absolute differences can lead to high relative differences.

The RBL boundary layer is characterised by higher turbulence intensities compared to the MRBL (compare Fig 4.14 and Fig. 4.20). This difference in the turbulence intensities is also visible in Fig. 6.3 and Fig. 6.4. The turbulence intensities in the model area are in general higher for the RBL compared

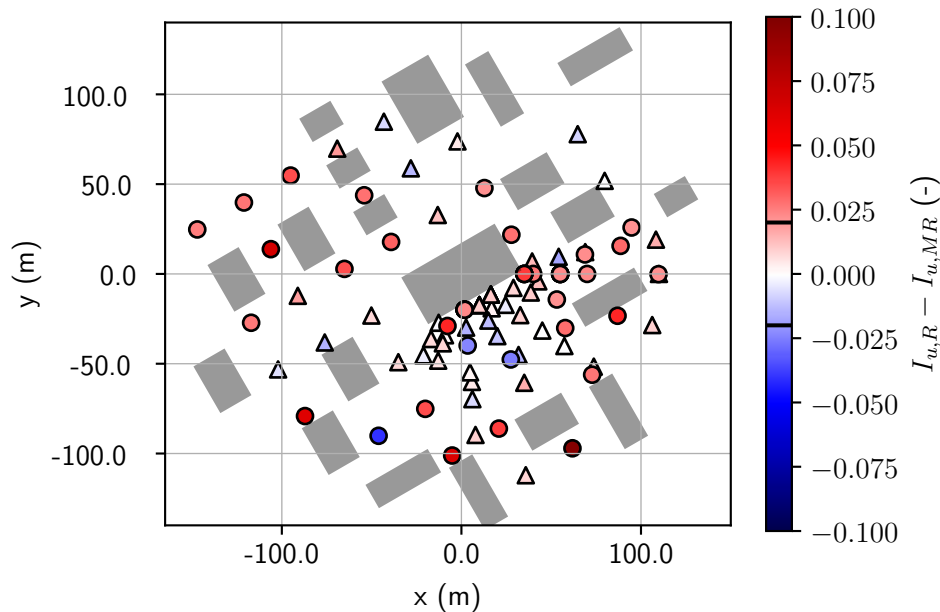


Figure 6.3: Absolute difference of turbulence intensity I_u between the rough boundary layer inflow and the moderate rough boundary layer inflow. Wind direction from left to right (M3). Maximum measurement uncertainty (± 0.02) indicated with black lines on the colour bar. Measurement points within the range of the measurement uncertainty are indicated with triangles. Measurement height is 2 m.

to the MRBL. Similar, as for the horizontal mean wind speeds (Fig. 6.2) the positive differences are most significant at the beginning model area and diminish the further down stream the measurement locations are. In negative y -direction from the main hall positive and negative absolute differences in the turbulence intensities are visible. Overall differences between RBL and MRBL are higher for the turbulence intensities in v -direction compared to the turbulence intensities in u -direction. Similar to Fig. 6.2, measurements with differences within the measurement uncertainty are indicated with triangles.

The area in positive x - and negative y -direction of the main hall is of special interest because it is in the near field of the source. Differences in the flow and the turbulence in the near field between both boundary layers can result in substantial changes in the dispersion of neutral density and heavy gases. In the near field of the main hall (in the positive x - and negative y -direction of the building in the middle of Fig. 6.3) the local horizontal wind speeds are approximately 10% lower in the RBL. Differences in I_u are mostly between 0 - 0.035. These values are however partly within the uncertainty of the turbulence intensities of 0.02. Differences in I_v in the vicinity of the main hall range between 0.01 and 0.05.

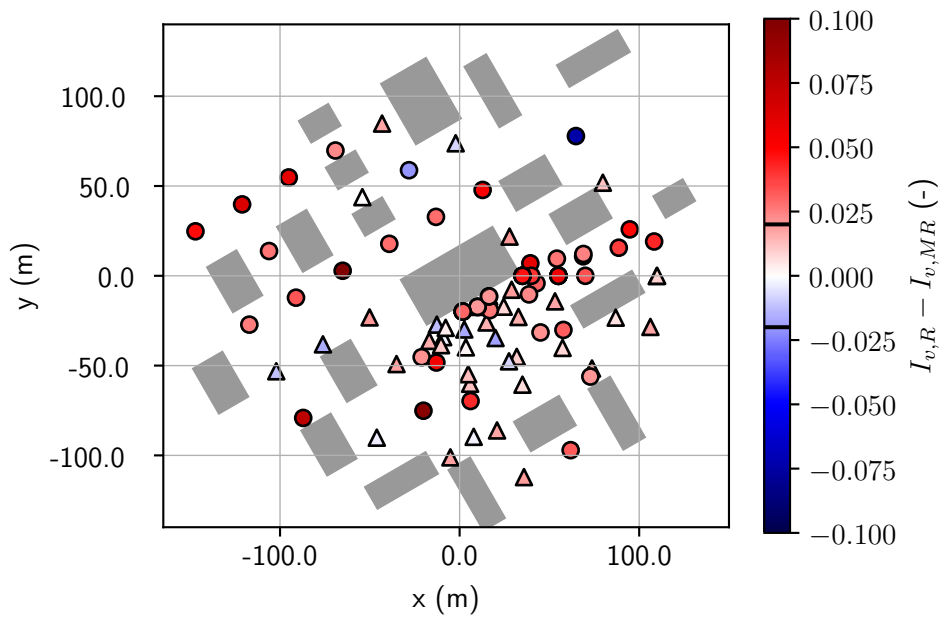


Figure 6.4: Absolute difference of turbulence intensity I_v between the rough boundary layer inflow and the moderate rough boundary layer inflow. Wind direction from left to right (M3). Measurement height is 2 m. For more information read caption of Fig. 6.3.

Comparisons of the mean horizontal wind speed and the turbulence intensities I_u and I_v between RBL and MRBL for the two other wind directions are not shown here, but are attached in Appendix C (M1: Figures C.1, C.2, C.3 and M2: Figures C.5, C.6, C.7). For the two other mean wind directions the influence of the change in the boundary layer has a comparable influence on the horizontal wind speed and the turbulence intensities inside the model configuration. Horizontal wind speeds are generally slower for the rougher boundary layer and the influence of the boundary layer change becomes less significant further downstream in the second half of the model area. Also, turbulence intensities are generally higher, however the trend which is observable in M3 is not as clear as in M1 and M2.

Since the influence of the boundary layer change is significant and observable in the three different wind directions it can be assumed that the findings can also be generalized to other model geometries. Depending on the magnitude of the change in roughness length the influence on the flow inside the model area might be substantial. In this thesis a boundary layer change of $z_0 = 0.06$ m and $\alpha = 0.16$ to $z_0 = 0.29$ m and $\alpha = 0.23$ showed significant impact on the flow inside the model configuration. The change in the z_0 and α represents a jump of one roughness class (VDI, 2000). So it can be assumed that changes in the boundary layer flow of the same or greater magnitude should result in a similar or greater change of the flow inside model configuration. Changes of the roughness class of the atmospheric boundary layer up to two classes are not unrealistic. For example a factory located at a lake or a sea coast on the one side and a city on the other side would experience a slightly rough boundary layer for one wind direction and a rough to very rough boundary layer for wind coming from the city side.

6.1.2 Influence of a Boundary Layer Change on the Neutral Density Gas Dispersion

The transport of a neutral density gas (in essence a passive tracer) at typical atmospheric wind speeds is dominated by advection and turbulent mixing. As seen in Section 6.1.1 the turbulence intensities increase with an increase of the roughness of the inflow boundary layer. However, also the horizontal wind speed decreases. In this section, the influence of the boundary layer change from MRBL to RBL on the neutral density gas dispersion will be investigated.

For this, the dimensionless concentrations measured in both boundary layers are compared. Fig. 6.5 shows a section of the M3 configuration of the idealized industrial area model on the downwind side of the main hall and focusses on the dispersion area. The wind direction of this configuration is 30° .

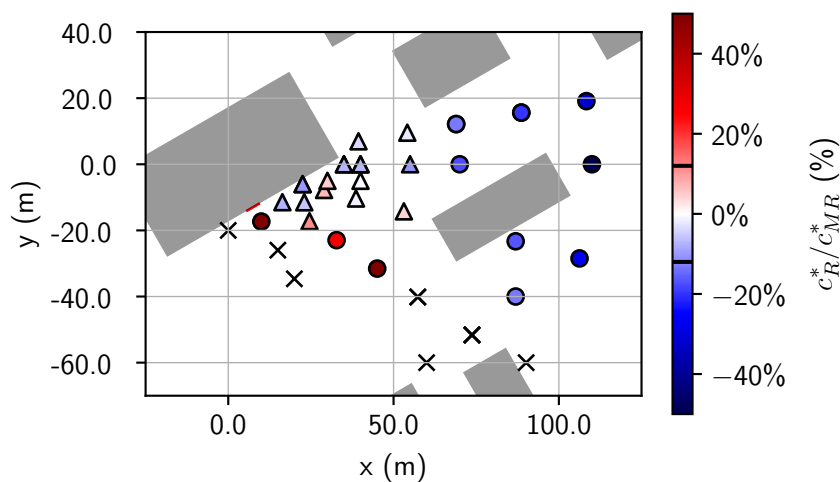


Figure 6.5: Relative difference between the dimensionless concentration measurements of the RBL and the MRBL. Red colours indicate higher concentrations for the RBL compared to MRBL. Similar to the Figures 6.2 or 6.4 measurement points where the relative difference is below the double of the confidence interval ($\pm 12\%$) are indicated with a triangle instead of a circle. The measurement uncertainty is indicated with black lines on the colour bar. Measurement locations where in both boundary layers no concentration is measured are indicated with a cross. Wind direction is from left to right (M3). Source is marked with a red line on the large building in the left side of the figure. Measurement height is 2 m.

The effect of the boundary layer change is clearly visible in Fig. 6.5. In the inner parts of the gas plume the dimensionless concentration is significantly lower in the rough boundary layer flow (blue colours) compared to the moderately rough boundary layer. At the edge of the gas plume the dimensionless concentrations are higher (red colours) in comparison to the moderately rough boundary layer. Similarly to the figures in Section 6.1.1 measurement locations with differences below the double of the confidence of the measurements are indicated with a triangle. Values at these measurement locations are not inherently wrong, but need to be regarded with caution.

While the significance of the difference of the flow between RBL and MRBL decreased with further distance from the beginning of the model, the significance of the difference of the neutral density dispersion increases with increasing distance from the source. This can be explained with the fact that the differences due to a change in the roughness layer are integral quantities and increase over time. E.g.

at measurement points far away from the source the gas cloud was subject to more mixing due to the higher turbulence intensities of the rough boundary layer.

The higher turbulence intensities are also causing the gas cloud to become wider. Therefore, the higher concentrations at the edge of the gas cloud are higher. However, the high relative differences at the edges of the plume need to be considered with caution because the low concentrations at the edge of the gas cloud potentially skew the comparison.

Similar to the non-ambiguous influence on the flow parameters for the 90° wind direction case (Fig. C.5, C.6 and C.7) the relative differences of the dimensionless concentrations are less systematic compared to the 30° wind direction case (Fig. 6.6).

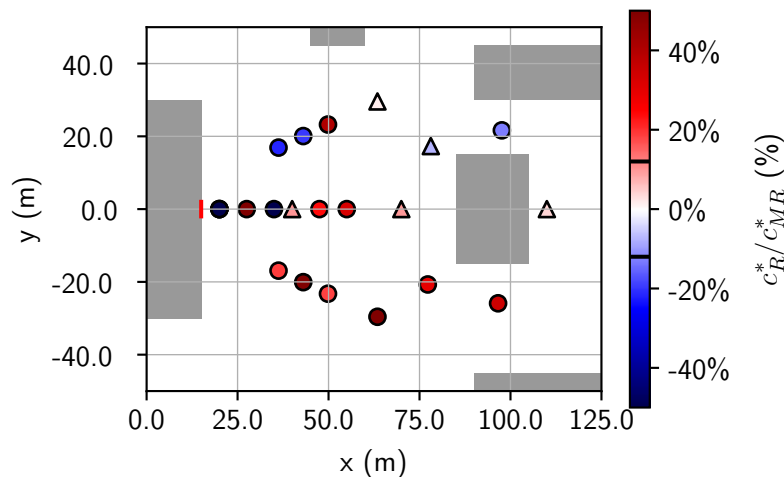


Figure 6.6: Relative difference between the dimensionless concentration of the RBL and the MRBL. For more information read subtitle of Fig. 6.5. Wind direction is from left to right (M2). Source is marked with a red line on the large building in the left side. Measurement height is 2 m.

For the M2 case (90° wind direction) the dimensionless concentrations are generally lower inside the recirculation zone behind the large main hall on the left side of Fig. 6.6 for the rough boundary layer. The recirculation zone of the main hall is visible in the mean wind direction and wind speed (Fig. 6.7). Here the mean wind direction is opposite to the main wind direction. Outside of the recirculation zone of the main hall the dimensionless concentrations are generally higher in the RBL. Further downstream in the vicinity of the building in the middle ($y = 0$ m) on the right side (x -coordinate wise) the relative differences are smaller compared to the edge of the recirculation zone.

The comparison of the dimensionless concentrations between the rough and moderately rough boundary layer for the 0° wind direction case (M1) show similar results as in the M3 case (Fig. 6.8). Dimensionless concentrations at the edge of the gas cloud are higher for the rough boundary layer. However, lower dimensionless concentrations are, with some exceptions which are within the measurement uncertainty, generally not observed in a measurement height of 2 m. Relative differences at the edge of the gas cloud are significant albeit high relative differences are partially caused by the comparison with very small dimensionless concentrations in the MRBL.

It is possible that the relative concentration difference is lower for the rough boundary layer in higher measurement heights, however this is not observed in the measured vertical profiles of the dimensionless

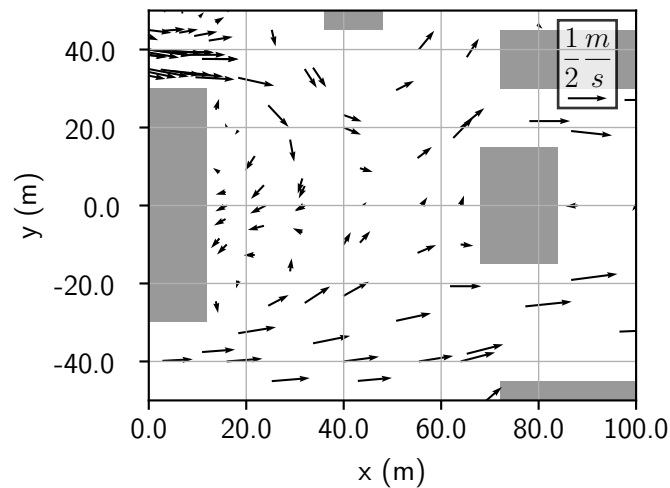


Figure 6.7: Mean wind direction and wind speed in a measurement height of 4 m. Wind direction is from left to right (M2) and the boundary layer is the MRBL.

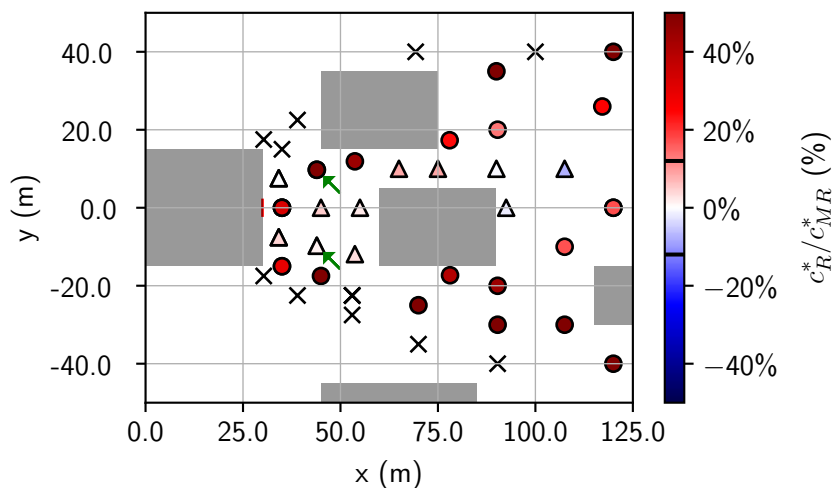


Figure 6.8: Relative difference between the dimensionless concentration of the RBL and the MRBL. For more information read subtitle of Fig. 6.5. Wind direction is from left to right (M1). Source is marked with a red line on the large building in the left side. Two locations with vertical profiles are marked with green arrows. Measurement height is 2 m.

concentration (Fig. 6.9). Regrettably, only two vertical profiles have been measured in this configuration. With the results from the comparison between the mean dimensionless concentrations of the neutral density dispersions in the RBL and MRBL it is hard to draw general conclusions regarding the influence of the boundary layer change on the mean concentrations. There are indications that the stronger turbulence can lead to a wider gas plume and lower concentrations within the plume inside the model area, but this is not visible for the three wind directions. For the neutral density dispersion for the 0° and 90° wind direction this general trend due to the influence of the boundary layer change is potentially obfuscated by the recirculation zones behind the buildings. The mean wind speed and mean wind direction for the 30° wind direction case (M3) of the idealized industrial zone model is shown in the

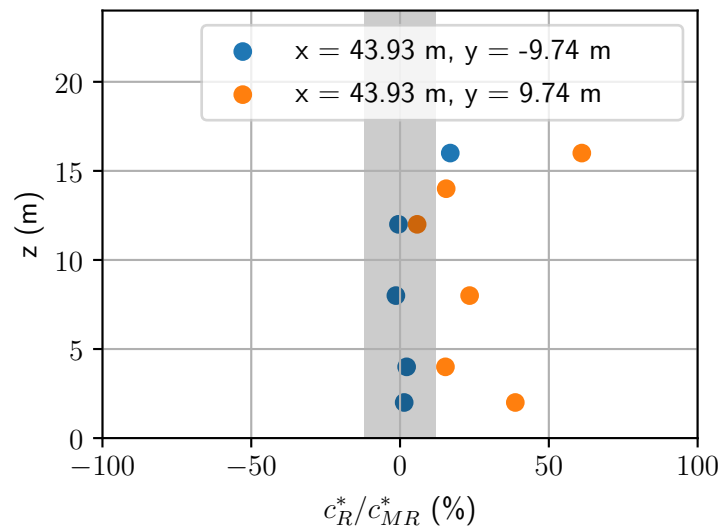


Figure 6.9: Relative difference between the dimensionless concentration of the RBL and the MRBL for two measured vertical dimensionless concentration profiles. The measurement locations of the vertical profiles are marked with green arrows in Fig. 6.8. The grey area marks the combined uncertainty of both measurements ($\pm 12\%$).

Appendix in Fig. C.9. In this figure measurements for both boundary layers are included. It can be seen that the locally measured wind direction does not significantly change with a change of the boundary layer. Furthermore, it can be observed that only a small recirculation zone is in the near field of the source which has been used in Fig. 6.5.

6.1.3 Influence of a Boundary Layer Change on the Heavy Gas Dispersion

In this section the influence of the boundary layer change on the heavy gas dispersion is presented. The influence on the mean relative concentrations is showcased (Fig. 6.10) for one configuration of the idealized industrial park (M3). As shown in Fig. 6.3 and Fig. 6.4 the turbulence in the near field of the source is stronger for the rough boundary layer compared to the moderately rough boundary layer. Furthermore also the mean horizontal wind speeds are lower for the RBL compared to the MRBL. This influence of the change of the flow inside the model area is visible in the relative differences of the mean concentrations. In close vicinity of the source and the source building the mean concentrations are higher. Further away from the source the mean concentrations are lower for the RBL compared to the MRBL.

One potential reason for this change in the mean concentrations is the stronger turbulent mixing which results in more vertical mixing of the heavy gas into higher elevations. This is visible close to the building, where the heavy gas concentrations close to the ground are high enough to still have a significant heavy gas effect. Another potential effect on the change of the dispersion of the heavy gas is the change of the mean horizontal wind speed. As seen in Fig. 6.2 the mean horizontal wind speeds are up to 10% lower in the vicinity of the source in the RBL compared to the MRBL. This change to lower mean horizontal wind speed changes the ratio between the buoyancy effect of the heavy gas and the advection and potentially results in a slightly stronger heavy gas effect.

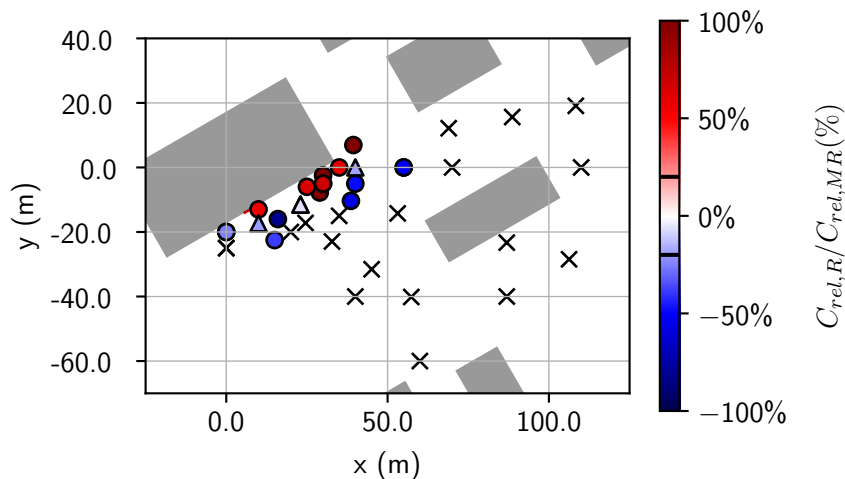


Figure 6.10: Relative difference between the mean relative concentration of a heavy gas dispersion for the RBL and the MRBL. Similar to the Figure 6.2 measurement points where the relative difference is below the double of the confidence interval ($\pm 20\%$) are indicated with a triangle instead of a circle. The measurement uncertainty is indicated with black lines on the colour bar. Measurement locations are indicated with a cross, if in both boundary layers the relative concentration is below 0.5%. Wind direction is from left to right (M3). This represents a wind direction of 30° . Source volume flow is $3.3 \text{ m}^3/\text{s}$ and reference wind speed is 1 m/s . The source is marked with a red line on the large building on the left side. Measurement height is 2 m.

The influence of the boundary layer change on the mean relative concentration for heavy gas dispersions in the configurations M1 (Fig. C.4) and M2 (Fig. C.8) are presented in the Appendix C. Overall, the relative concentrations in a height of 2 m are lower for both wind directions (M1 and M2) for the RBL compared to the MRBL.

In general, a significant change in the neutral density and heavy gas dispersion caused by the change of the boundary layer flow from moderately rough to rough is observable. However, observing a general trend is difficult. There are indications that the higher turbulence of the rougher boundary layer leads to a wider gas plume for the neutral density gas dispersion (Fig. 6.5). But this is only well observable for the 30° wind direction case (M3). For the other wind directions (0° and 90°) the influence of the buildings and their large recirculation zones lead to a more mixed picture, where no clear trend can be observed. This also applies for the heavy gas dispersion where a clear trend due to the change of the boundary layer is also difficult to observe. For the 0° and 90° wind direction it can be observed that the mean concentrations in a height of 2 m are generally lower for the heavy gas dispersion in the rough boundary layer. In the model configuration with the 30° wind direction mean concentrations close the source are higher in the rough boundary layer and lower outside of the close vicinity of the source and main hall (Fig. 6.10).

The findings of the influence of a boundary layer change in this section correspond with Britter and McQuiad (1988) (Section 3.3.2) who rank the influence of the surface roughness and the turbulent length scales in the ABL as significant but of lesser importance for a heavy gas dispersion. Britter and McQuiad (1988) describe the influence of the mean wind speed on the heavy gas dispersion as one of

the dominant factors. However, the presented heavy gas dispersion measurements were carried out at similar wind speeds and thus, the effect of a change of the mean wind speed can not be analysed.

6.2 Statistical Characterization of Measured Concentration

The statistical evaluation of heavy gas dispersions is still lacking in many field campaigns, wind tunnel experiments, dispersion models or guidelines. In many cases the simple arithmetic mean is still used to describe concentration distributions of gas dispersions. International norms (IEC, 2020) classifying areas in terms of explosion risk show deficiencies regarding the statistical measures and the description of presented CFD data is lacking. In the early days of field campaigns and wind tunnel experiments sensors and equipment were not able to capture time resolved concentrations and often measured dosages, which were transferred into means. With the technological advancement in the last 30 to 40 years better equipment was developed to capture instantaneous concentrations. For more recent field campaigns instantaneous concentrations are available. Dispersion models based on RANS only have mean values as their model output. In the case of intermittent concentration fluctuations it however begs the question if a mean value of a concentration is sufficient to address safety concerns. For example, Burgess et al. (1972) were able to achieve burning back to the LNG spillage source, while the mean concentration (averaged over 3 1/2 minutes) was just about 10% of the lower flammability limit (LFL). In this section the following research question will be addressed: *Is the arithmetic mean an adequate statistical measure to investigate heavy gas dispersions?*

The research question will be addressed by first identifying the issues with the arithmetic mean and then offering better suited statistical parameters to describe gas dispersions.

6.2.1 Issues with the Arithmetic Mean

In Fig. 6.11 two exemplary snippets are presented for two relative concentration time series measured in the idealized commercial area model. Both time series are measured at the same location and are rescaled to the same wind conditions and release conditions. The only difference between the concentration measurements in the two time series is the density of the gases.

The mean concentrations of both releases (red in Fig. 6.11) are relatively similar to each other (neutral 1.5%, heavy 2.6%). However, the fluctuations of the instantaneous concentrations differ significantly. The maximum neutral density gas concentrations measured in this snippet are around 4% (maximum in the total time series around 10%), whereas the maximum concentrations of the heavy gas release are almost one magnitude larger at approximately 30% (maximum in the total time series approximately 50%).

In case of a hydrogen sulfide gas release, which has a LFL of 4.3% (IFA, 2020), the interpretation of the mean concentration of the neutral density and heavy gas time series would result in a false sense of security because both mean values are below the LFL. However concentration peaks exceed the LFL of 4.3%. This is the case for the example of the heavy gas release and the total time series of the neutral density gas release (not shown in Fig. 6.11b).

The issue with using the arithmetic mean for determining safety distances in case of a heavy gas dispersion scenario becomes even more apparent in Fig. 6.12. Fig. 6.12 shows a two-dimensional view

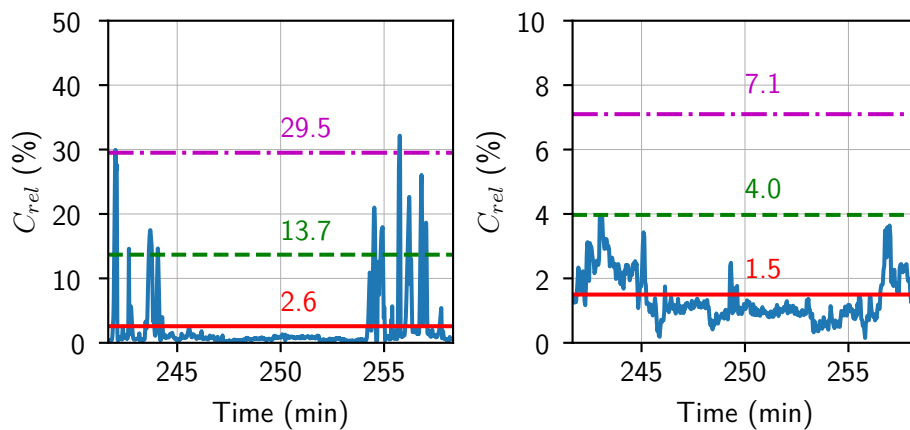


Figure 6.11: Relative concentrations for a heavy gas dispersion (left, a) and a neutral density gas dispersion (right, b). Measurement location at $x = 47.5$ m, $y = 0$ m, $z = 4$ m. Release conditions: M2, S1, the volume flow is $21 \text{ m}^3 \text{ s}^{-1}$, reference wind speed is 1 m/s . Mean concentration of the whole time series in red, 95th percentile in green (dashed), 99th percentile in magenta (dash dotted). Measurement uncertainties ($\pm 10\%$) are omitted for better visibility.

of measurement points where the LFL of a concentration of 4.3% is exceeded by either the mean (Fig. 6.12a) or the maximum value of the whole time series (Fig. 6.12b). By using the mean concentration to determine safety distances (mean concentration below the LFL of 4.3%), distances of 30 to 40 m from the source (red line at the side of the building in the left of Fig 6.12a) would be estimated. However, maximum concentrations of the individual time series are exceeding the LFL for all except one measurement location (Fig. 6.12b). It however begs the question if the maximum occurring concentration is a better measure for a safety evaluation, since singular measurements which might last for just a fraction of a second very likely do not pose a risk of deflagration or explosion (Britter and McQuiad, 1988).

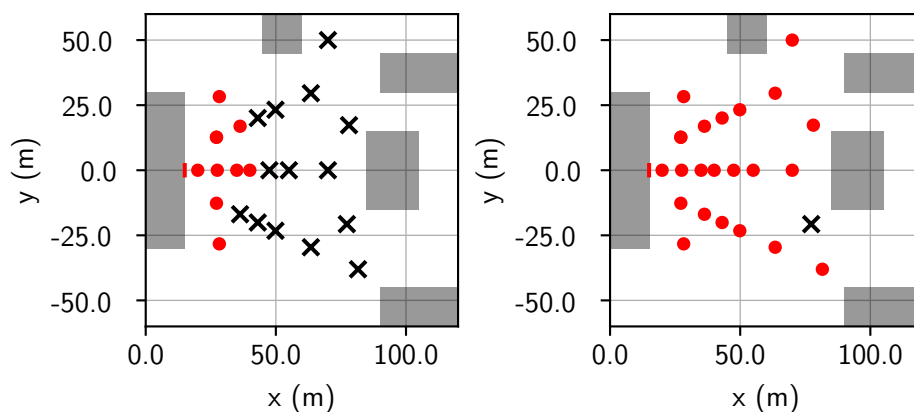


Figure 6.12: Left (a): Mean relative concentration of a heavy gas dispersion in 2 m height above (red dots) and below (black crosses) 4.3% for the release conditions stated in Fig. 6.11. Right (b) maximum relative concentrations in 2 m height above (red dots) and below (black crosses) 4.3% for the same conditions as in (a).

In regards to toxicological risk assessments the arithmetic mean is useful to calculate the toxic load (Boris and Patnaik, 2014). Due to the complexity and vast amounts of different toxic materials with different effects and risks, toxicological assessments are not further discussed here and the reader is referred to Mannan (2012).

Summing up, the arithmetic mean is not able to capture short spikes in the time series of the measured concentration. Regarding the presented exemplary time series of the neutral density gas dispersion this might not be a big issue since the peak concentrations are not that high compared to the mean. This behaviour obviously changes if the measured time series has a high peak to mean ratio. For the presented heavy gas dispersion the arithmetic mean fails to capture the variability of the concentration fluctuations and the concentration maxima. The importance to capture peaks in the concentration fluctuations are supported by the findings of Burgess et al. (1972), who were able to achieve burning back to source, while the mean concentration was approx. 10% of the LFL.

6.2.2 Suitable Statistical Measures for the Analysis of Gas Dispersion

To investigate the measurement data of neutral density and heavy gas dispersions in detail a deeper view into the concentration distribution is needed. For example a more robust statistical parameter is the k -th percentile. A k -th percentile is a measure which divides a set of data below a specific percentage k . So for example, a 95th percentile describes the value below which 95% of values of the time series are found. The 50th percentile which divides a data set into two halves, is also better known as the median.

The concentration distributions of the previously shown neutral density and heavy gas dispersion time series (Fig. 6.11) are shown in Fig. 6.13. The 95th or 99th concentration percentiles of both time series are included in Fig. 6.11 and 6.13. For the neutral density gas dispersion the 95th concentration percentile is a relative concentration of 4% and the 99th concentration percentile is a relative concentration of 7.1%. With these values the initial assessment of the comparison of the mean concentration of 1.5% and the LFL of 4.3% becomes questionable. For the heavy gas dispersion time series the comparison becomes even more lopsided. Here the 95th concentration percentile is 13.7% and the 99th concentration percentile is 29.5%. Both greatly exceed the LFL.

Percentiles, however, disregard the temporal and highly variable aspect of the concentration fluctuations. Very short concentration peaks of less than a couple of seconds might not be dangerous in regard to explosions or fire. For example in RIVM (2021) an averaging period of 18.75 s is given. So a short term exceedance of just a couple of seconds of a LFL would be accounted for as a "non-exceedance".

To account for short term peaks event statistics can be used. So for example a suitable condition for an event is the exceeding of a certain threshold like a LFL. Selecting an event duration is not trivial since there is very few experimental data on the risk of inflammation or deflagration regarding short concentration peaks. As a starting point, the previously stated 18.75 s (RIVM, 2021) is chosen. For simplicity this is rounded up to a minimum event duration time of 20 s. With an event duration of 20 s and a mean local wind speed of 1 m/s a gas cloud with a minimum size of 20 m which exceeds the chosen LFL can be observed. An inflammation or deflagration of such a gas cloud would already result in a severe health and security risk.

A statistical representation of such an event view on the dispersion scenario already presented in Fig. 6.12 is shown in Fig. 6.14. Close to the source (red line on the left building) the frequency of

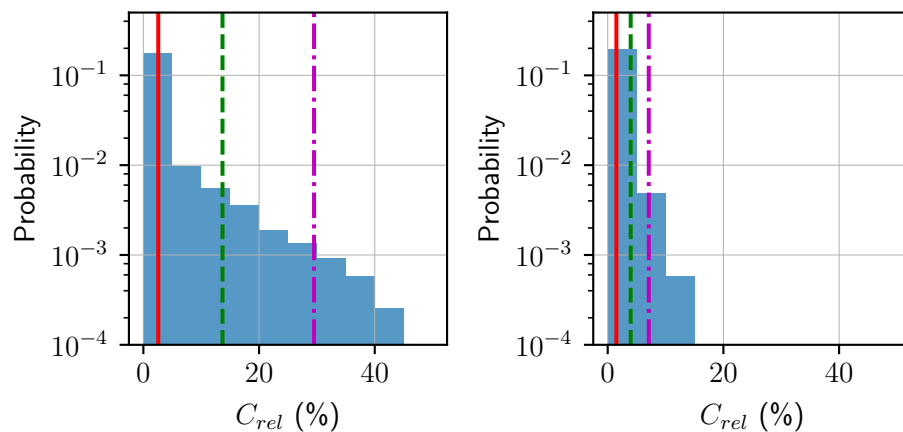


Figure 6.13: Normalized distribution of relative concentrations measured at the same location and conditions as in Fig. 6.11. Left (a) heavy gas dispersion, right (b) neutral density gas dispersion. Bin width is 5%. Mean concentration in red, 95% concentration percentile in green (dashed) and 99% concentration percentile in magenta (dashed dotted).

such an event, which exceeds the LFL, is almost 100% of the sampling time. With increasing distance from the source the frequency of an event with a duration of 20 s decreases substantially. However, at a distance of 70 m from the source the relative frequency of such an event is still approximately 2%. For the measurement duration of approximately 8.5 hours this translates into approximately 15 minutes where the presented event is measured. The upper most point (y-axis wise) shows no exceedance when the LFL is compared to the mean (Fig. 6.12a), whereas in the event view it shows an event frequency of approximately 1% (approximately 8 minutes in full-scale).

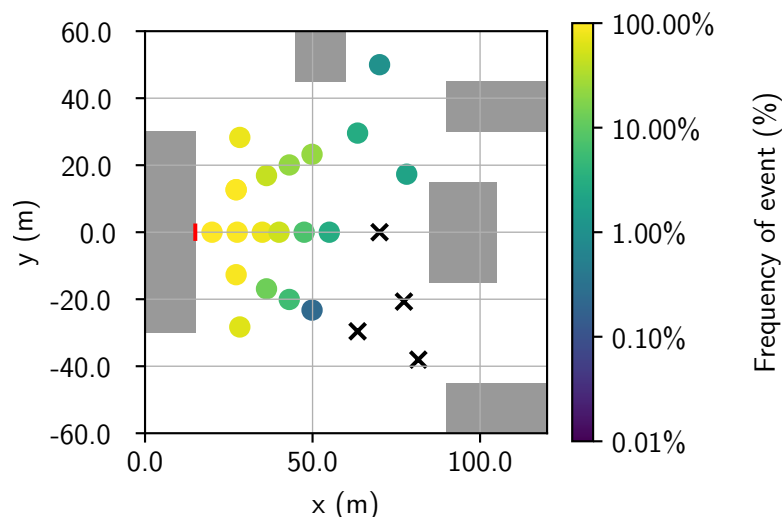


Figure 6.14: Frequency of a concentration event which exceeds a LFL of 4.3% over a duration of at least 20 seconds. Same release conditions as in Fig. 6.11.

In this section the advantages and disadvantages of various statistical parameters have been presented. The arithmetic mean is a simple statistical parameter which can give a quick but albeit shallow view

into time series of concentration data. For flammability risks assessments the arithmetic mean is only a crude proxy to get a general overview. However, in case toxic dispersion scenarios the mean is a useful statistical measure to calculate the toxic load (Boris and Patnaik, 2014). For a more in-depth view on the statistics of gas dispersion of flammable materials the usage of percentiles or more complex statistical measures like event statistics appear more suitable.

6.3 Local Concentration Statistics

Locally measured concentrations in dispersion scenarios are influenced by a multitude of factors. The main drivers of a dispersion scenario are the upwind and local wind conditions, building geometries, type of release, release parameters and the gas itself. Depending on the density of the released gas large differences can be expected in the distribution of the locally measured concentration. By investigating the local concentration distribution indications whether the location is affected by a heavy gas effect and how strong the heavy gas effect is can be found.

Four exemplary local concentration distributions of a heavy gas dispersion measured inside the idealized commercial area model (M2) are presented in Fig. 6.15. The concentration distributions are measured along the $y = 0$ m axis at varying heights and varying distances from the source. In terms of proximity to the source and the ground the distributions are ranked from 6.15a (farthest, red dots) to 6.15d (closest, green dots).

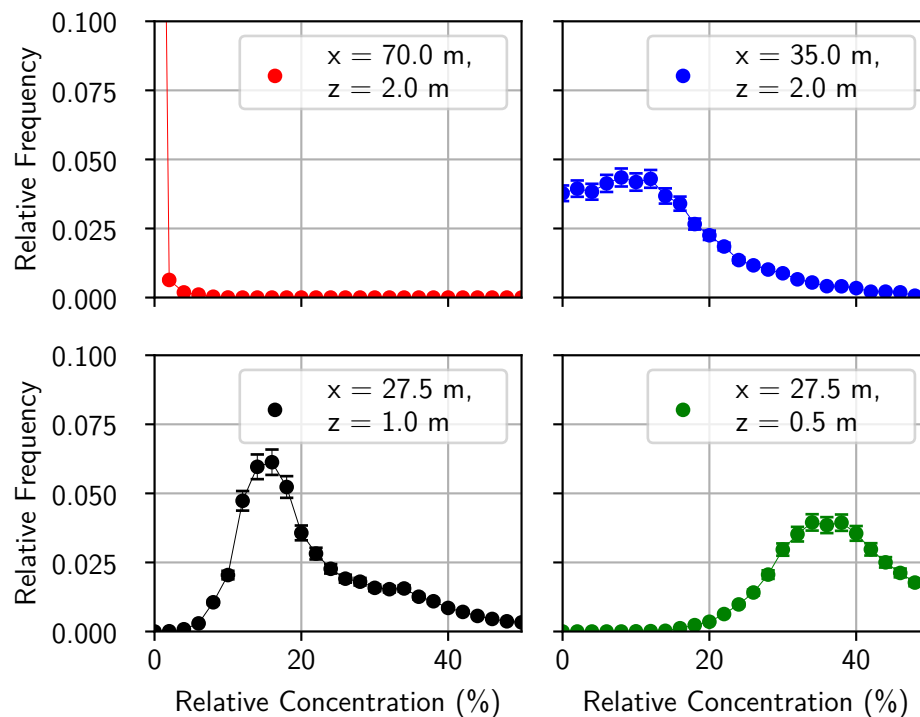


Figure 6.15: Normalized distribution of relative concentrations measured in the same configuration and under the same conditions as in Fig. 6.11a. The measured relative concentrations are binned into 50 bins with a width of 2%. The concentration distribution in red in the top left is sub figure (a), (b) is in the top right, (c) in the bottom left and (d) in the bottom right.

The concentration distribution shown in Fig. 6.15a (red curve on the top left) is measured at a distance of 55 m from the source and in a height of 2 m above ground. The relative concentration with the highest relative frequency is between 0% and 2% (out of frame). Approximately 99% of the measurements show a relative concentration of less than 2%. The relative frequency of higher concentration sharply decreases and concentrations above 2% are observed with a relative frequency of less than 1%. In a distance of 20 m to the source ($x = 35$ m, $y = 0$ m, $z = 2$ m) the distribution shifts to the right (Fig. 6.15b, blue curve on the top right). Here the relative frequency of the 0% to 2% relative concentration bin is approximately 8%. Up to the most frequently measured concentrations (approximately 12%) the relative frequencies of measured relative concentrations is almost constant. At higher concentration bins above the maximum at 12% the relative frequencies decrease. Relative concentrations above 50% occur with a frequency of less than 0.5%. Closer to the source ($x = 27.5$ m, $y = 0$ m, $z = 1$ m) (Fig. 6.15c, black curve on the bottom left) the distribution shifts further to the right. At this measurement position no fresh air was present for the entire sampling duration. Relative concentrations below 5% are measured with a relative frequency of less than 0.5%. Most frequently measured concentrations are around a concentration of 16%. Another local maximum of the frequency is observable at concentrations of 35%. At the closest measurement location to the source at a height of 0.5 m presented in Fig. 6.15d (green curve on the bottom right) the most frequent observed concentrations are around 36%. Relative concentration below 20% are very rare. To maintain comparability to the other concentration distributions (Fig. 6.15a-c) concentration values above 50% are left out of frame. Relative concentration measurements of 80% are observed with a frequency of approximately 0.5%. Overall it can be observed that by moving closer to the source and closer to the ground, the concentration distribution shifts to higher concentrations.

The shape of the presented concentration distributions measured inside a configuration with obstacles are subject to a multitude of factors as stated above. However, in the following only the influence of the distance to the source and height above ground is described.

Concentration measurements in this model configuration at locations in distances of more than 40 to 50 m to the source and in measurement heights of 2 m or higher show a similar concentration distribution as the distribution presented in Fig. 6.15a. With increasing proximity to the source and the ground the concentration distributions generally shift to higher concentrations as above and as expected. In this intermediate area, where the concentration distribution shifts from a behaviour shown in Fig. 6.15a, greatly varying concentration distributions like Fig. 6.15b and c are observed. The two presented distributions are not intended to cover the entire range of observed distributions but present examples of possible concentration distributions in the intermediate area. Measurements in close proximity to the source and the ground show concentration distributions similar to Fig. 6.15d. Depending on the distance to the source and height of the measurement the peak of the distribution is shifted or scaled (wider or narrower). From this observation of the concentration distributions, three different regimes are discernible: distributions characterised by generally low concentrations and no heavy gas effect, distributions inside an intermediate region where a significant heavy gas effect can be observed and distributions close to the source where a strong heavy gas effect is observed.

To find general properties of the concentration distributions and to accurately discern between the different regimes, a fitting distribution function is searched. From the plethora of different probability density functions (PDFs) the gamma distribution and the log-normal distribution appear suitable. Both

PDFs are able to describe the behaviour of the measured concentration distributions with a strong heavy gas effect and without a locally present heavy gas effect. The behaviour of the PDFs of the gamma and log-normal distribution is very similar (Vaz and Fortes, 1988, Wiens, 1999 and Bromideh and Valizadeh, 2014) and fits of both PDFs to the measured concentration distributions show good agreement. However, the representation of the different concentration regimes is more clear in the PDF of the gamma distribution. This will be shown in the following.

The PDF of gamma distribution in the shape-rate parametrisation has the following form

$$f(x; a, b) = \frac{x^{\alpha-1} e^{-\beta x} \beta^\alpha}{\Gamma(\alpha)} \text{ for } x > 0 \quad \alpha, \beta > 0, \quad (6.1)$$

with the shape parameter α , the rate parameter β and where $\Gamma(\alpha)$ is the gamma function. The $\Gamma(\alpha)$ function, for any positive real number α , is defined as

$$\Gamma(\alpha) = \int_0^\infty x^{\alpha-1} e^{-x} dx, \text{ for } \alpha > 0. \quad (6.2)$$

For more information on the gamma distribution the reader is referred to Hogg and Craig (1979). An example on how the PDF of the gamma distribution varies for arbitrary values is shown in Fig. 6.16. For values of $\alpha \leq 1$ the PDF of the gamma distribution decreases monotonously. If $\alpha > 1$, the rate

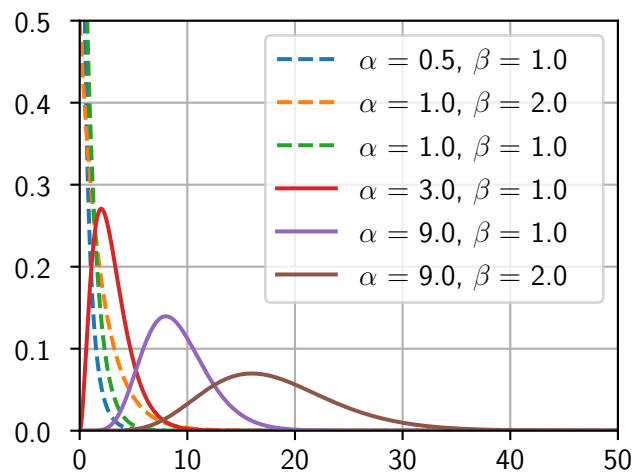


Figure 6.16: Examples for arbitrary gamma distributions for varying parameters of α and β .

parameter β determines the rate of the decrease. For higher values of β the decrease is smaller (compare the orange and blue line in Fig. 6.16). Concentration distributions without a significant heavy gas effect and which are monotonous decreasing can be described by a PDF of the gamma distribution with a shape parameter of $\alpha \leq 1$.

For values of $\alpha > 1$ the shape of the PDF of the gamma distribution changes and is no longer monotonously decreasing. Now the PDF originates from the origin, increases to a certain value and decreases afterwards. The combination of α and β determines the position, the height of the peak and the width of the PDF (red, purple and brown lines in Fig. 6.16).

Due to the rather simple behaviour of the PDF of the gamma distribution in regard to the shape parameter α , which alone can model the behaviour of concentration distributions without a heavy gas effect ($\alpha \leq 1$) or with a strong heavy gas effect ($\alpha > 1$), the gamma distribution is chosen for further analysis. The log-normal distribution is rejected because the shape of its PDF depends on a combination of two parameters instead of one.

Fits of the PDFs of the gamma distribution to the already presented measured relative concentration distributions (Fig. 6.15) are shown in Fig. 6.17. In case of the measurement with the highest distance to the source (Fig. 6.17a, red line) and the measurement closest to the source (Fig. 6.17d, green line) a fit of a gamma distribution is able to capture the characteristics of the measured concentration distribution. The fit to the concentration measurements with the largest distance to the source has an $\alpha \leq 1$, which represents a measurement location without a significant heavy gas effect, whereas the fit to the measurements closest to the source leads to an $\alpha > 1$ which is characterised by a location with a strong heavy gas effect.

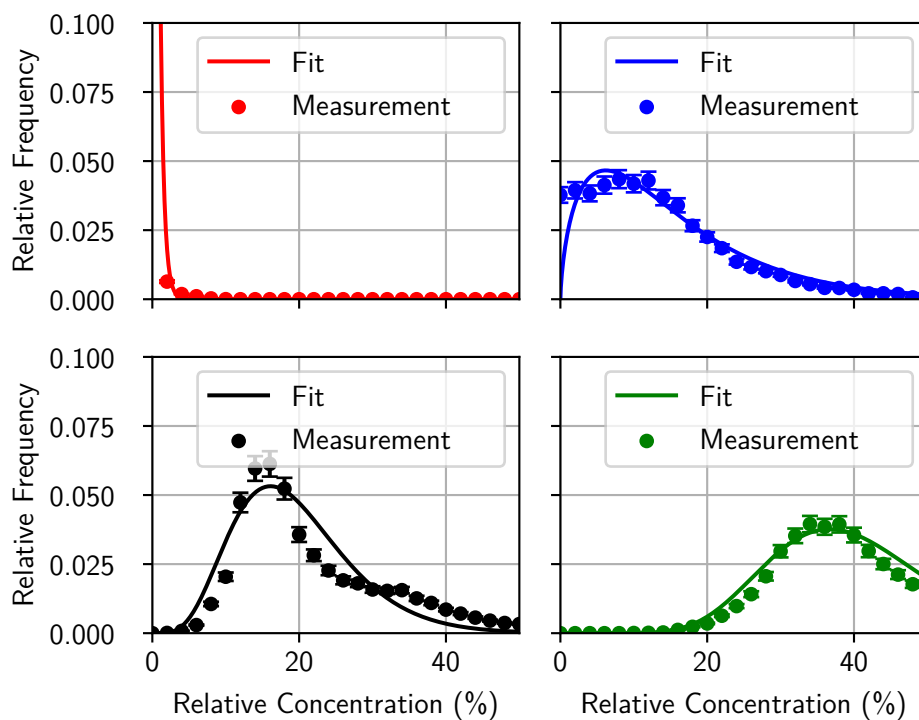


Figure 6.17: Normalized distributions of measured relative concentrations as shown in Fig. 6.13 including fits of PDFs of the gamma distribution. The concentration distribution in red in the top left is sub figure (a), (b) is in the top right, (c) in the bottom left and (d) in the bottom right.

The concentration distributions at the two measurement locations (Fig. 6.17b and c, blue and black lines) in the intermediate region are not well represented by the fit. The fit in Fig. 6.17b is not able to capture the frequency of concentrations below 4%. The fit in Fig. 6.17c roughly represents the shape of the concentration distribution but is not able to capture the local maxima on the tail of the distribution around relative concentrations of 34% and underestimates the frequency of higher relative concentrations. In general, fits with a singular gamma distribution are not able to accurately describe concentration distributions in the intermediate regime.

The lack of accuracy of the gamma distribution fits to the measured concentration distributions in the intermediate region shows a need for more sophisticated fitting. Concentration distributions in locations in the intermediate region are characterised by a combination of the other two regimes. In the intermediate region the concentration distributions, are in a transition from concentration distribution typical for a location without a significant heavy gas effect to a concentration distribution typical for a location with a strong heavy gas effect. Therefore, a combination of two gamma distributions is used to describe the distributions in the intermediate region. The PDF for the double gamma distribution has the following form:

$$f(x; \alpha, \beta, \gamma, \delta) = \frac{1}{2} \left(\frac{x^{\alpha-1} e^{-\beta x} \beta^\alpha}{\Gamma(\alpha)} + \frac{x^{\gamma-1} e^{-\delta x} \delta^\gamma}{\Gamma(\gamma)} \right) \text{ for } x > 0 \quad \alpha, \beta, \gamma, \delta > 0, \quad (6.3)$$

where α and β are the shape and rate parameter of the first distribution and γ and δ are the shape and rate parameter of the second distribution respectively. The used double gamma distributions is a simple sum of both individual distributions where each PDF is multiplied with factor of 1/2. Even though the approach of the double gamma distribution is more sophisticated compared to the single gamma distribution fit it makes no claim to be exhaustive. The combination of two gamma distributions is an idealistic attempt to combine the properties of a distribution without a significant heavy gas effect and a distribution with a strong heavy gas effect.

The introduced double gamma distribution (Eq. 6.3) is now fitted to the concentration distributions of the intermediate region (Fig. 6.17b and c). This is shown in Fig. 6.18. The fits in Fig. 6.18a and d are single gamma distributions, whereas the fits to Fig. 6.18b and c are now in the form of a PDF of a double gamma distribution.

The fits of PDFs of the double gamma distribution are able to reasonably describe the measured concentration distributions. In case of Fig. 6.18b the fit of the double gamma distribution now includes the low concentration values between 0% and 4% the singular gamma distribution was not able to capture. Furthermore, also the peak of the measured concentration distribution is better matched with the fit of the double gamma distribution. The fit for this concentration distribution is a combination of two gamma distributions, where one shape parameter $\alpha \leq 1$ and the shape parameter of the other distribution is greater than one. Good results for the fit are also achieved for the concentration distribution in Fig. 6.18c. With the fit of the double gamma distribution the peak of the distribution is well matched and also the tail of the distribution is sufficiently represented. Both shape parameters of this double gamma distribution are greater than one.

In case of the concentration distribution in Fig. 6.18d the argument can be made that a fit with a double gamma distribution would result in a better representation of the measured concentration. This is however a moot point because every distribution can be reproduced more accurately with a fit of a higher degree of freedom. The presented approach of fitting a single gamma distribution for distributions with or without a heavy gas effect attempts to model a distribution while remaining as simple as possible.

By now applying the previously described single and double gamma distribution fitting to each measured concentration distribution and categorizing the points into the three regimes on two-dimensionally distributed measurement points an insight into the spatial distribution of the specific regimes is possible. Such a categorization is presented in Fig. 6.19. In Fig. 6.19a (left) a configuration with a source volume

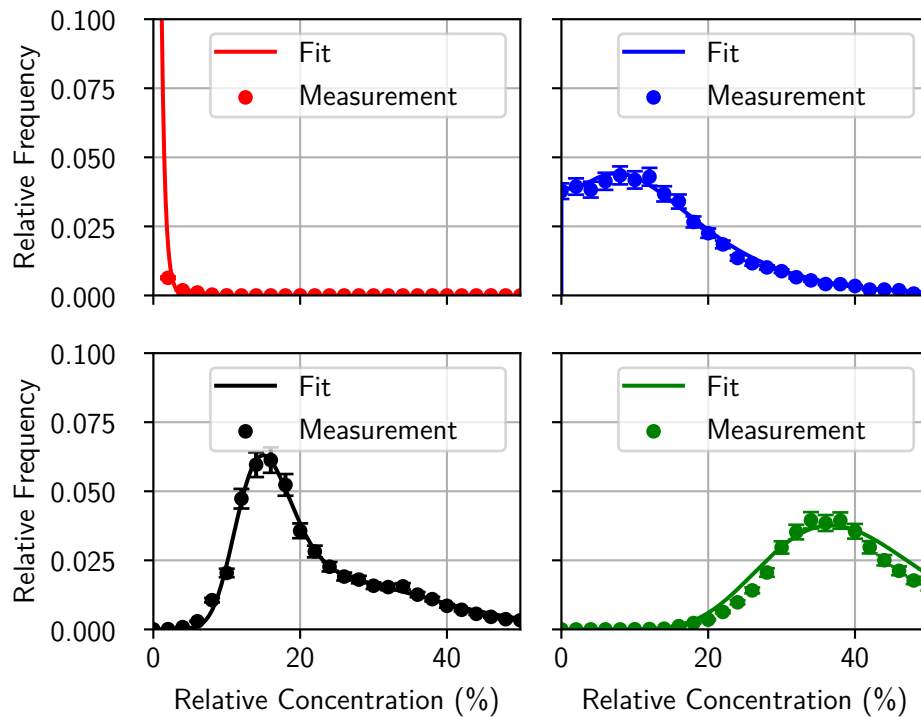


Figure 6.18: Normalized distributions of measured relative concentrations as shown in Fig. 6.17 including fits of PDFs of the gamma distribution. The fits in a and d (red and green lines) are singular gamma distributions (Eq. 6.1) and the fits in b and c (blue and black) are double gamma distributions (Eq. 6.3).

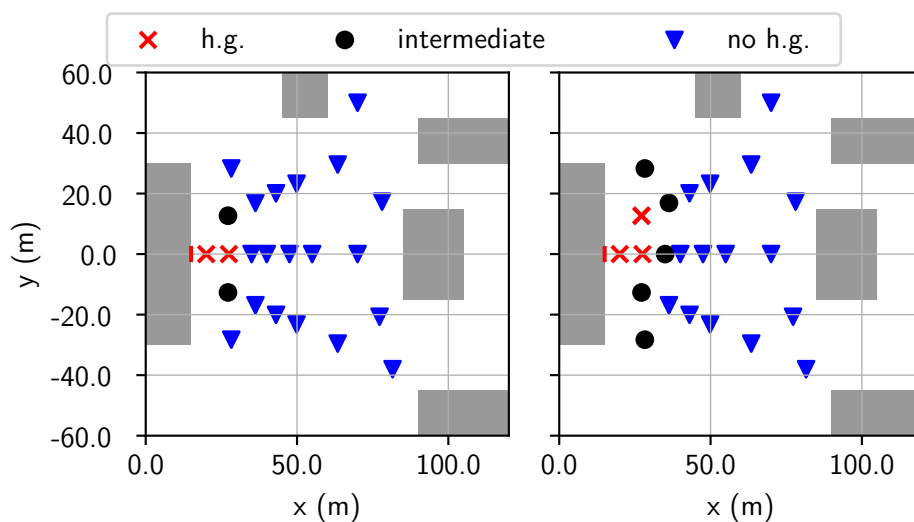


Figure 6.19: Classification of local concentration distributions into near field, intermediate region and far field based on the shape of the fit of the gamma distribution. 'h.g.' is an abbreviation for heavy gas and 'no h.g.' is an abbreviation for no heavy gas. Measurement height is 2 m. Left (a) release rate: $8.3 \text{ m}^3/\text{s}$, right (b) release rate: $21 \text{ m}^3/\text{s}$. Other release conditions are the same between the two cases and are listed in Fig. 6.11a.

flow rate of approximately $8 \text{ m}^3/\text{s}$ is presented, while in Fig. 6.19b (right) the source volume flow rate is approximately $21 \text{ m}^3/\text{s}$. When the applied single gamma distribution fit has a shape parameter of $\alpha \leq 1$ the measurement point is categorized as a point without a significant heavy gas effect. When the measured concentration distribution is representable by a double gamma distribution fit the measurement point is categorized as a point of the intermediate region. If the best fit is a single gamma distribution and has a shape parameter $\alpha > 1$ the measurement point is categorized as a measurement point with a strong heavy gas effect.

In case of Fig. 6.19a the majority of measurement points are characterised to be without a heavy gas effect. Only the measurement points close to the source show a significant heavy gas effect. By increasing the volume flow rate (Fig. 6.19b) the number of measurement points with a significant heavy gas effect increases. Here three points show a strong heavy gas effect whereas only two are characterised by a strong heavy gas effect for Fig. 6.19a. The number of points of the intermediate region also increases from two to five.

Up to this point in this section the influence of changes in the distance to the source, height above ground and release rate on the concentration distribution has been investigated. However, also the mean wind speed has a significant influence on the local concentration distribution. With higher mean wind speeds the densimetric Froude number increases and the heavy gas effect diminishes, which results in a shift in the local concentration distributions. This shift of the concentration distributions is also visible in the classification of the measurement locations.

In Fig. 6.20 the influence of a change in reference wind speed of a heavy gas dispersion in the model of the area source without obstacles (Section 4.3.1) on the spatial distribution of the distribution classes is presented. The reference wind speed is increased from 1 m/s (Fig. 6.20a, top), over 2 m/s (Fig. 6.20b, left) to 4 m/s (Fig. 6.20c, right). In Fig. 6.20a the majority of measurement points is in the intermediate region class. Only the measurement points at the edges of the gas plume fall into the class without a significant heavy gas effect. The transition between the intermediate class to the class without a significant heavy gas effect at the edges of the gas plume is very gradual and a clear distinction is difficult. This gradual transition and a minor lateral inhomogeneity of the gas plume are potential causes for the slight asymmetry in the spatial distribution. By doubling the reference wind speed to 2 m/s (Fig. 6.20b) the number of points in the intermediate class decreases. The influence of the buoyancy on the heavy gas dispersion becomes less significant and the local concentration distributions are shifted to lower concentrations. This is observable in the decrease of the width of the points in the intermediate region class. However on the $y = 0 \text{ m}$ axis the spatial distribution of the classes does not change. After another doubling of the reference wind speed to 4 m/s (Fig. 6.20c) the number of points of the intermediate region class further decreases and shifts to the class without a significant heavy gas effect. All measurement points along the $x = 25 \text{ m}$ axis change from the intermediate class to the class without a significant heavy gas effect. Points along the $y = 0 \text{ m}$ axis further downstream remain in the intermediate class. Regrettably, the number of available measurement points in 1 m height for the higher wind speeds is lower compared to the other reference wind speeds.

Fig. 6.21 shows the spatial distribution of the classes of the concentration measurements in the industrial chemical model (Section 4.3.3). As written in Sec. 5.5 Reynolds number independence in the industrial chemical park model is achieved at reference wind speeds of 2 m/s , which leads to a diminished heavy gas effect. The effect of the relatively high reference wind speed on the heavy gas effect is visible

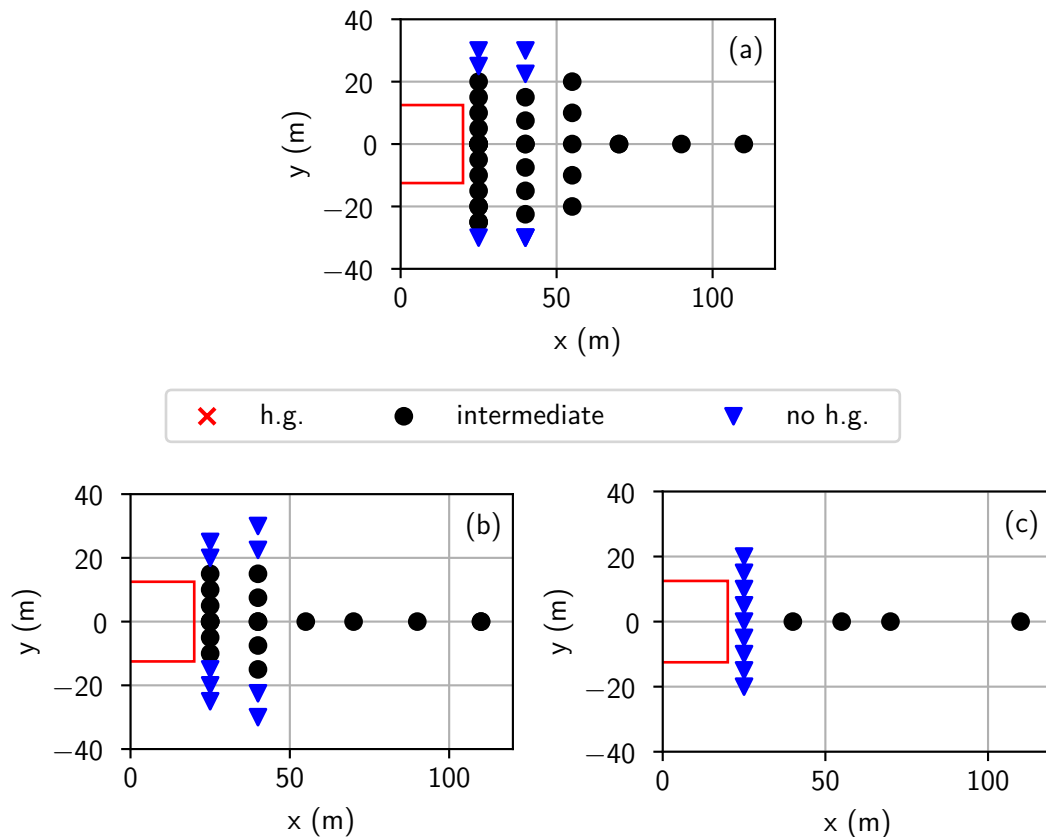


Figure 6.20: Classification of local concentration distributions into near, intermediate and far field based on the shape of the fit of the gamma distribution. Configuration is the area source model without obstacles (Section 4.3.1). Measurement height is 1 m and the wind direction is from left to right. Volume release rate is approximately $50 \text{ m}^3/\text{s}$. Source is indicated with the red rectangle in the left. In the three plots the reference wind speed is varied: top (a) 1 m/s, left (b) 2 m/s and right (c) 4 m/s. For additional information read caption of Fig. 6.19.

in the spatial distribution of the classes of the gamma distribution fits. All measurement points except one fall into the class without a significant heavy gas effect. Only the measurement point in negative x - and negative y -direction of the source (red rectangle in Fig. 6.21) belongs to the intermediate class. This measurement point is situated in the recirculation zone of the big building in the bottom left half of Fig. E.1 in the Appendix E. Here, the local wind direction of the mean flow is against the general flow and transports the gas in the negative x - and negative y -direction. Due to the higher spatial resolution of the measurement points the recirculation is better visible in the model configuration with all tanks (Fig. E.2). No points fall into the class with a strong heavy gas effect. Aside from the reduction of the heavy gas effect due to the relatively high reference wind speed, further reduction is also caused by the strong turbulence from the structures in the model area. The strong turbulence is visible in the standard deviation of the u and v -component of the flow (compare Fig. E.3 and Fig. E.4 to Fig. E.1).

Since transport processes of gases and especially of heavy gases in boundary layer flows in building configurations are complex, it is expected that the rather simple fits of single and double gamma

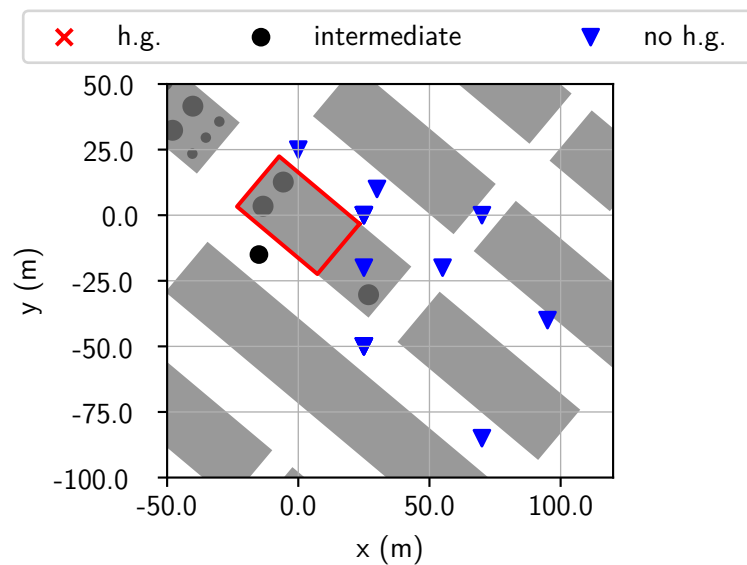


Figure 6.21: Classification of local concentration distributions into near, intermediate and far field based on the shape of the fit of the gamma distribution. Configuration is the industrial chemical park (Section 4.3.3). Measurement height vary from point to point, but the majority of measurement point is measured at a height of one metre. The wind direction is from left to right. Volume release rate is approximately $50 \text{ m}^3/\text{s}$ and the reference wind speed is 2 m/s . Source is indicated with the red rectangle in the left. The grey circles with a black border are tanks. For additional information read caption of Fig. 6.19.

distributions oversimplify or miss features and characteristics of the measured concentration distributions. Two exemplary cases of concentrations measurements inside the idealized industrial zone of 'poor' fits are shown in Fig. 6.22. In these two cases the fit of a double gamma distribution is not able to fully capture the structure of the measured concentration distribution. For example in Fig. 6.22a (black line) the fit overestimates the relative frequency of the events where the relative concentration is between 0% and 2% relative concentration. The fit in Fig. 6.22b fails to reproduce the distribution of between 0% and 10% relative concentration.

There are various ways to tackle the 'poor' fits and improve their quality. In the following, two approaches will briefly be presented and discussed. However, the focus is not on refining the method directly but rather to present potential ideas for future improvements.

One approach to improve the quality of the fit and also improve the understanding of the intermediate region is to use a weighted form of the double gamma distribution. The previously presented form of the double gamma distribution is a simple sum, where both gamma distributions are weighted equally. By changing this weighting factor to be variable it is possible that the intermediate region can be described more accurately. For example at the interface between a region with a strong heavy gas effect and the intermediate region a stronger weighted gamma distribution where the shape parameter $\alpha \leq 1$ might improve the overall fit and lead to a better understanding of the influencing factors in the double gamma distribution.

Another possible approach to improve the accuracy of the fits is to change the number of bins of the histogram. The previously presented approach uses 50 bins with a relative concentration bin width of

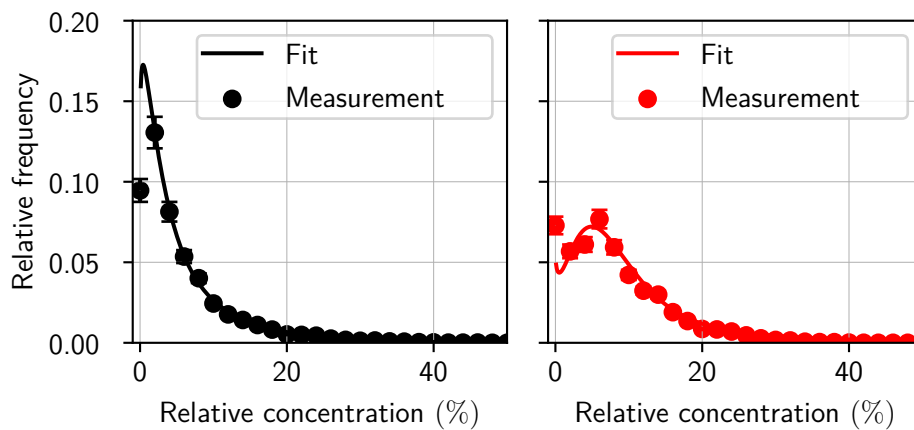


Figure 6.22: Two examples for fits of double gamma distributions to measured concentration data, where the fit is not able to accurately represent the measured data. Measurement conditions are the same as in Fig. 6.11. Measurement location for (a, black) is $x = 36.3$ m, $y = 16.9$ m and $z = 2$ m and for (b, red) is $x = 28.3$ m, $y = 28.3$ m and $z = 2$ m.

2%. By increasing the number of bins more data points are available for the fit. However, the variability between the data points can also increase.

There are several applications for the gamma distribution approach to classify measurement points in regards to the local heavy gas effect. For example in case of an accidental release of hazardous material a concentration measurement which shows the characteristics of a near field or intermediate region can help first responders localizing the source or facilitate a better management of evacuations. This obviously also depends on several other parameters like the surrounding buildings, the type of gas and atmospheric conditions.

A potential use case of the described method might also be the evaluation of CFD models. CFD models like for example LES models are able to simulate time resolved gas dispersion and can output concentration distributions for individual locations. These simulated local concentration distributions should show a similar behaviour which is presented in this section. CFD models are often evaluated by comparing mean concentrations between the model and reference data sets. However, as shown in Section 6.2.1 the mean concentration as a metric has several issues. One rough approach could be a comparison between the spatial distribution of three classes between the model and the reference measurements. A more direct comparison of the PDFs of gamma distribution between the model and the reference data can provide a deeper insight into the behaviour of the CFD model and its capabilities to sufficiently predict concentration distributions.

Another interesting potential use case is the development of a statistical model to predict local concentration PDFs depending on location (distance to the source and height above ground), wind speed, density of the gas, the boundary layer and other factors. The presented behaviour of the concentration distribution shows a potentially systematic behaviour which could be a basis for a systematic model. However, the measured data is not substantial enough to develop such a model and such a development is outside the scope of this thesis. For the development of such a systematic model extensive systematic variations of the contribution factors are necessary.

6.4 Influence of Individual Roughness Elements on the Flow and the Gas Dispersion

The wind tunnel model presented in Section 4.3.1 is a very idealistic model just consisting of a large area source (25 m by 40 m) flush with the ground and a homogenous floor roughness of the roughness elements (Fig. 4.3). A goal of performing flow and gas dispersion measurements in this model configuration was the generation of reference data for the verification of CFD models. This configuration was designed as an academic case where disturbing influences of obstacles were eliminated as far as possible and the performance of CFD models could be evaluated without the interfering effects of large obstacles on the flow. However, the model configuration is not completely devoid of obstacles. To model the boundary layer (Section 4.4) roughness elements are placed in the wind tunnel. As visible in Fig. 4.3, the roughness elements are also placed downwind of the area source. In case of the used boundary layer (Sec. 4.4.2) these roughness elements have a full-scale height and width of 2 m and a thickness of 0.2 m. With Eq. 3.5, a source volume flow in full-scale of approximately $50 \text{ m}^3/\text{s}$ and CO_2 as released gas, the L_{cc} of the heavy gas release is approx. 3 m. Using the L_{cc} , the vertical dimension of the gas cloud can be approximated to a height of approximately 3 m. The expected height of the gas cloud is of the same order of magnitude as the height and width of the roughness elements. On the y -axis (lateral direction) the roughness elements are placed staggered every 20 m and on the x -axis (along wind direction) every 10 m with a gap of 20 m after three elements (Fig. B.2). This placement results in a low density of roughness elements where the roughness elements can be considered as individual objects. To match the configuration and include the influence of individual roughness elements, the CFD models would need to also model the individual roughness elements which is difficult to implement due to the necessary spatial resolution to accurately model the roughness elements.

However, the removal of the roughness elements also has an impact for the flow. Due to the absence of the roughness elements on the emission source and the local reduction of ground roughness, the initial boundary layer changes and adapts to the new ground roughness. The removal of roughness elements can lead to a reduction of turbulence and an increase in the local wind speed. This change in the flow influences the gas dispersion.

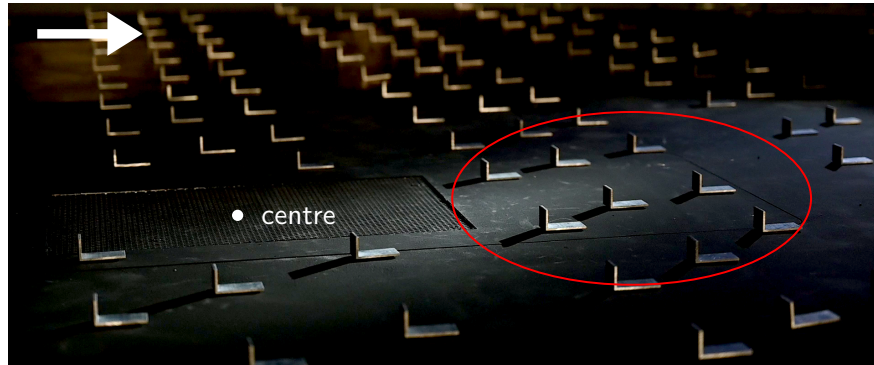
In this section the influence of the removal of the roughness elements on the flow and on the gas dispersion is investigated. This addresses the research question: *Is it necessary to treat the used roughness elements as individual obstacles?*

6.4.1 Influence of Individual Roughness Elements on the Flow

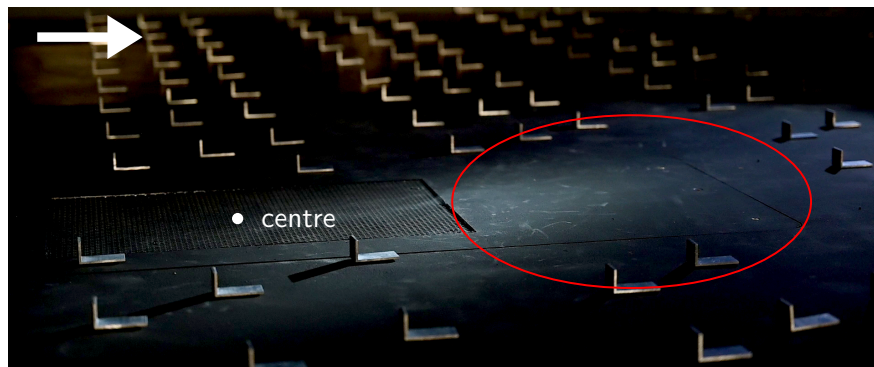
To investigate the influence of the presence or absence of individual roughness elements on the flow, measurements in two model configurations were performed. In one case flow measurements were performed with the local absence of roughness elements. And the other case was designed as a reference where the roughness elements were not removed. The flow measurements in the reference case are in essence, a repetition of the boundary layer measurements presented in Section 4.4.2.

Fig. 6.23 depicts a view into the wind tunnel with both model setups of the area source with (Fig. 6.23a) and without (Fig. 6.23b) roughness elements downstream of the source. The roughness elements were only removed in the path of the released gas. Roughness elements further away from the $y = 0 \text{ m}$

axis (middle of the wind tunnel) were not removed so that the original wind tunnel boundary layer was disturbed as little as possible. When measurements were performed further downstream the roughness elements were also removed there (not included in Fig. 6.23).



(a) Roughness elements present downstream of the source.



(b) Roughness elements absent downstream of the source.

Figure 6.23: Picture of the area source model configuration with and without roughness elements downstream of the source. The area where the roughness elements were removed is marked with a red ellipse. The area source is the rougher surface in the left centre of the image. Centre of the area source is marked with white dot. Wind direction is from left to right and indicated by the white arrow.

Over a distance of up to 80 m away from the centre of the source four vertical flow profiles are shown in Fig. 6.24. Three vertical profiles were measured with an absence of roughness elements downstream of the source (blue, green and orange). These vertical profiles are located at the centre of the source (0 m) and at a distance of 40 m and 80 m downstream from the centre of the source. As a reference one vertical profile was measured at a distance of 80 m from the centre of the source which has no absence of roughness elements (red).

With an increasing distance from the source a shift in the vertical profile of mean wind speed can be observed. At the centre of the area source ($x = 0$ m) the U -mean wind speed is slightly higher compared to the reference profile (red). As visible in Fig. 6.23 no roughness elements are on top of the area source. This means that at the location of the vertical profile at $x = 0$ m one line of roughness elements in front of the measurement location is already removed. With an increasing fetch distance with missing roughness elements the difference between the U -mean wind speed and the reference profile increases near the ground. While the profile of the mean U -wind speeds at $x = 0$ m generally are still within the measurement uncertainty in regard to the reference profile, the mean U -wind speeds at a

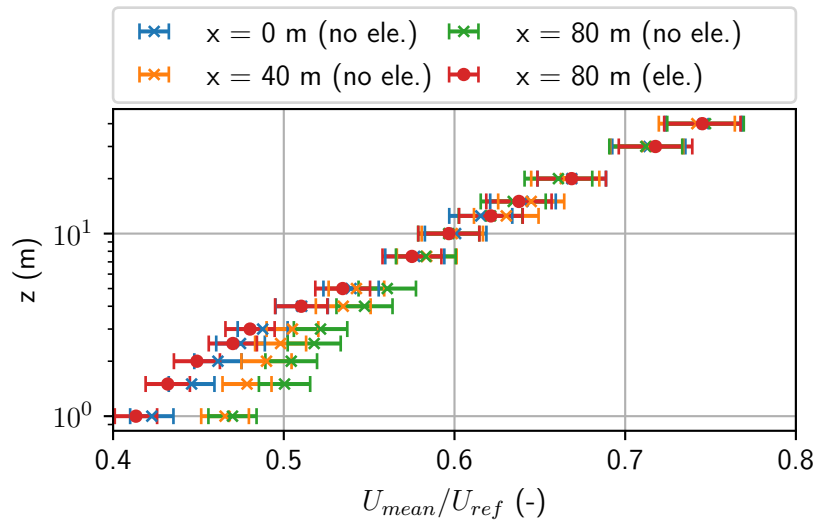


Figure 6.24: Vertical profiles of u windspeeds along the $y = 0$ - axis. Vertical profiles at their respective x coordinates and at 0 m on the y axis. The abbreviation *no ele.* in the legend stands for *no roughness elements* and *ele.* stands for *with roughness elements*. Measurement uncertainty is stated in Tab. 4.3.

distance of 40 m and 80 m show a higher mean U -wind speed of approximately 10% and 14% close to the ground respectively. Differences of the mean U -wind speeds between the vertical profiles decrease with increasing height. Above a height of 9 m no significant differences between the individual vertical profiles are observable.

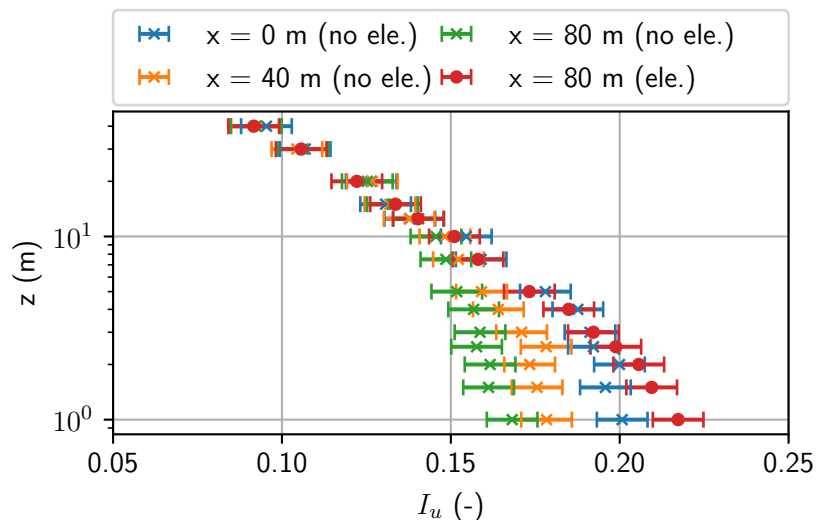


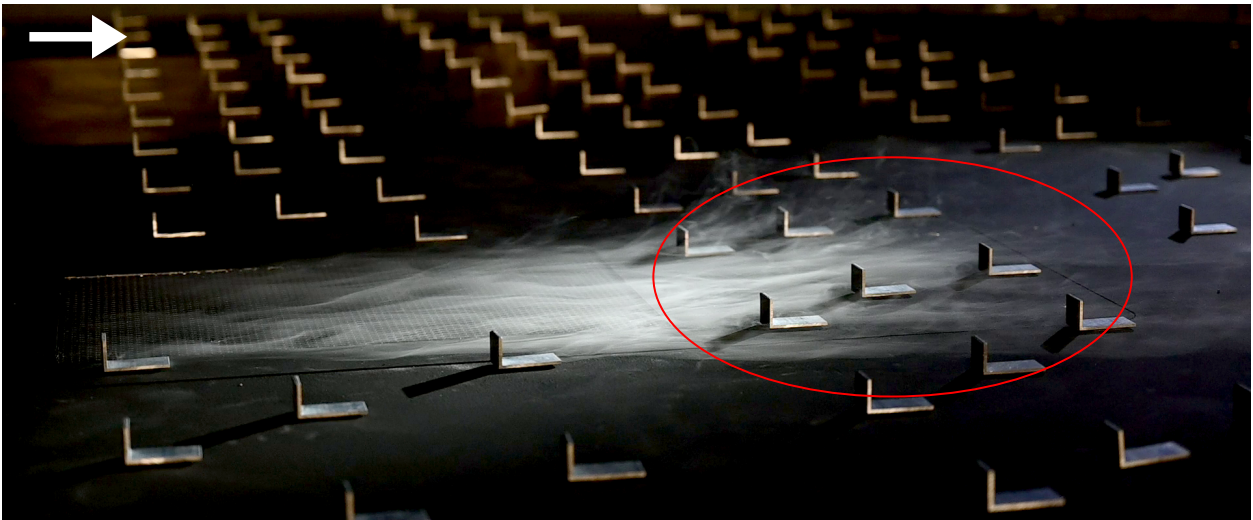
Figure 6.25: Vertical profiles of turbulence intensities of the main wind direction (I_u) along the $y = 0$ - axis. Vertical profiles at their respective y coordinates and at 0 m on the y axis. For more explanations read the subtitle of Fig. 6.24. Measurement uncertainty is stated in Tab. 4.3.

The turbulence intensity of u wind velocity component also shows significant changes caused by the removal of the roughness elements. Fig. 6.25 shows vertical profiles of the turbulence intensity of the u wind velocity component at increasing distances from the source (same distances from the source

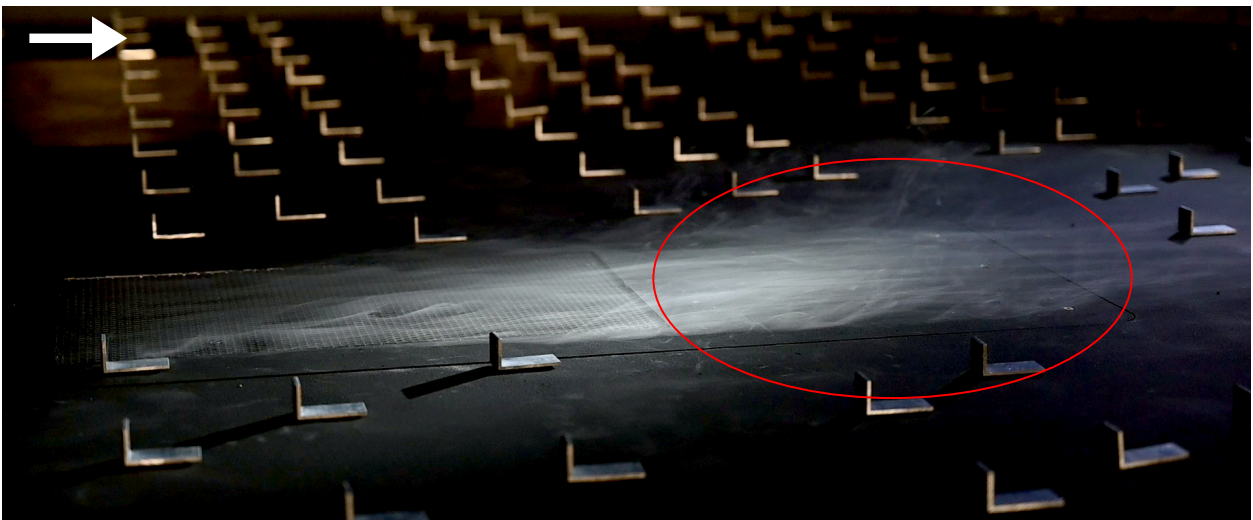
as the vertical profiles in Fig. 6.24). The highest turbulence intensities are measured for the reference wind profile. A comparison of the vertical profile over the centre of the area source to the reference vertical profile shows slightly weaker turbulence intensities up to a height of 3 m. With further increasing distance without the presence of roughness elements the turbulence intensity continues to decrease. In a height of 2 m the turbulence intensity of the u -component decreases from 0.21 (reference) to 0.17 ($x = 40$ m) and 0.16 ($x = 80$ m). Similar to the vertical profiles of the U -mean wind speeds differences due to the absence of the roughness elements are observable up to a height of approx. 10 m.

In a more qualitative approach Fig. 6.26 shows the influence of roughness elements on a visualisation of a dispersion of CO_2 with a fog tracer. Similar to Fig. 6.23a and 6.23b in Fig. 6.26a roughness elements are present, while in Fig. 6.26b the roughness elements are removed. As already seen in Fig. 6.25 the absence of the roughness elements leads to a decrease in the turbulence intensities. The weaker turbulence is also observable in the flow visualisation in Fig. 6.26. In Fig. 6.26a more fog is transported upwards and more disturbances are visible in the gas cloud. Furthermore the gas cloud is slightly wider in Fig. 6.26a compared to Fig. 6.26b. This trend of a slightly wider gas cloud is a general observation and not limited to the single snap shots of the presented continuous release.

In addition to the general change in the flow structure the roughness elements also have a direct impact on the flow in their direct vicinity. This, for example, is visible upwind of the roughness elements where the roughness elements have a blocking effect on the flow. Furthermore, less dense fog is observable in the wakes of the roughness elements.



(a) Roughness elements present downstream of the source.



(b) Roughness elements absent downstream of the source.

Figure 6.26: Picture of the area source model configuration with and without roughness elements downstream of the source. The area where the roughness elements were removed is marked with a red ellipse. In both configurations a mixture of CO_2 and haze is released from the source with a model-scale volume flow rate of approximately 2000 l/h.

6.4.2 Influence of Individual Roughness Elements on the Gas Dispersion

As seen in Section 6.4.1 the absence of roughness elements results in a decrease of the turbulence intensities and an increase of the mean wind speed. This deviation from the original boundary layer increases with a longer fetch without roughness elements.

Fig. 6.27 shows two longitudinal profiles of relative concentrations for a heavy gas dispersion with roughness elements present and with roughness absent inside the gas cloud. The heavy gas dispersion was performed with a volume flow rate of approximately $50 \text{ m}^3/\text{s}$ and a reference wind speed of approximately 1 m/s . Over the measured distance the profile with roughness elements shows higher concentration values

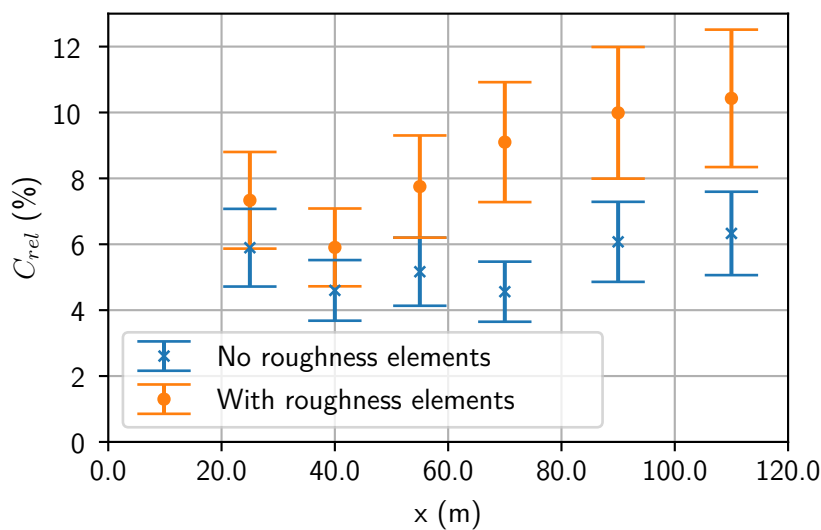


Figure 6.27: Longitudinal profiles of relative concentrations at height of 2 m along the $y = 0$ axis for a dispersion with (orange) and without (blue) roughness elements inside the gas plume. The used source has an extent up to a distance of $x = 20 \text{ m}$. $x = 0 \text{ m}$ represents the centre shown in Fig. 6.23. The measurement uncertainty is $\pm 20\%$.

compared to the profile with the absence of roughness elements. This difference between the two profiles is likely caused by the higher vertical mixing in the presence of the roughness elements. The stronger vertical mixing results in an increased vertical entrainment of the heavy gas into higher elevations.

This stronger vertical mixing is also visible in the trend of the relative concentration with increasing distance from the source. Whereas the concentrations of the heavy gas dispersion in the absence of roughness elements is relatively constant with increasing distance, the concentration of the dispersion with roughness elements increases with increasing distance. Due to the stronger mixing more heavy gas, which has a higher concentration close to the ground, is mixed upwards. Both profiles show slightly higher concentrations at $x = 25 \text{ m}$ which are probably caused by a small edge at the end of the area source at $x = 20 \text{ m}$.

The stronger vertical mixing in the presence of roughness elements is also visible in Fig. 6.28. Here two vertical concentration profiles measured at $x = 25 \text{ m}$ are shown. The profile in orange is with roughness elements present and blue profile is with roughness elements removed inside the gas plume. Between a height of one and two metres the two vertical profiles of relative concentration intersect. Below this height the concentrations are higher in the case of the heavy gas dispersion without roughness

elements. Above the intersection concentrations for the profile with roughness elements are higher. This again, shows the effect of stronger mixing due to the presence of the roughness elements. The vertical profile measured at $x = 25$ m is the only vertical profile where a comparison of the vertical concentration distribution can be made. These vertical profiles are measured close to the source and the flow has not yet been influenced drastically by the change of the roughness elements. Vertical profiles further downstream are expected to show bigger differences if roughness is removed all along the dispersing plume. Future experiments should investigate this problem in detail to quantify the effect of roughness removal.

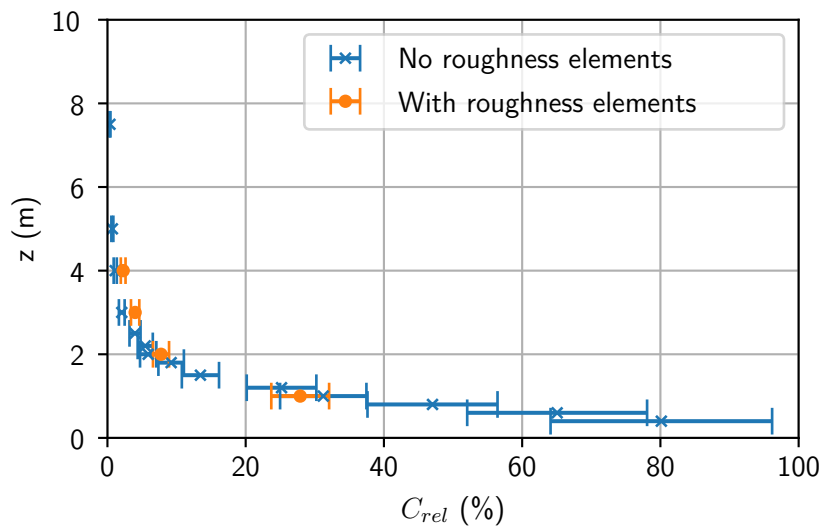


Figure 6.28: Vertical profiles of the relative concentration for a dispersion with (orange) and with the absence (blue) of roughness elements. Vertical profiles measured at $x = 25$ m and $y = 0$ m. Measurement uncertainty is $\pm 20\%$.

Summing up, individual roughness elements have a substantial impact on flow and dispersion. The removal of roughness elements has an effect on the flow and resulting from this, an influence on the gas dispersion. The decrease in the turbulence resulting from the removal of the roughness elements leads to less vertical mixing and thus higher concentrations near the ground. For the creation of the reference data set it was decided to perform the measurements without the presence of the roughness elements, because the CFD models which were developed by project partners were not able to model the individual roughness elements due to resolution constraints and comparatively small size of the roughness elements. In the given data set the few locally missing roughness elements are not expected to spoil model evaluation at heights above a measurement height of two metres.

The general findings of influence on the heavy gas dispersion are comparable with findings of Michálek and Zacho (2012) who also investigated the influence of a boundary layer change on the dispersion of a heavy gas and found that in the presence of a smoother surface the vertical mixing is weaker and the gas cloud is generally shallower.

Chapter 7

Conclusion

Although heavy gas dispersion experiments have been performed in the field and in boundary layer wind tunnels since the 1960s and 1970s knowledge gaps are still apparent. In the past, measurements have mainly been conducted in flat open terrain or with obstacles of low complexity. In more recent measurement campaigns the focus shifted to dispersion scenarios inside build up areas (Jack Rabbit II, Spicer and Smith, 2021 and MODITIC, Robins et al., 2016). However, systematic reference data for the verification of dispersion models for complex environments is still lacking.

This thesis deals with the realisation of a heavy gas dispersion measurement campaign in complex environments and presents findings regarding heavy gas dispersion measurements. For this flow, neutral density and heavy gas dispersion experiments were performed in three different model configurations of increasing complexity. The models ranged from a very idealistic dispersion scenario of an area source without obstacles, over an idealistic industrial area to a dispersion in a complex industrial chemical park. To investigate the influence of external factors on the gas dispersion like a change of the reference wind speed or the inflow boundary layer, these parameters were varied for the idealistic area source without obstacles and the idealised industrial park model. Further aspects like for example the influence of individual roughness elements on the gas plume and how a gas dispersion with a significant heavy gas effect can be achieved are presented.

The most important prerequisite for successful physical modelling of a heavy gas dispersion is a Reynolds number independence at a reference wind speed as low as possible to enable an as low densimetric Froude number as possible. With this, a wide range of possible densimetric Froude numbers can be modelled and resulting from this a wider range of heavy gas dispersion scenarios can be realised. The density of the released heavy gas also substantially influences the possible modelling range of densimetric Froude numbers. However, a free selection of a specific heavy gas is often not possible because of health risks in case of flammable or toxic gases, issues with the instrumentation, the greenhouse potential or the costs of the gas.

Using a large scale of 1:100 allows the experimenter to use large volume flow rates in model-scale which still represent realistic release cases in full-scale. However, the large model-scale of 1:100 leads to issues while performing wind tunnel experiments. One issue is the limited size of the wind tunnel. As seen in Sec. 4.4 the large dimensions of the WOTAN wind tunnel are still not sufficient to model a boundary layer flow at a scale of 1:100 which has integral lengths scales similar to nature. Large turbulent structures are underrepresented in comparison to reference values (VDI, 2000 and Erdmann, 2017). The size of the large turbulent structures is also limited by thickness of the modelled boundary layer of approximately 80 m - 90 m. Another issue is the large size of obstacles of the models and the size of the model itself. The chemical industrial model slightly exceeded the blockage criteria of VDI

(2000). Achieving a turbulent flow around the cylinders of the industrial chemical park model proved to be difficult. Due to the large size of the cylinders of a diameter of up to 8 cm in model-scale the flow separation of the cylinders showed Reynolds dependence up to a reference wind speed of 2 m/s. All in all achieving a heavy gas effect is not a trivial endeavour and is heavily dependent on the model and the dispersion scenario itself, as well as the capabilities of the used boundary layer wind tunnel. However, with careful planning heavy gas dispersions in complex environments can be physically modelled.

Four major research questions arose before and during the measurement campaign. In the following the findings regarding the research questions will be summarized.

Does a change of the boundary layer inflow have a significant effect on the gas dispersion inside the model area? To address this research question, flow, neutral density and heavy gas dispersion experiments have been performed in the idealistic industrial park model with a variation of the boundary layer from moderately rough to rough (Section 6.1). At first the changes in the flow were investigated. Changes in the flow in the model area due to the boundary layer change are significant. Mean wind speeds decrease by up to approximately 20%, where the majority of the measurement points shows a decrease in the order of approximately 10%. The change in the mean wind speed is comparable for all three wind directions (M1-M3). Changes in the turbulence intensities are also significant. In general the turbulence intensities increase by up to 0.05. The change of the turbulence intensities of the v flow component are generally higher than the changes of the u -component. At the beginning of the model area the change in the flow is strongest and decreases with further distance into the model area.

For the neutral density gas dispersion a widening of the gas plume for the rougher boundary layer is observable. The widening of the plume leads to lower concentrations within the plume and higher concentration at the edges of the plume compared to the less rough boundary layer. This widening of the plume is best visible in the M3 configuration (mean wind direction of 30°) of the idealized industrial model. In case of the heavy gas dispersion in general a reduction in the mean concentrations in a height of 2 m is observed. This is potentially caused by the increased turbulent mixing which results in a stronger entrainment of the heavy gases in to greater heights. In the M3 configuration higher concentrations are observed close to the source building. This is likely also caused by the increased turbulent mixing but here a higher concentration of heavy gas is closer to the ground and mixed up into a height of 2 m.

Is the mean an adequate statistical measure for heavy gas dispersions? The arithmetic mean is still often used in describing the dispersion field of a heavy gas release. However, single point measurements of heavy gases releases are often very intermittent and the PDFs are asymmetric. Using the arithmetic mean to determine the modelling quality of CFD models or as an estimation of safety distances can lead to errors. It was shown that for exemplary time series the 99th percentile of the relative concentration is up to one order of magnitude higher than the mean and that the arithmetic mean is not able to capture the variability of the concentration time series. A better suited statistical measure is the 95th or the 99th percentile which is able to capture concentration peaks. To also include the temporal fluctuations of the concentration signal an event occurrence is introduced. This event view captures short events where the concentration rises above a certain threshold and remains above that threshold for a specific duration. The introduction of this event measure is motivated by the issue that very short exceedances of a LFL of just a few seconds might not lead to an inflammation or deflagration. By viewing events with longer durations on the order of 10 to 20 seconds this issue is alleviated. Specific information when a gas cloud ignites or explodes is still rare and more research is needed to find the

necessary conditions for such an event. With better knowledge the specific parameters of the event measure can be refined.

Is it possible to characterise model regions by the local concentrations distribution and distinguish different regions in regards to a potential heavy gas effect? The concentration distribution at a measurement location depends on the distance from the source, height above ground, wind speed, turbulence intensity, density of the released gas, source release rate and additional factors. Concentration distributions measured close to the source and the ground and at low wind speeds vary greatly to concentration distributions measured at measurement locations at larger distance from the source or at higher reference wind speeds. Both concentration distributions are well represented with a PDF of the gamma distribution. Measured concentration distributions at locations which experience a strong heavy gas effect have a shape parameter greater than one, whereas concentration distributions without a significant heavy gas influence have a shape parameter smaller or equal to one. Measurement locations between those two regimes belong to an intermediate regime. Here the shape of the concentration distribution is very variable and cannot be represented with a single gamma distribution. In this intermediate regime the concentration distribution was found to be best represented by a sum of two gamma distributions. With the classification into the three regimes measurement regions in model areas can be determined where a heavy gas effect is still observable and where the heavy gas effect has become negligible.

Is it necessary to treat roughness elements as individual obstacles? During the measurement campaign in the area source model without obstacles it became apparent, that the roughness elements which shape the boundary layer have a significant influence on the local flow. This proved to be an issue, because the measurement data in this model configuration is also intended as reference data for CFD models. Due to the small size of the roughness elements and the resulting necessary very fine meshing and high computational power current CFD models are generally not able to accurately model the individual roughness elements and their influence on the flow.

To quantify the influence of individual roughness elements on the flow and the gas dispersion, measurements were performed with roughness elements present and absent. It was observed that the u -component of the wind speed increases by about 14% over a distance of 80 m when the roughness elements are removed. Over the same distance the turbulence intensities of the u -component decreased from 0.21 to 0.16. The influence of the removal of roughness elements on the flow was observed up to a height of 9 m. For the heavy gas dispersion the 2 m mean concentrations decreased with a removal of the roughness elements. This is likely caused by the reduced turbulent mixing which resulted in a lower vertical mixing of the heavy gas which remained closer to the ground. The heavy gas dispersion with roughness elements present also showed a slightly wider gas plume compared to the case without roughness elements in and in the vicinity of the plume.

The clear influence of the roughness elements on the flow and the gas dispersion makes it is necessary to treat the roughness elements which are used in this thesis as individual obstacles. This finding obviously depends on the size and density of the used roughness elements. For more generalisable statements systematic tests with roughness elements with varying sizes are necessary.

The extensive flow, neutral density and heavy gas measurements from the measurement campaign, which accompanied the writing of this thesis, are published as a potential future reference data set (Michel et al., 2023).

7.1 Outlook

This thesis proves the feasibility of the physical modelling of heavy gas dispersion in complex environments. However, the exact influence of changes in the boundary conditions on the physical processes of the heavy gas dispersion are still not completely understood. For general statements and deeper knowledge more systematic studies of heavy gas dispersions have to be performed. In this thesis it was shown that a change in boundary layer roughness has an influence on the gas dispersion but a generalizable relation cannot be drawn. More thorough systematic testing of the individual parameters of heavy gas dispersion experiments in single model configurations can lead to better understanding of how the measured concentration changes with a change in the driving external factors.

With more systematic variations of the driving factors like the reference wind speed or the release rate a statistical model which aims to predict changes in local concentration distributions can be developed. The basic concept of such a statistical model is presented in this thesis in Sec. 6.3. Depending on the strength of the present heavy gas effect the shape of the measured local concentration distribution varies and can be well represented by a gamma distribution or a combination of two gamma distributions. This idea could be further improved and potentially lead to a development of a statistical model.

Another potential idea to the overall concept of heavy gas dispersion experiment is to use gases which have a lower density than air and perform gas dispersion experiments on the roof of a boundary layer wind tunnel. This obviously need a change and switch of the whole experimental setup to the top of wind tunnel including the boundary layer development section, but this could alleviate the issue of finding a suitable heavy gas which is not flammable, corrosive, toxic or very expensive (Sec. 5.1). Helium could for example be released from a source on the underside of the roof of a wind tunnel. Due to its lower density compared to air helium would stay on top of the wind tunnel and acts like a heavy gas which stays at the floor of the wind tunnel.

Appendices

Appendix A

Quality Assurance

A.1 Quality Assurance of the Boundary Layers

This section contains figures which describe further quantities of the modelled boundary layers and are referenced in Sec. 4.4, 4.4.2 and 4.4.3.

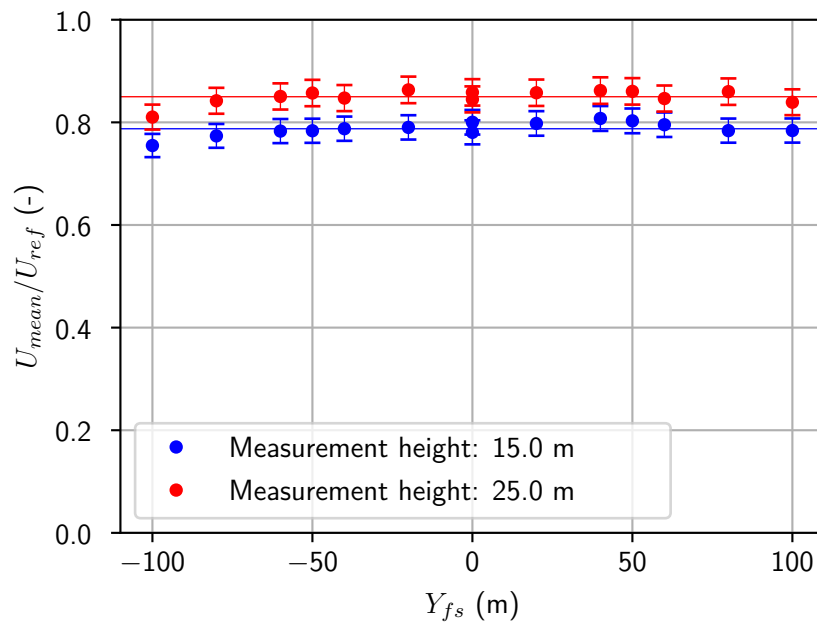


Figure A.1: Lateral wind profile of the moderately rough boundary layer measured in two heights in front of the model area at the end of the development section of the wind tunnel. Measurement uncertainty is stated in Tab. 4.3.

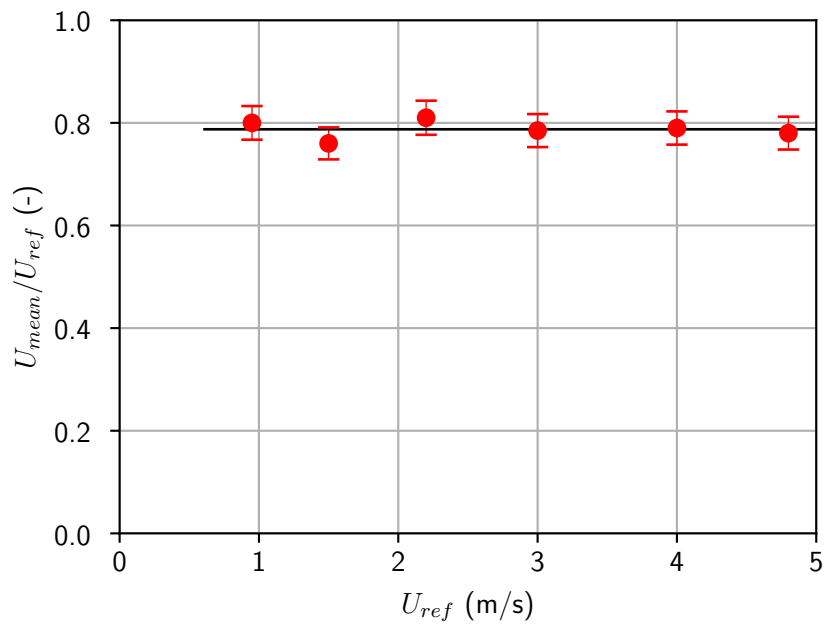


Figure A.2: Reynolds number independence test of the flow in the moderately rough boundary layer in a height of 15 m. Measurements have been performed in front of the model area at the end of the development section of the wind tunnel. Measurement uncertainty is stated in Tab. 4.3.

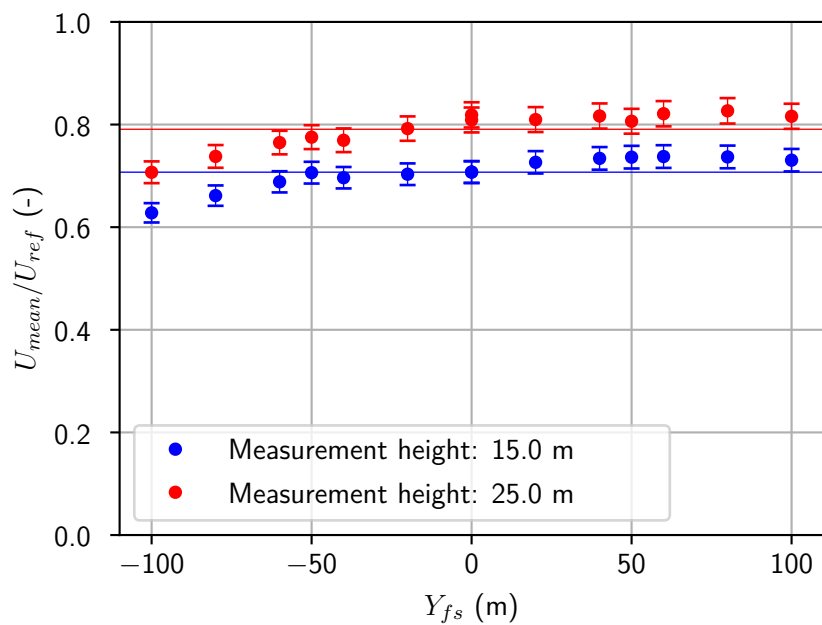


Figure A.3: Lateral wind profile of the rough boundary layer measured in two heights in front of the model area at the end of the development section of the wind tunnel. Measurement uncertainty is stated in Tab. 4.3.

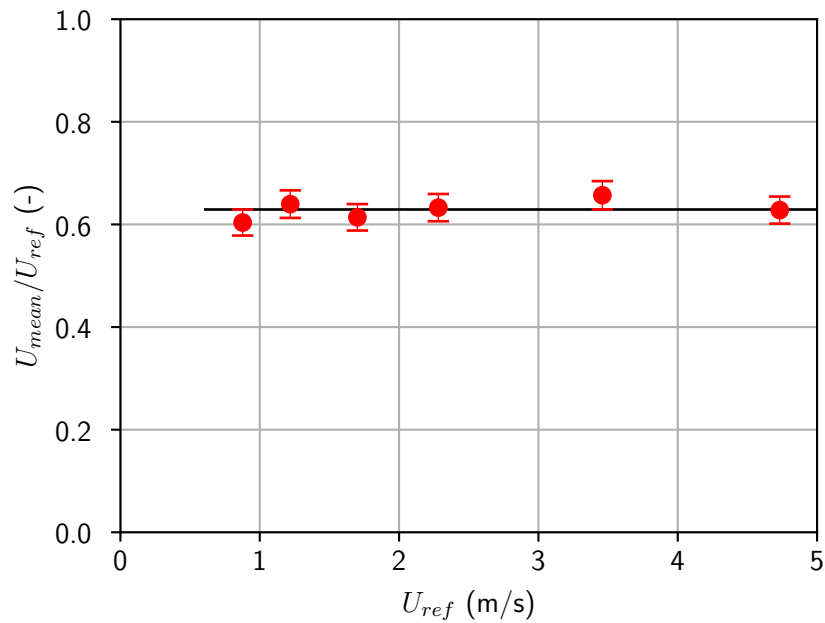


Figure A.4: Reynolds number independence test of the flow in the rough boundary layer in a height of 15 m. Measurements have been performed in front of the model area at the end of the development section of the wind tunnel.

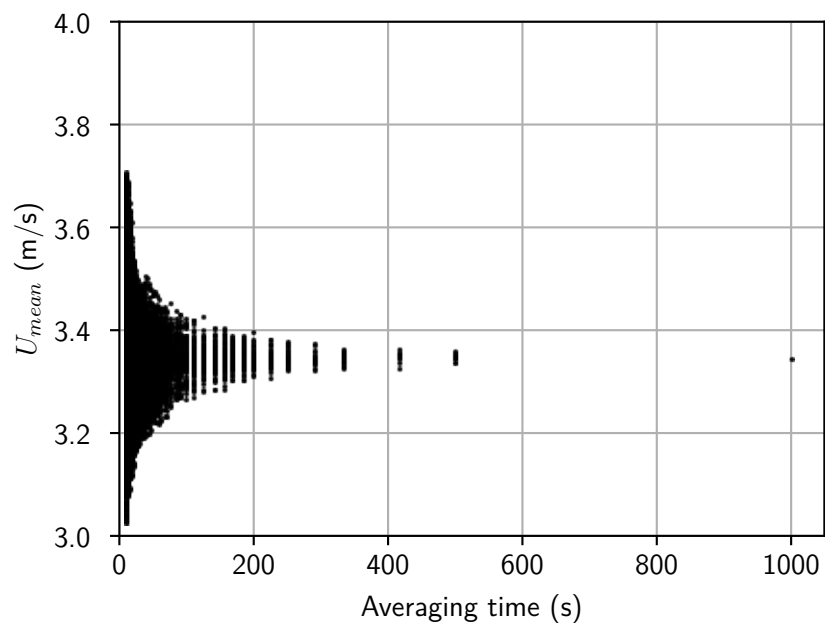


Figure A.5: Blockwise convergence test for an exemplary timeseries of the U -component of the wind speed. Measurement performed in a height 10 m in the rough boundary layer at the end of the development section. At an averaging time of approximately 180 s the total spread between the maximum and minimum wind speed is approximately 2.5% of the mean wind speed. At an averaging time of approximately 300 s this total spread has decreased to approximately 1% of the mean wind speed.

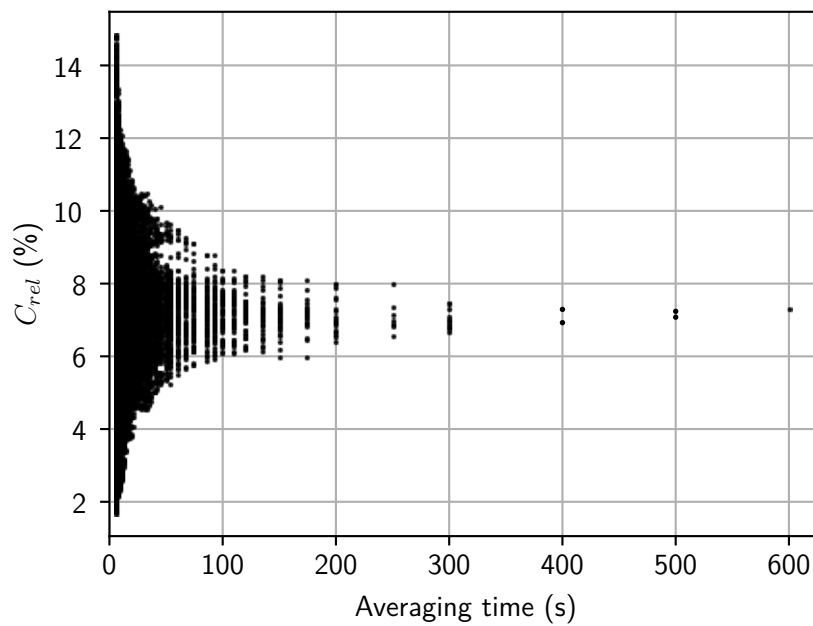


Figure A.6: Blockwise convergence test for an exemplary timeseries of a relative concentration measurement. Measurement performed behind the area source at $x = 25$ m, $y = 0$ m and $z = 2$ m. At an averaging time of approximately 200 s the total spread between the maximum and minimum concentration is approximately 20% of the mean concentration. At an averaging time of approximately 300 s this total spread has decreased to approximately 10% of the mean wind speed.

Appendix B

Boundary Layer Setup

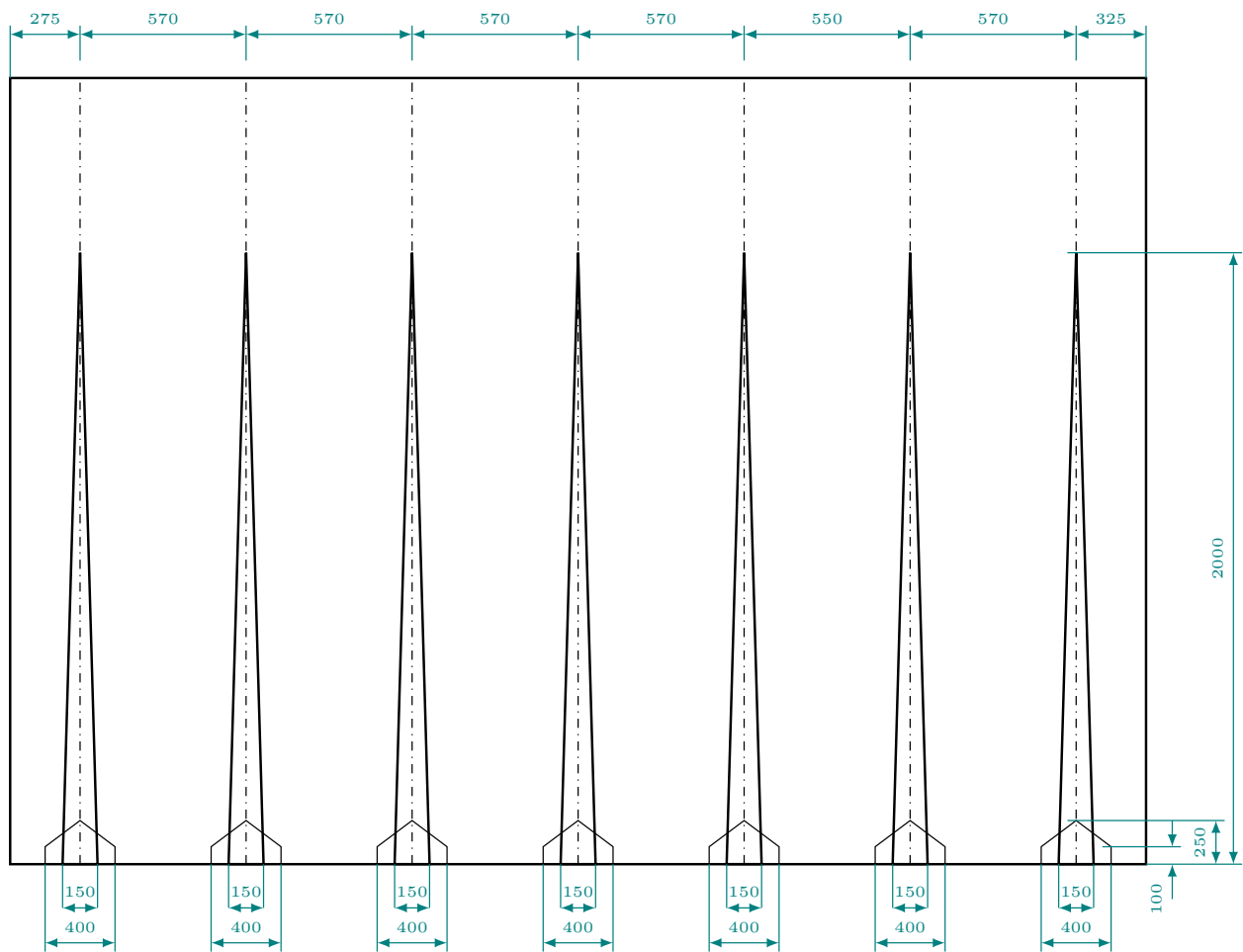


Figure B.1: Vortex generator setup for the moderately rough boundary layer.

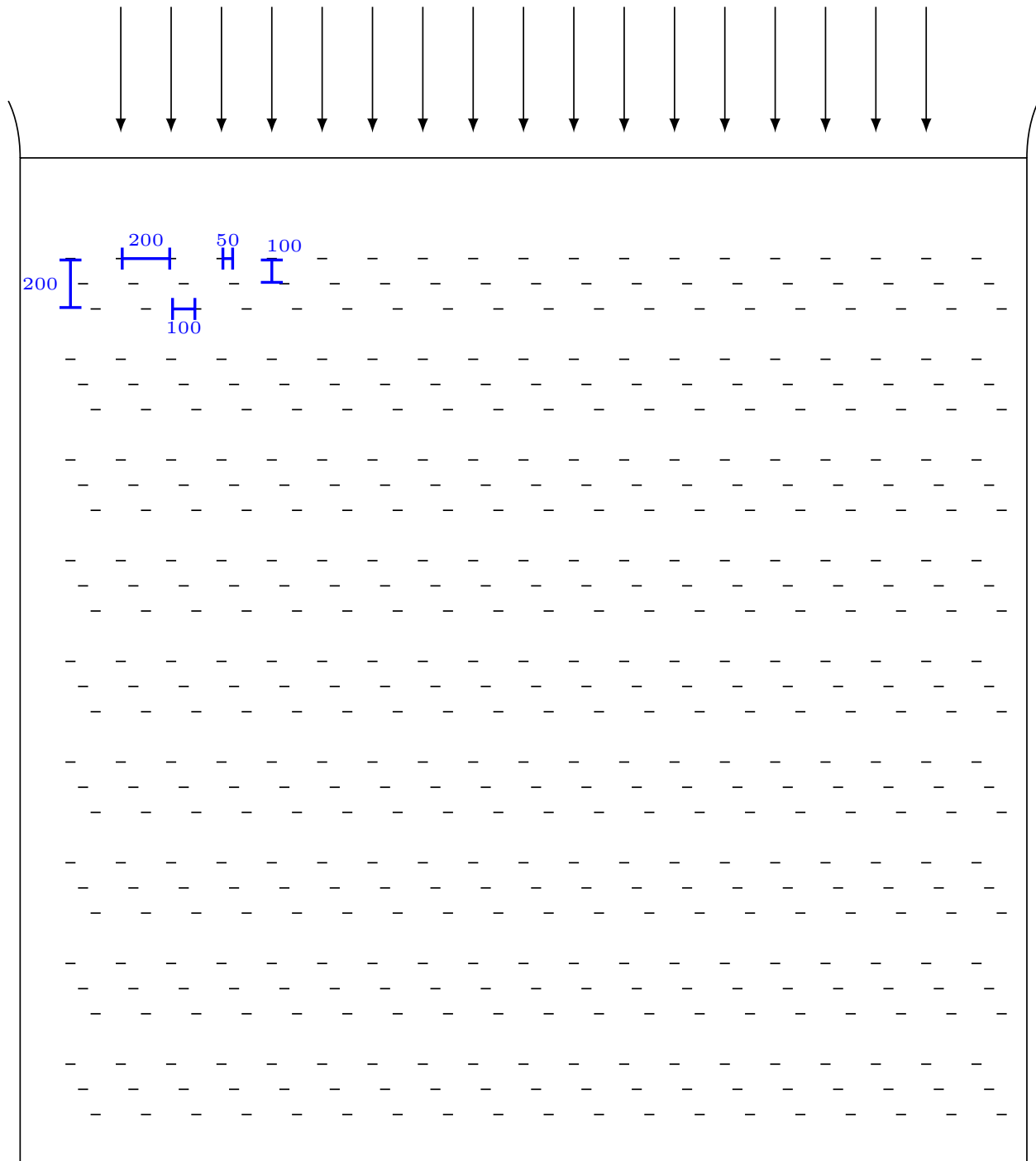


Figure B.2: Roughness element setup for the moderately rough boundary layer, all elements have the size of 20 mm x 20 mm (model-scale).

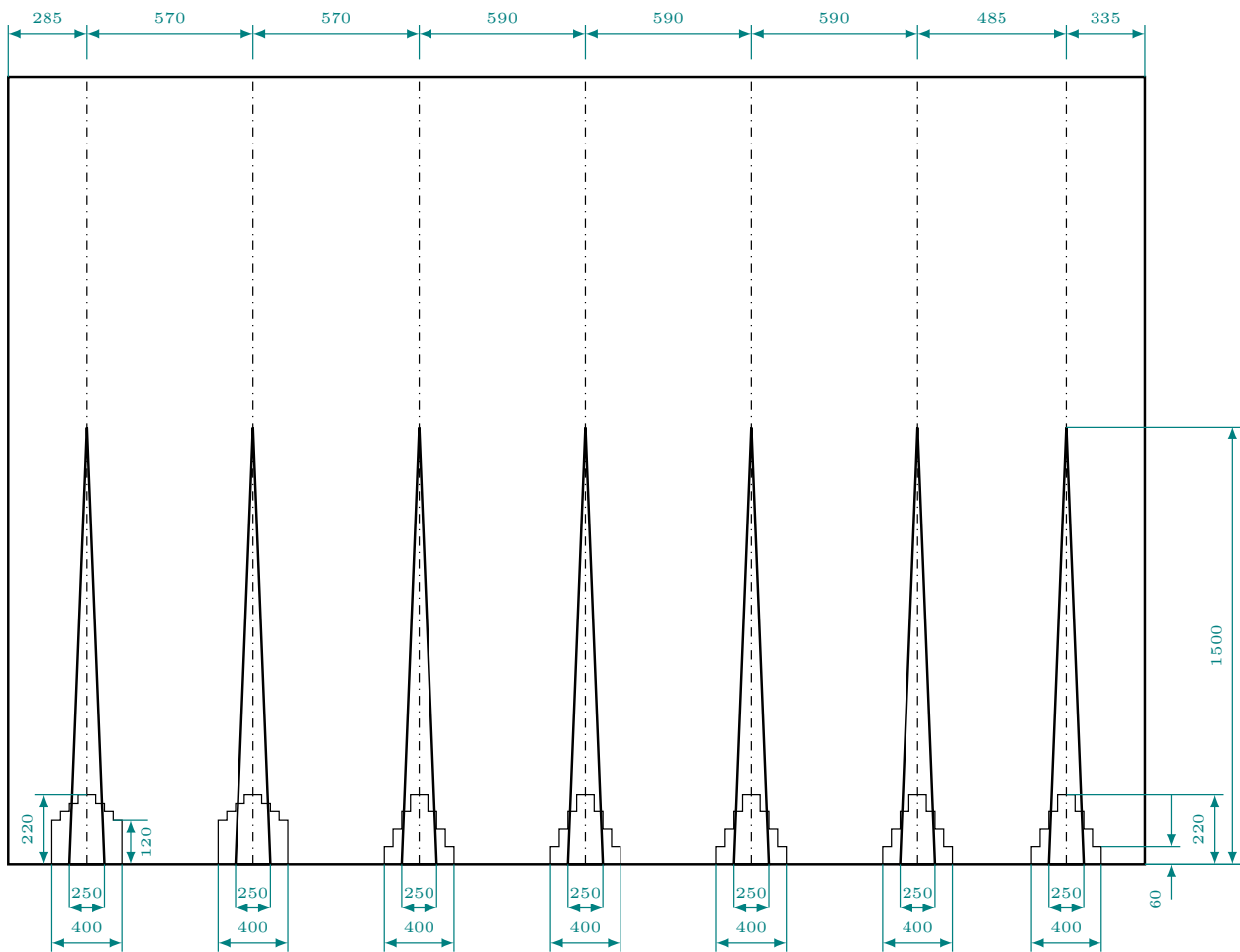


Figure B.3: Vortex generator setup for the rough boundary layer.

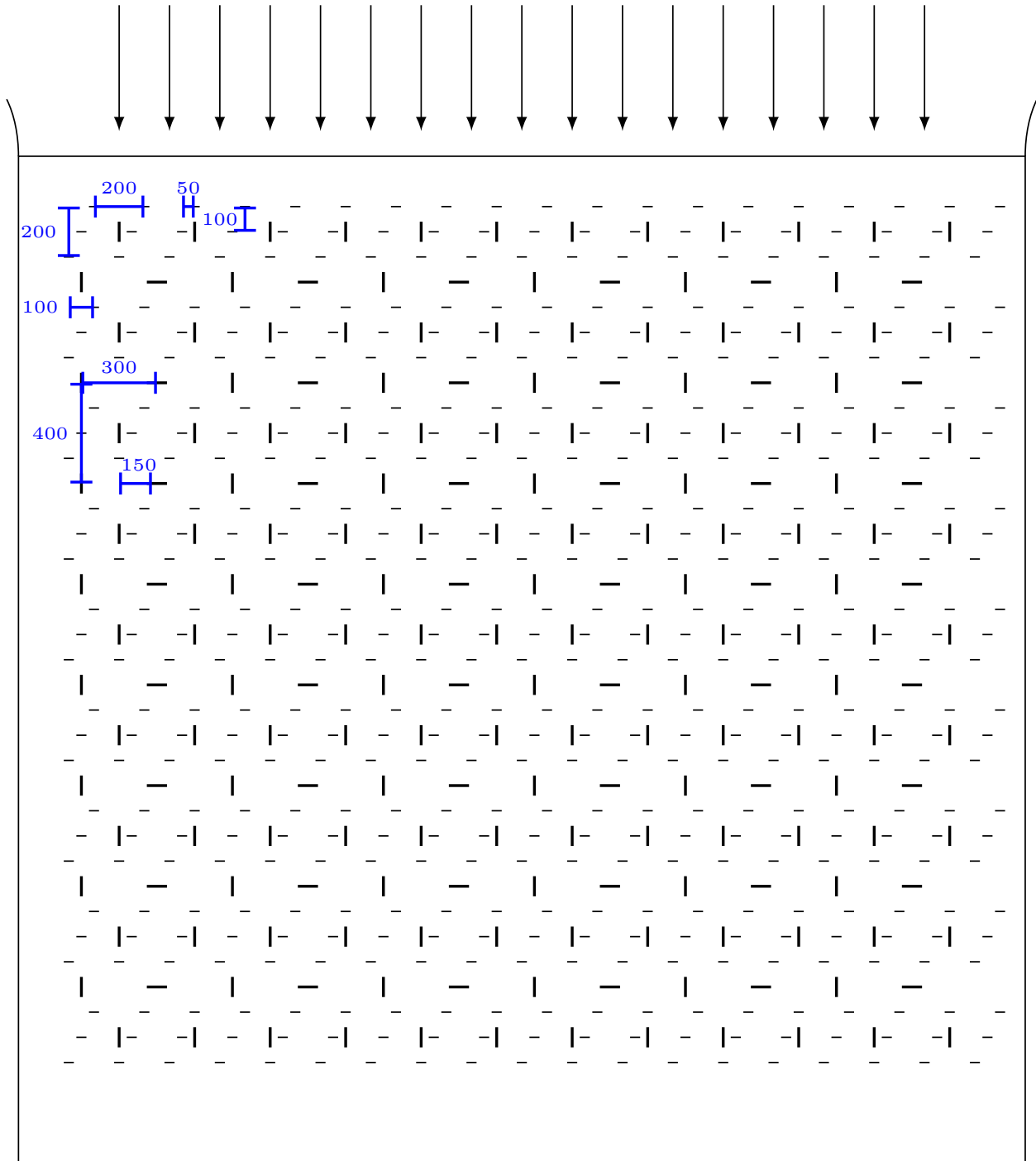


Figure B.4: Roughness element setup for the moderately rough boundary layer, the small elements have a size of 20 mm x 20 mm and the large elements have a size of 50 mm x 50 mm (model-scale).

Appendix C

Additional Measurement Results

C.1 Measurement results: Model 1

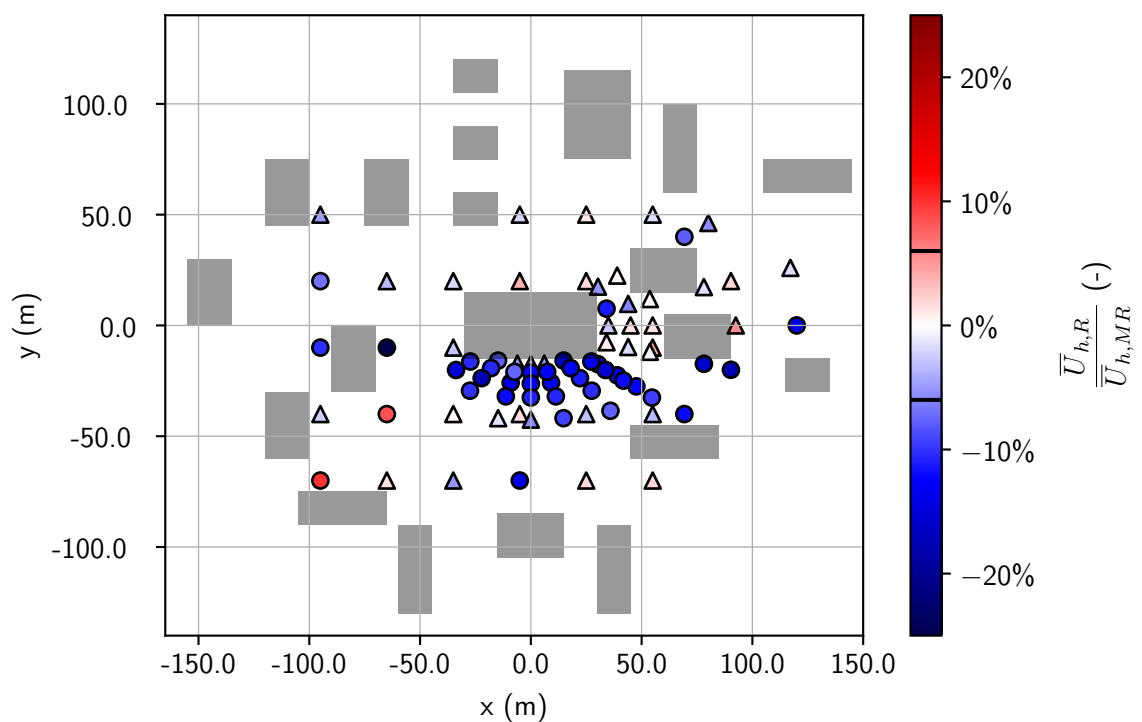


Figure C.1: Relative difference of magnitude (horizontal wind speed) between the rough boundary layer inflow and the moderate rough boundary layer inflow. Measurement height is 4 m and the wind direction is from left to right. For more information read caption of Fig. 6.2.

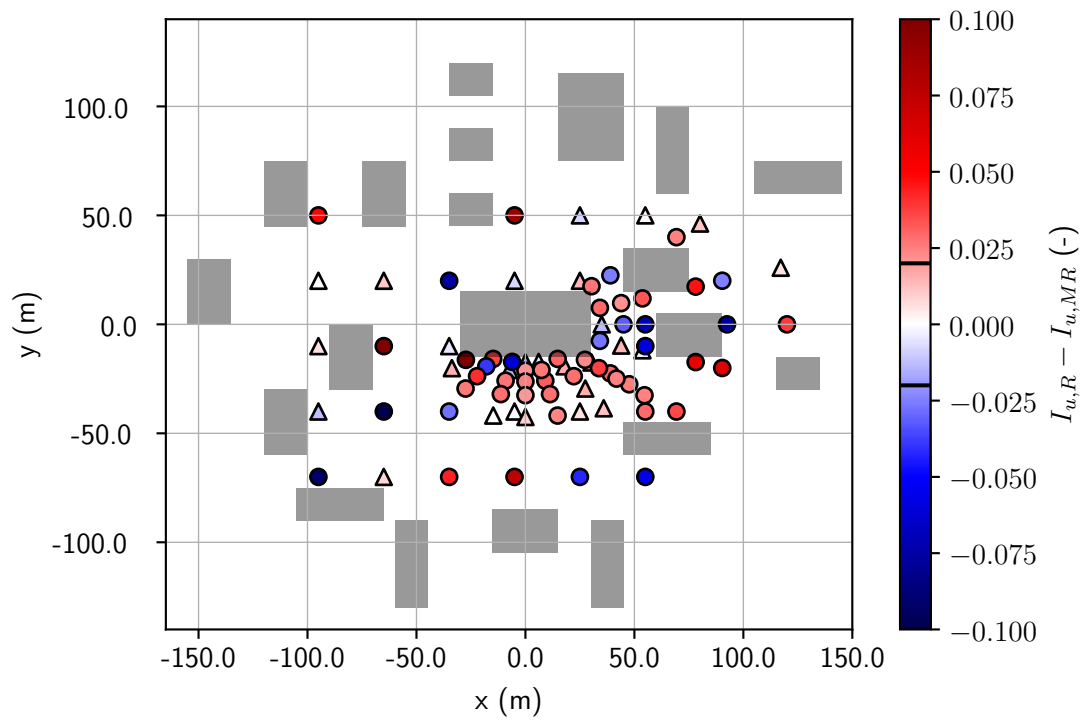


Figure C.2: Absolute difference of turbulence intensity I_u between the rough boundary layer inflow and the moderate rough boundary layer inflow. Measurement height is 4 m and the wind direction is from left to right. For more information read caption of Fig. 6.3.

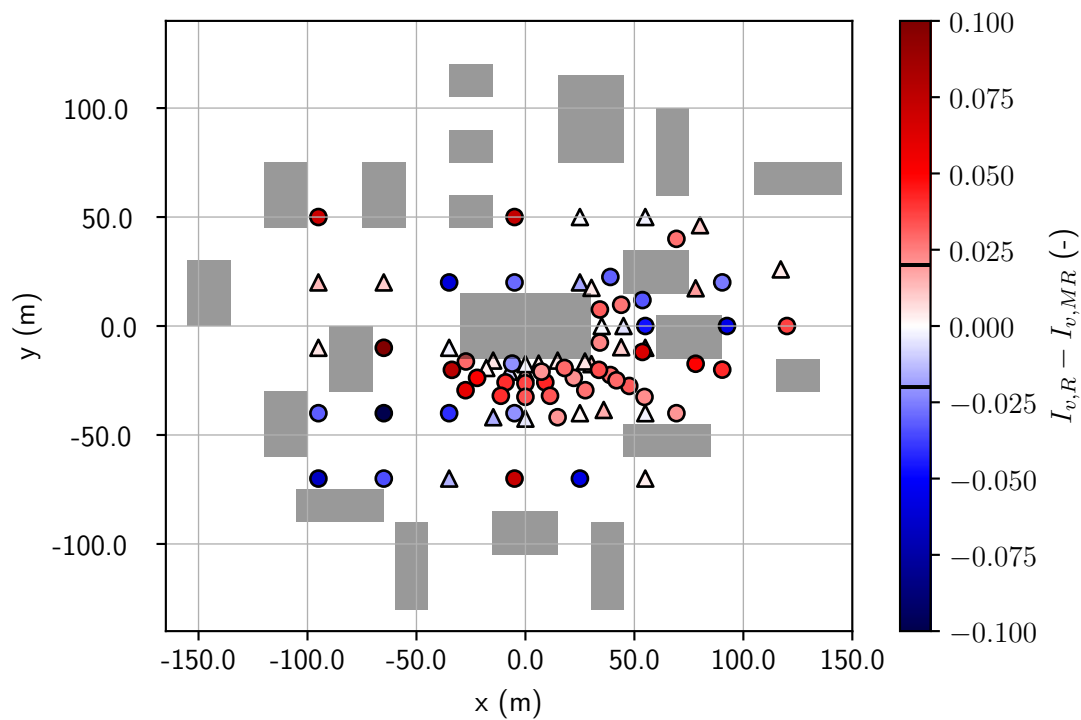


Figure C.3: Absolute difference of turbulence intensity I_v between the rough boundary layer inflow and the moderate rough boundary layer inflow. Measurement height is 4 m and the wind direction is from left to right. For more information read caption of Fig. 6.4.

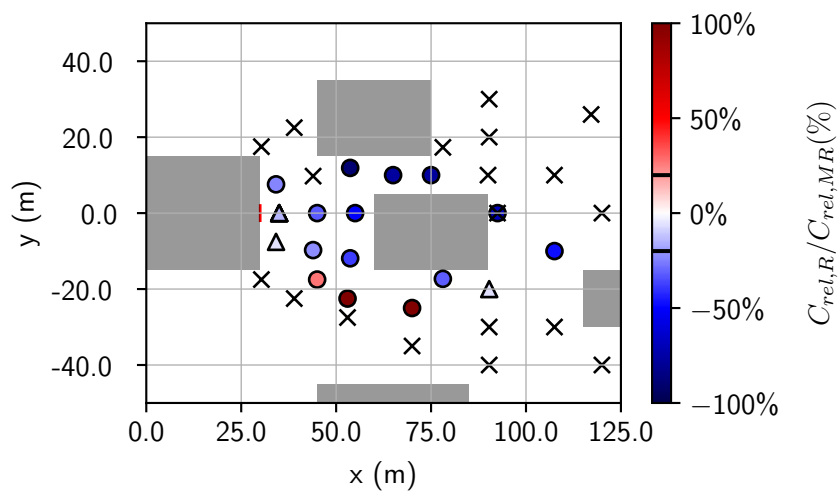


Figure C.4: Relative difference of the mean relative concentration for a heavy gas dispersion between the rough boundary layer (R) and the moderate rough boundary layer (MR). Wind direction is from left to right (M1). This represents a wind direction of 0° . Source is marked with a red line on the large building on the left side. Measurement height is 2 m. For more information read caption of Fig. 6.10.

C.2 Measurement results: Model 2

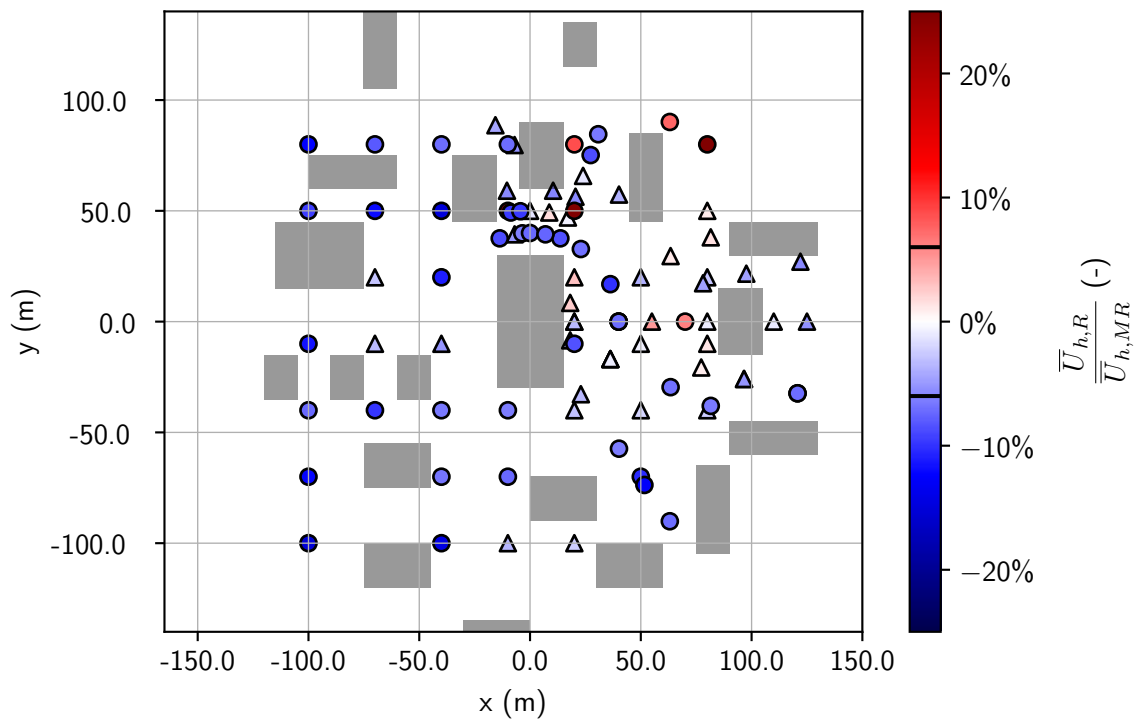


Figure C.5: Relative difference of magnitude (horizontal wind speed) between the rough boundary layer inflow and the moderate rough boundary layer inflow. Measurement height is 4 m.

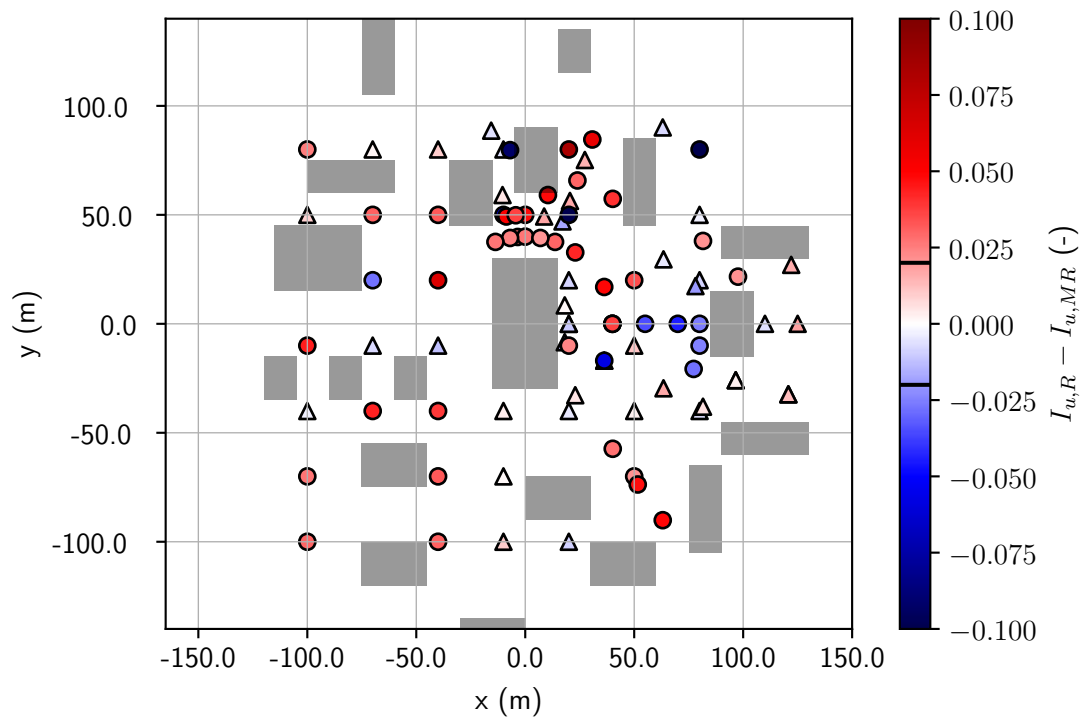


Figure C.6: Absolute difference of turbulence intensity I_u between the rough boundary layer inflow and the moderate rough boundary layer inflow. Measurement height is 4 m.

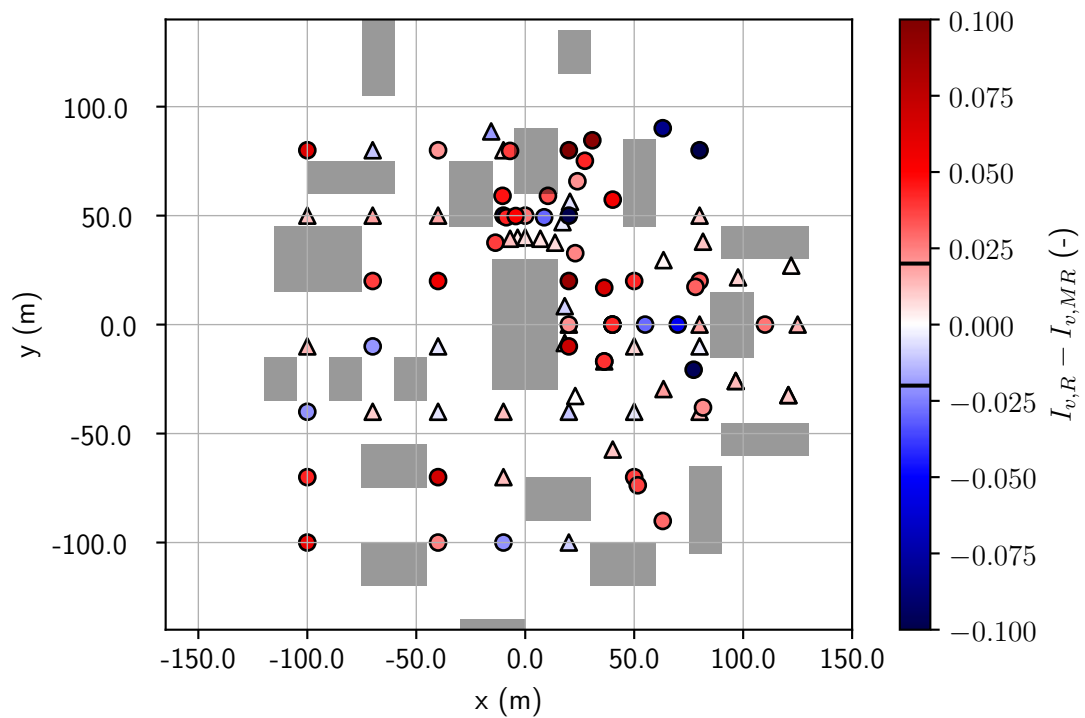


Figure C.7: Absolute difference of turbulence intensity I_v between the rough boundary layer inflow and the moderate rough boundary layer inflow. Measurement height is 4 m.

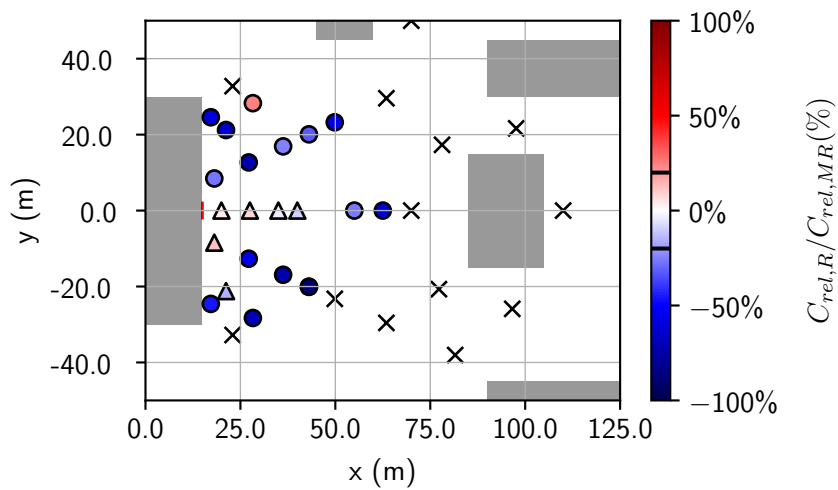


Figure C.8: Relative difference of the mean relative concentration for a heavy gas dispersion between the rough boundary layer (R) and the moderate rough boundary layer (MR). Wind direction is from left to right (M2). The M2 configuration is a wind direction of 90° . Source is marked with a red line on the large building on the left side. Two locations with vertical profiles are marked with green arrows. Measurement height is 2 m.

C.3 Measurement results: Model 3

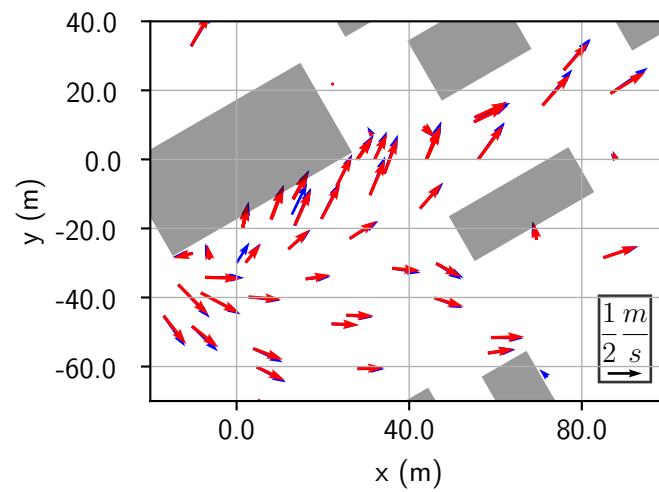


Figure C.9: Mean wind direction and wind speed in a measurement height of 2 m for the moderately rough boundary layer in blue and the rough boundary layer in red. Wind direction is from left to right. Used configuration is the idealized industrial model (M3).

Appendix D

Measurement results: Area Source without Obstacles Model

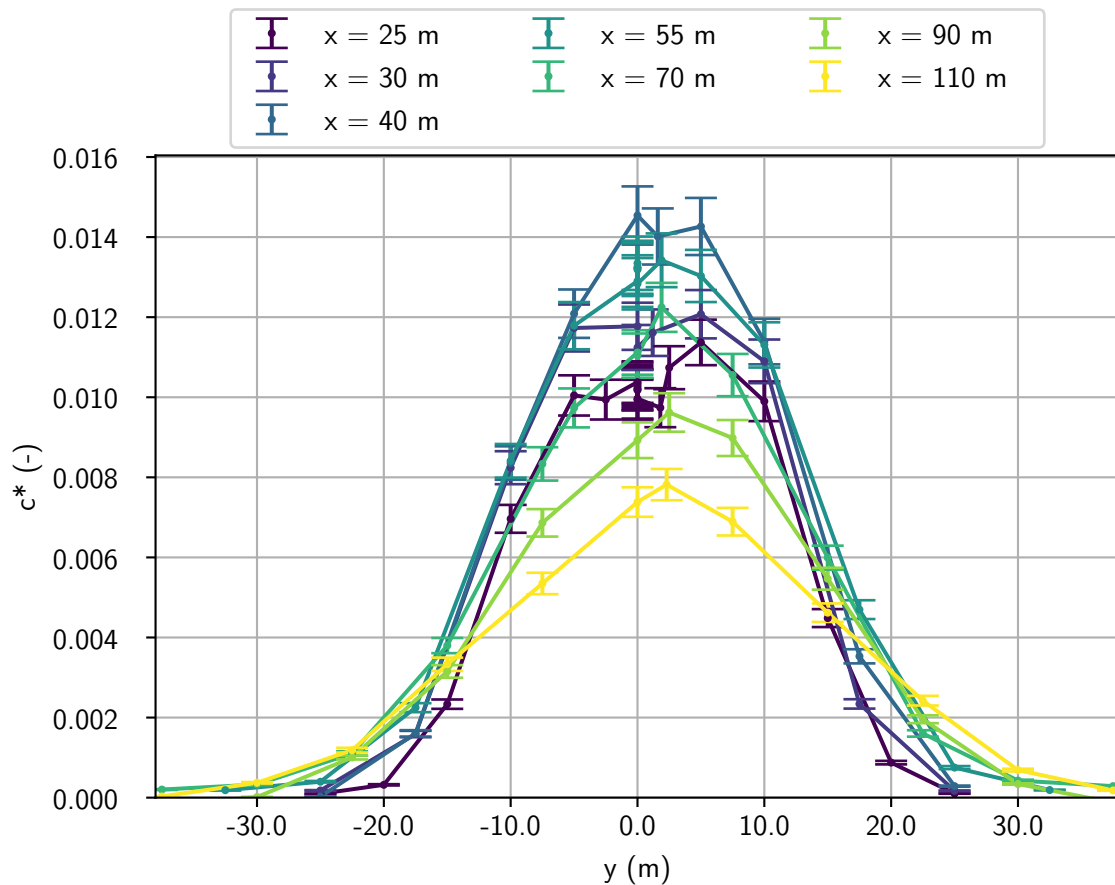


Figure D.1: Lateral profile of dimensionless concentrations measured in the area source model without obstacles in a measurement height of 2 m. Lateral profile measurements are performed in seven different distances from the centre point of the area source (Sec. 4.3.1).

Appendix E

Measurement results: Industrial Chemical Park Model

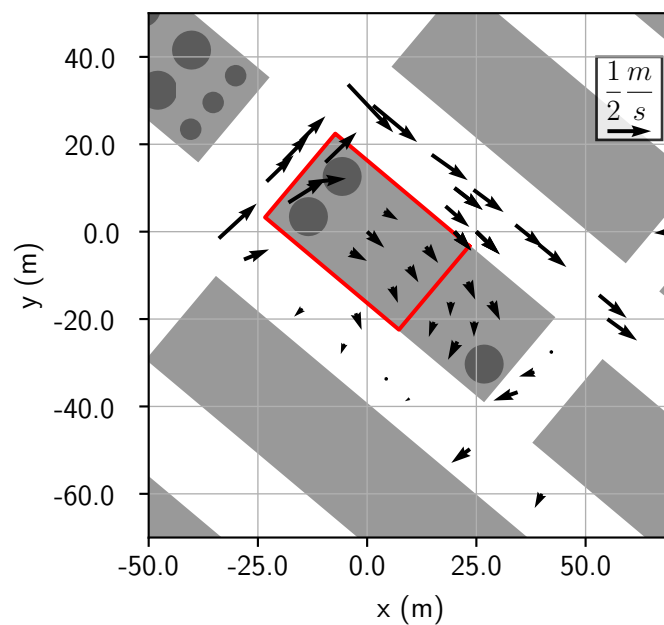


Figure E.1: Mean wind direction and wind speed in the chemical park model configuration with 10 tanks. Measurement height is 2 m. Measurement height is 2 m. The wind direction is from left to right and the used boundary layer is moderately rough. Used source is marked with a red rectangle.

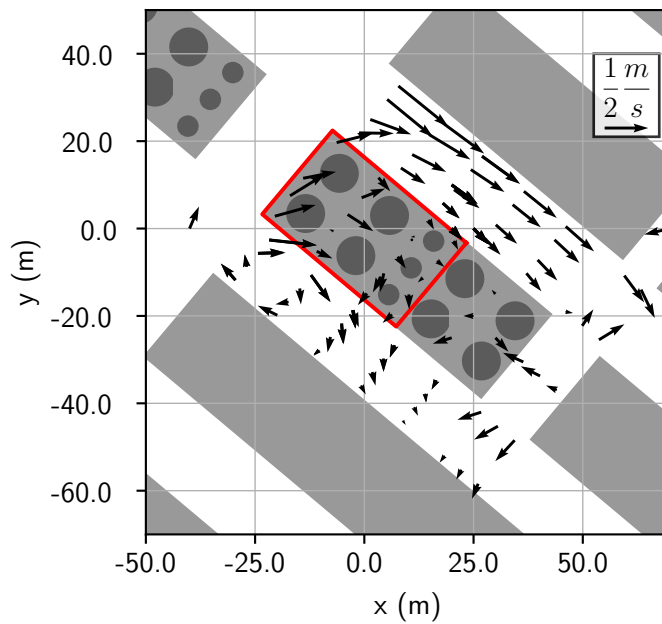


Figure E.2: Mean wind direction and wind speed in the chemical park model configuration with full number of tanks (19 tanks). Measurement height is 2 m. The wind direction is from left to right and the used boundary layer is moderately rough. Used source is marked with a red rectangle.

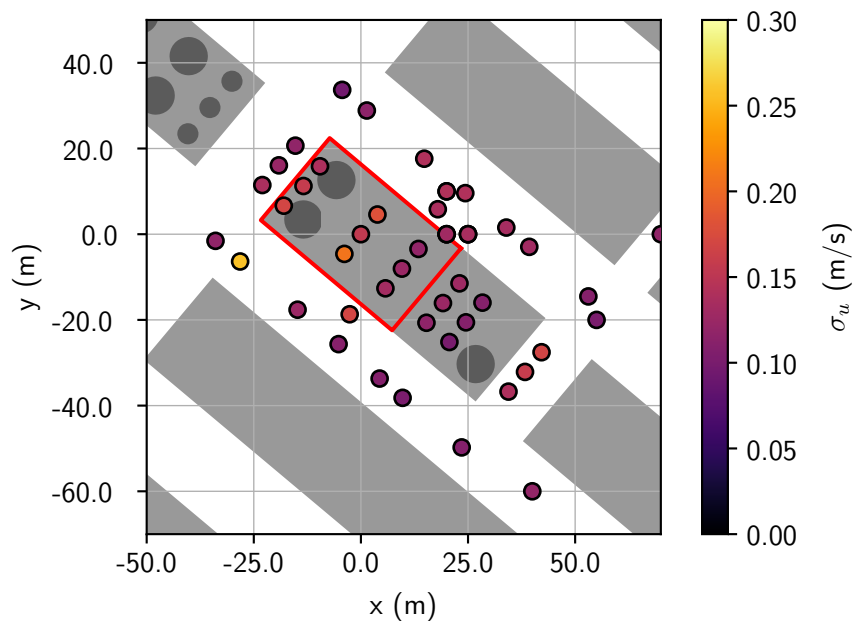


Figure E.3: Standard deviation of the u -component of the wind. Measurement height is 2 m. The wind direction is from left to right and the used boundary layer is moderately rough. Used source is marked with a red rectangle.

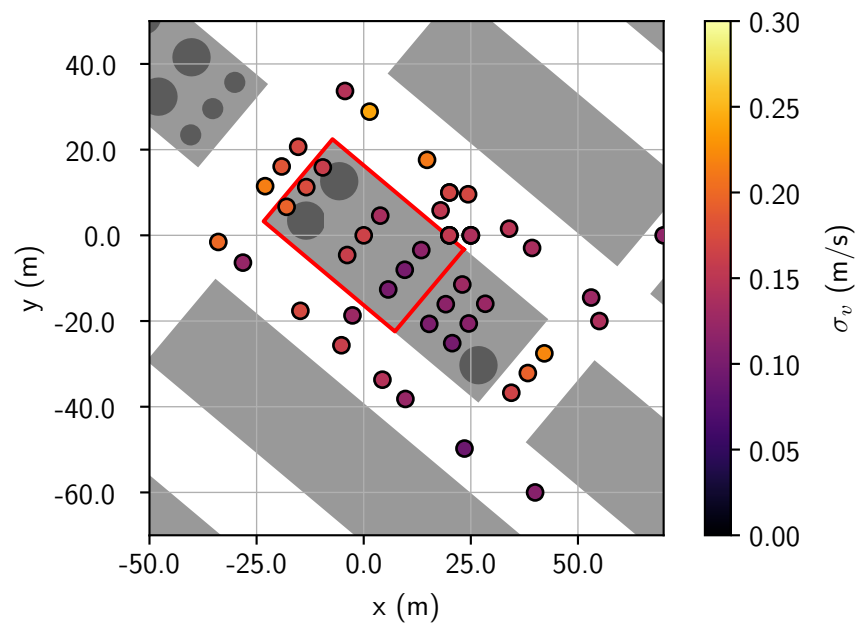


Figure E.4: Standard deviation of the v -component of the wind. Measurement height is 2 m. The wind direction is from left to right and the used boundary layer is moderately rough. Used source is marked with a red rectangle.

Bibliography

- Albrecht, H.-E., Borys, M., Damaschke, N., and Tropea, C. (2003). *Laser Doppler and Phase Doppler Measurement Techniques*. Springer Berlin Heidelberg. 24
- Arya, S. (1982). Atmospheric boundary layers over homogeneous terrain. 46
- Basu, S. and Lacser, A. (2017). A cautionary note on the use of monin–obukhov similarity theory in very high-resolution large-eddy simulations. *Boundary-Layer Meteorology*, 163(2):351–355. 54
- Batt, R., Gant, S., Lacombe, J.-M., Truchot, B., and Tucker, H. (2016). CFD modelling of dispersion in neutral and stable atmospheric boundary layers : results for prairie grass and Thorney Island. 7
- Bertazzi, P. A. (1991). Long-term effects of chemical disasters. lessons and results from seveso. *Science of The Total Environment*, 106(1-2):5–20. 2
- Boris, J. P. and Patnaik, G. (2014). Acute exposure guideline levels (aegls) for time varying toxic plumes. 70, 72
- Brautmeier, L. (2015). Untersuchung des quellnahen ausbreitungsverhaltens schwerer gase - eine machbarkeitsstudie. Master's thesis, Universität Hamburg. 51
- Briggs, G., Britter, R., Hanna, S., Havens, J., Robins, A., and Snyder, W. (2001). Dense gas vertical diffusion over rough surfaces: Results of wind-tunnel studies. *Atmospheric Environment*, 35:2265–2284. 8
- Britter, R., Weil, J., Leung, J., and Hanna, S. (2011). Toxic industrial chemical (TIC) source emissions modeling for pressurized liquefied gases. *Atmospheric Environment*, 45(1):1–25. 18
- Britter, R. E. and McQuiad, J. (1988). *Workbook on the Dispersion of Dense Gases*. HSE. 1, 13, 17, 21, 67, 69
- Bromideh, A. A. and Valizadeh, R. (2014). Discrimination between gamma and log-normal distributions by ratio of minimized kullback-leibler divergence. *Pakistan Journal of Statistics and Operation Research*, 9(4):443. 74
- Broughton, E. (2005). The bhopal disaster and its aftermath: a review. *Environmental Health*, 4(1). 1, 2
- Burgess, D. S., Biordi, J., and Murphy, J. N. (1972). Hazards of spillage of lng into water. report no. 4177. Technical report, Pittsburgh Mining and Safety Research Center, U.S. Bureau of Mines. 68, 70
- CEA (2003). Co2 systems planning and installation. 50
- Counihan, J. (1975). Adiabatic atmospheric boundary layers: A review and analysis of data from the period 1880–1972. *Atmospheric Environment (1967)*, 9(10):871–905. 6, 38, 40, 41, 43, 45, 46, 47, 48
- Department of Energy (1979). Liquefied gaseous fuels safety and environmental control assessment program: a status report. Technical report, Colorado State University. 5
- D'Silva, T. (2006). *The Black Box of Bhopal: A Closer Look at the World's Deadliest Industrial Disaster*. Trafford. 1
- Erdmann, F. (2017). Wind tunnel study of terrain induced flow modification aand spatial resolution effects. Master's thesis, University Hamburg. 41, 42, 43, 46, 48, 89

- ESDU-85020 (1985). Characteristics of atmospheric turbulence near the ground. part ii: single point data for strong winds (neutral atmosphere). 42
- EU (2012). Directive 2012/18/eu of the european parliament and of the council of 4 july 2012 on the control of major-accident hazards involving dangerous substances, amending and subsequently repealing council directive 96/82/ec. 2
- EWTL (2006). Compilation of experimental data for validation of microscale dispersion models. <https://mi-pub.cen.uni-hamburg.de/index.php?id=433>. 54
- Fay, J. A. (1980). Risks of LNG and LPG. *Annual Review of Energy*, 5(1):89–105. 1, 2
- Forster, P., Ramaswamy, V., Artaxo, P., Berntsen, T., Betts, R., Fahey, D. W., Haywood, J., Lean, J., Lowe, D. C., Myhre, G., Nganga, J., Prinn, R., Raga, G., Schulz, M., and Van Dorland, R. (2007). Changes in atmospheric constituents and in radiative forcing. In Solomon, S., Qin, D., Manning, M., Chen, Z., Marquis, M., Averyt, K. B., Tignor, M., and Miller, H. L., editors, *Climate Change 2007: The Physical Science Basis. Contribution of Working Group I to the Fourth Assessment Report of the Intergovernmental Panel on Climate Change*, book section 2. Cambridge University Press, Cambridge, United Kingdom and New York, NY, USA. 51
- Fox, S. B. (2011). Project jack rabbit: Field tests. Technical report, Chemical Security Analysis Center. 8
- Hall, D. J. and Waters, R. (1985). Wind tunnel model comparisons with the thorney island dense gas release field trials. *Journal of Hazardous Materials*, 11:209–235. 7
- Hanna, S., Britter, R., Argenta, E., and Chang, J. (2012). The jack rabbit chlorine release experiments: Implications of dense gas removal from a depression and downwind concentrations. *Journal of Hazardous Materials*, 213-214:406–412. 53
- Hanna, S., Mazzola, T., Chang, J., Spicer, T., Gant, S., and Batt, R. (2021). Gaps in toxic industrial chemical model systems: Improvements and changes over past 10 years. *Process Safety Progress*, 41(1):151–166. 3, 11
- Hanna, S. and Steinberg, K. (2001). Overview of petroleum environmental research forum (PERF) dense gas dispersion modeling project. *Atmospheric Environment*, 35(13):2223–2229. 8
- Hanna, S. R. and Chang, J. C. (2001). Use of the kit fox field data to analyze dense gas dispersion modeling issues. *Atmospheric Environment*, 35(13):2231–2242. 8, 52, 53
- Hardee, H. C., Lee, D. O., and Benedick, W. B. (1978). Thermal hazard from LNG fireballs. *Combustion Science and Technology*, 17(5-6):189–197. 1, 2
- Harms, F. (2010). *Systematische Windkanaluntersuchungen zur Charakterisierung instationärer Ausbreitungsprozesse einzelner Gaswolken in urbanen Rauigkeitsstrukturen*. PhD thesis, Staats- und Universitätsbibliothek Hamburg Carl von Ossietzky. 46
- Havens, J. (1977). Predictability of lng vapor dispersion from catastrophic spills onto water: An assessment. Technical report, University of Arkansas. 2
- Havens, J. (1992). Review of dense gas dispersion field experiments. *Journal of Loss Prevention in the Process Industries*, 5(1):28–41. 1, 5, 6, 53
- Havens, J., Walker, H., and Spicer, T. (2012). Bhopal atmospheric dispersion revisited. *Journal of Hazardous Materials*, 233-234:33–40. 1, 2
- Heinrich, M. and Gerhold, E. (1986). Praxisgerechte bestimmung der zündentfernung bei der freisetzung schwerer gase (lpg), 3. zwischenbericht. Technical report, TÜV Norddeutschland. 7

- Hertwig, D. (2013). *On aspects of large-eddy simulation validation for near-surface atmospheric flows*. PhD thesis, Universität Hamburg. 24, 41, 46
- Hirst, W. J. S. and Eyre, J. A. (1983). Maplin sands experiments 1980: Combustion of large LNG and refrigerated liquid propane spills on the sea. In *Heavy Gas and Risk Assessment — II*, pages 211–224. Springer Netherlands. 7
- Hogg, R. V. and Craig, A. T. (1979). *Introduction to Mathematical Statistics*. Macmillan Publishing Co., Inc. 74
- IEC (2020). Explosive atmospheres - part 10-1: Classification of areas - explosive gas atmospheres. Standard IEC 60079-10-1, International Electrotechnical Commission, Geneva, CH. Edition 3.0. 68
- IFA (2020). Schwefelwasserstoff. <https://gestis.dguv.de/data?name=001130>. Accessed: 22.11.2022. 68
- IFA (2021). Kohlenstoffdioxid. <https://gestis.dguv.de/data?name=001120>. Accessed: 26.01.2023. 51
- Kaimal, J. C. (1994). *Atmospheric Boundary Layer Flows: Their Structure and Measurement*. Oxford University Press. 42
- Kaimal, J. C., Wyngaard, J. C., Izumi, Y., and Coté, O. R. (1972). Spectral characteristics of surface-layer turbulence. *Quarterly Journal of the Royal Meteorological Society*, 98(417):563–589. 42
- Kolmogorov, A. N. (1991). The Local Structure of Turbulence in Incompressible Viscous Fluid for Very Large Reynolds Numbers. *Proceedings of the Royal Society A: Mathematical, Physical and Engineering Sciences*, 434:9–13. 47
- Koopman, R., Cederwall, R., Ermak, D., Goldwire, H., Hogan, W., McClure, J., McRae, T., Morgan, D., Rodean, H., and Shinn, J. (1982). Analysis of burro series 40-m3 lng spill experiments. *Journal of Hazardous Materials*, 6(1-2):43–83. 6
- König-Langlo, G. (1987). *Windkanalmodellierung der Ausbreitung störfallartig freigesetzter Gase schwerer als Luft*. PhD thesis, Universität Hamburg. 7, 17, 18, 20
- König-Langlo, G. and Schatzmann, M. (1991). Wind tunnel modeling of heavy gas dispersion. *Atmospheric Environment. Part A. General Topics*, 25(7):1189–1198. 7, 19
- Leitl, B., Harms, F., Michel, S., Turnow, J., Plischka, H., Schalau, B., and Schalau, S. (2021). Simulation kurzzeitiger Gefahrstofffreisetzungen aus Industrieanlagen/simulation of short-term hazmat releases from industrial facilities – challenges and possible solutions. *Gefahrstoffe*, 81(07-08):257–270.
- Mannan, M. S. (2012). Chapter 18 - toxic release. In Mannan, S., editor, *Lees' Loss Prevention in the Process Industries (Fourth Edition)*, pages 1679–1760. Butterworth-Heinemann, Oxford, fourth edition edition. 70
- McQuaid, J., Roebuck, B., and Wilde, D. G. (1985). Large-scale field trials on dense vapour dispersion. In *Safety of Thermal Water Reactors*, pages 179–189. Springer Netherlands. 6, 52, 53
- Meroney, R. and Neff, D. (1977). Dispersion of vapor from lng spills - simulation in a meteorological wind tunnel. Technical report, Colorado State University. 5
- Meroney, R. and Neff, D. (1979). Dispersion of vapor from lng spills – simulation in a meteorological wind tunnel of spills at china lake naval weapons center, california. Technical report, Colorado State University. 5, 6
- Meroney, R. and Neff, D. (1982). Dispersion of vapor from liquid natural gas spills— evaluation of simulation in a meteorological wind tunnel: Five-cubic-meter china lake spill series. *Journal of Wind Engineering and Industrial Aerodynamics*, 10(1):1–19. 6

- Meroney, R. N. (1982). Wind-tunnel experiments on dense gas dispersion. *Journal of Hazardous Materials*, 6(1-2):85–106. 1, 7
- MESA (2019). *WSWD SONIC Anemometer User Manual*. MESA Systemtechnik GmbH, Turmstraße 8, 78467 Konstanz Germany, version 1.5 edition. 24
- Michálek, P. and Zacho, D. (2012). Effect of surface roughness on neutral and dense gas dispersion in the BLWT. In *Air Pollution XX*. WIT Press. 88
- Michel, S., Leitl, B., Harms, F., Schalaus, S., Schalaus, B., Plischka, H., Turnow, J., and Kornev, N. (2023). Störfallartige Ausbreitung von dichte-neutralen und schweren Gasen in komplexen Umgebungen. 10.25592/UHHFDM.11779. 91
- NDR (2022). Bundestag verabschiedet Ing-gesetz. <https://www.tagesschau.de/wirtschaft/bundestag-fluessiggas-terminals-101.html>. Accessed: 20.05.2022. 2
- Nicholson, D., Lian, N., Hedrick, A., and Schmidt, E. (2017). Final test report for jack rabbit (jr) ii. Technical report, West Desert Test Center. 8, 9
- NRC (2007). *Acute Exposure Guideline Levels for Selected Airborne Chemicals: Volume 5*. The National Academies Press, Washington, DC. 2
- Odsæter, L. H., Skarsvåg, H. L., Aursand, E., Ustolin, F., Reigstad, G. A., and Paltrinieri, N. (2021). Liquid hydrogen spills on water—risk and consequences of rapid phase transition. *Energies*, 14(16):4789. 2
- Oke, T. (1984). Methods in urban climatology. *Applied Climatology*, 14:19–29. 15, 16
- Oke, T. (1988). The urban energy balance. *Progress in Physical Geography: Earth and Environment*, 12(4):471–508. 15, 16
- Panofsky, H. A. (1974). The atmospheric boundary layer below 150 meters. *Annual Review of Fluid Mechanics*, 6(1):147–177. 38, 45, 46
- Pasquill, F. (1961). The estimation of the dispersion of windborne material. *Meteorol. Mag.*, 90:33. 7
- Peckham, M. (2006). *HFR400 Fast Response Hydrocarbon Measurement System User Manual*. Cambustion, 347 Cherry Hinton Road Cambridge UK, 3.5 edition. 26
- Petersen, R. and Cochran, B. (1995). A wind tunnel evaluation of methods for estimating surface roughness length at industrial facilities. *Atmospheric Environment*, 31(1):45–57. 8
- Philipson, L. L. (1978). The safety of LNG systems. *Energy Sources*, 4(2):135–155. 1
- Plate, E. (1982). Wind tunnel modelling of wind effects in engineering. *Engineering meteorology*, pages 573–639. 39
- Plischka, H., Michel, S., Turnow, J., Leitl, B., and Kornev, N. (2022). Comparison of turbulent inflow conditions for neutral stratified atmospheric boundary layer flow. *Journal of Wind Engineering and Industrial Aerodynamics*, 230:105145.
- RIVM (2021). Handleiding risicoberekeningen bevi. techreport, Rijksinstituut voor Volksgezondheid en Milieu (RIVM). 70
- Robins, A., Castro, I., Hayden, P., Steggel, N., Contini, D., Heist, D., and Taylor, T. J. (2001). A wind tunnel study of dense gas dispersion in a stable boundary layer over a rough surface. *Atmospheric Environment*, 35(13):2253–2263. 8
- Robins, A., Hayden, P., and Wingstedt, E. M. M. (2016). Moditic wind tunnel experiments. Technical report, Forsvarets Forskningsinstitut FFI. 10, 11, 52, 53, 89

-
- Schalau, S., Habib, A., and Michel, S. (2021). Atmospheric wind field modelling with OpenFOAM for near-ground gas dispersion. *Atmosphere*, 12(8):933.
- Schalau, S., Habib, A., and Michel, S. (2023). A modified k-epsilon turbulence model for heavy gas dispersion in built-up environment. *Atmosphere*, 14(1):161.
- Schatzmann, M., König, G., and Lohmeyer, A. (1986). Dispersion modeling of hazardous materials in the wind tunnel. In *Air Pollution Modeling and Its Application V*, pages 641–652. Springer. 17
- Schneider, A. L., Lind, C. D., and Parnarouskis, M. C. (1980). Us coast guard liquefied natural gas research at china lake. Technical report, COAST GUARD WASHINGTON DC. 5
- Simiu, E. and Scanlan, R. (1978). *Wind effects on structures: an introduction to wind engineering*. A Wiley-Interscience publication. Wiley. 42
- Snyder, W. (1995). Wind tunnel roughness array tests. Technical report, FMF, Research Triangle Park, NC 27711. 8
- Snyder, W. H. (1972). Similarity criteria for the application of fluid models to the study of air pollution meteorology. *Boundary-Layer Meteorology*, 3(1):113–134. 16, 17
- Snyder, W. H. (1981). Guideline for fluid modeling of atmospheric diffusion. fluid modeling report no. 10. Technical report, EPA. 13, 14, 15, 16, 17
- Spicer, T. and Smith, C. (2021). Jack rabbit ii mock urban environment trials: Wind tunnel model investigation and validation. Technical report, U.S. Department of Homeland Security Science and Technology Directorate, Chemical Security Analysis Center. 9, 52, 89
- Stull, R. B. (1988). *An Introduction to Boundary Layer Meteorology*. Springer Netherlands. 15, 16
- Taylor, G. I. (1938). The spectrum of turbulence. *Proceedings of the Royal Society of London. Series A-Mathematical and Physical Sciences*, 164(919):476–490. 40
- Tennekes, H. and Lumley, J. (1972). *A First Course in Turbulence*. MIT Press. 13
- Townsend, A. A. R. (1956). *The Structure of Turbulent Shear Flow (Cambridge Monographs on Mechanics)*. Cambridge University Press. 14
- Ulvestad, M. and Overland, I. (2012). Natural gas and co2 price variation: impact on the relative cost-efficiency of lng and pipelines. *International Journal of Environmental Studies*, 69(3):407–426. 2
- van Heugten, W. and Duijm, N. (1985). Some findings based on wind tunnel simulation and model calculations of thorney island trial no. 008. *Journal of Hazardous Materials*, 11:409–416. 7
- Vaz, M. F. and Fortes, M. (1988). Grain size distribution: The lognormal and the gamma distribution functions. *Scripta Metallurgica*, 22(1):35–40. 74
- VDI (1990). Environment meteorology - disperion of heavy gas emision by accidental releases - safety study, guideline 3783-2. *VDI-Richtlinien*. 7, 17, 18
- VDI (2000). Environment meteorology - physical modelling of flow and dispersion processes in the atmospheric boundary layer – application of wind tunnels, guideline vdi-3783-12. *VDI-Richtlinien*. 10, 17, 29, 31, 32, 33, 34, 35, 37, 38, 39, 42, 43, 45, 46, 48, 50, 52, 62, 89
- von Karman, T. (1948). Progress in the statistical theory of turbulence. *Proceedings of the National Academy of Sciences*, 34(11):530–539. 42
- Wiens, B. L. (1999). When log-normal and gamma models give different results: A case study. *The American Statistician*, 53(2):89. 74

Eidesstattliche Versicherung | Declaration on Oath

Hiermit erkläre ich an Eides statt, dass ich die vorliegende Dissertationsschrift selbst verfasst und keine anderen als die angegebenen Quellen und Hilfsmittel benutzt habe.

I hereby declare upon oath that I have written the present dissertation independently and have not used further resources and aids than those stated.

Simon Michel

Hamburg, 23.03.2023